Spin–Lattice Relaxation of Coupled Nuclear Spins with Applications to Molecular Motion in Liquids

DAVID M. GRANT,* CHARLES L. MAYNE, FANG LIU, and TIAN-XIANG XIANG

Department of Chemistry, University of Utah, Salt Lake City, Utah 84112

Received August 7, 1991 (Revised Manuscript Received August 23, 1991)

Contents

I. Introduction

The nuclear spin–lattice relaxation observed in nuclear magnetic resonance (NMR) involves a conserved transfer of energy between nuclear spin states and the lattice states associated with the environment of the spins. It was recognized in early experimental observations of the NMR phenomenon[1-3] that nuclear spin degrees of freedom would couple only weakly with their lattice environment. Consequently the spin–lattice relaxation time, T_1, for a nuclear spin system to attain thermal equilibrium with the lattice is on the order of milliseconds in solid samples to seconds in liquids, and in rare cases T_1 can even range up to minutes. These relatively long times compare with optical relaxation times of pico to nanoseconds. A significant benefit of these weak spin–lattice couplings is that the spins and the lattice may be treated, to zero order, as separate systems. Furthermore, the lattice is left essentially unperturbed due to exchange of energy with the spins because the heat capacity of the lattice at typical magnetic fields is orders of magnitude greater than that of the spins. When experimental measurements are made solely on the spin system, time-dependent perturbation theory is sufficiently accurate to explore the various important aspects of spin–lattice interactions.

Under these conditions, simple thermodynamic arguments lead to Bloch's equations of motion[2,3] which are adequate to predict the behavior of an ensemble of noninteracting nuclear spins interacting weakly with the lattice (see section II.A). The situation differs, however, when groups of nuclear spins couple with each other, and a more rigorous treatment is required involving a spin density matrix equation of motion with multiple spin–lattice relaxation parameters.[4-7] In low viscosity liquids, spin–lattice relaxation can be treated as temporal modulation of the various spin–lattice coupling terms as a consequence of thermally activated reorientation of a molecule. Therefore, the study of spin–lattice relaxation can contribute to a better understanding of molecular dynamics in liquids.

Historically, a single spin–lattice relaxation time was measured for each nucleus in an attempt to characterize the molecular motion. This oversimplification of relaxation processes may be due in part to the success of Bloch theory for isolated spins, but in the case of ^{13}C it is also due to the traditional ^1H decoupled experiment

0009-2665/91/0791-1591$09.50/0

David M. Grant was born in 1931 and educated in Utah with degrees from the University of Utah. He joined its chemistry faculty in 1958 after holding the DuPont instructorship at the University of Illinois. In addition to directing the thesis research of over 40 M.S. and Ph.D. students, Professor Grant served his institution as the Chemistry Department Chairperson (1962–73) and as the Dean of Science (1976–85). Professor Grant's research interests in nuclear magnetic resonance (NMR) spectroscopy has lead to nearly 300 research publications. He is best known for his pioneering work in the field of carbon-13 NMR. Molecular structural correlations of carbon-13 chemical shifts, both the istropic and tensor components, have exhibited the importance of carbon-13 shielding in the field of chemistry. His laboratory has also played a prominent role in the relationship between coupled spin relaxation, treated in this review, and molecular dynamics. His research work has been recognized in a variety of ways including the University of Utah Distinguished Research Award; the Gardner Prize and the Distinguished Service Award of the Utah Academy of Sciences, Arts and Letters; the California Section Gold Medal, the Utah Section Award of the American Chemical Society (ACS); and the 1991 National ACS Award in Petroleum Chemistry.

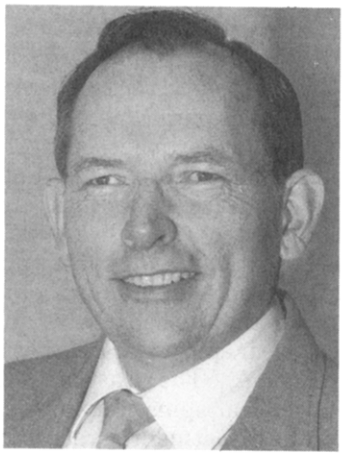

Charles L. Mayne is a native Utah. He earned a B.S. with honors in chemistry from New Mexico State University in 1970 while working as a chemist at the NASA White Sands Test Facility. His interest in NMR stems from his first year of graduate work at the Oregon Graduate Center under George Gray. Returning to Utah he completed a Ph.D. in Chemistry under David M. Grant in 1976. Dr. Mayne is currently manager of the Chemistry Department NMR facility at University of Utah and holds appointments as Adjunct Associate Professor of Chemistry at University of Utah and Brigham Young University. He has published on a wide range of topics in both solid- and liquid-state NMR.

Fang Liu was born in Anhui, P. R. China in 1963. She received her B.S. degree in 1983 from Wuhan University, and Ph.D. degree in physical chemistry in 1990 from University of Utah. She is currently a postdoctoral fellow at University of Utah with David M. Grant. She has been involved in the studies of molecular motion in solution explored via carbon-13 NMR coupled relaxation techniques and generalized Brownian dynamics simulations since 1985.

Tian-xiang Xiang was born in Wuhan, P. R. China in 1959. He received his B.S. degree in chemistry in 1982 from Wuhan University, and Ph.D. degree in physical chemistry (chemical dynamics) in 1986 from University of Utah. After a postdoctoral in the pharmaceutics department (University of Utah), he joined the faculty at Nanjing University (P. R. China) in 1988, where he is an associate professor in chemistry. His present research interests include basic studies in biological and artificial membrane transport, molecular dynamics and spectroscopy, statistical mechanics and molecular modeling, and molecular dynamics simulations.

that renders the ^{13}C relaxation essentially exponential in a single effective T_{1C}. To be strictly precise, however, such studies involving a single parameter per nucleus are unable to model adequately the complexity of coupled spin relaxation. Furthermore, these data, even if reasonably successful in modeling the spin dynamics, are unable to characterize the motion of molecules undergoing anisotropic reorientation. A single dynamical parameter would provide only one effective rotational correlation time per atom, and only a rigid spherical molecule rotating isotropically in its environment could be correctly described by such a simple approach. For real molecules with more complicated shapes, anisotropic motion obtains and additional diffusional parameters are required to characterize the reorientation.

The correlated motion of two or more nuclear spins produces modulation of the dipole–dipole interactions, and the resulting nuclear relaxation parameters in turn provide additional information about molecular motion. The motion of each pair of spins correlates either with itself (auto-correlation terms) or with that of other pairs

of spins (cross-correlation terms) in the coupled nuclear spin systems. One of the important aspects of complete relaxation data involving both auto and cross terms is that they may be interpreted in terms of an anisotropic rotational diffusion model. In liquids, molecules undergo collisions that modify their rotational states sufficiently frequently that small step diffusion models are usually appropriate for discussing these motional features.

Extensive reviews on coupled spin relaxation published by Werbelow and Grant[8] and by Vold and Vold[9] still are relevant. The review of coupled spin relaxation by Canet[10] provides a recent discussion of significant work completed during the past decade. Canet's elegant summary of the physical laws governing coupled spin relaxation emphasizes use of the spin operator basis. His use of irreducible spherical operators provides significant mathematical conveniences and insights to readers familiar with standard works on angular momentum,[11] and the serious worker in coupled spin relaxation can not avoid mastery of these powerful mathematical methods. However, many practicing chemists not conversant with such operator algebra may find this approach quite formidable thereby limiting their appreciation of coupled spin relaxation data and the associated molecular motional features elucidated by such information. As Canet has provided a recent comprehensive overview of coupled relaxation, the occasion of this review offers us the opportunity to put in one place an integrated and detailed presentation of coupled spin relaxation for the often used AX_2 case. This common system is the one important in proton coupled ^{13}C relaxation studies of the methylene spin moiety encountered often in the areas of organic and biochemistry. We also welcome the chance to unify definitions and notations. It is not our intent to duplicate the greater portions of the three previous reviews except as some material is needed in this manuscript for continuity. This review also focuses on the details of anisotropic molecular motion as it affects coupled spin relaxation in both rigid and flexible chain molecules.

It is our hope in this effort to provide the larger community of practicing chemists with a treatment that might give the nonspecialist a better appreciation of nuclear spin relaxation. The perception of simplicity often results from merely including a few extra details readily known to specialists in a field. Some aspects of NMR require a reasonably high level of complexity (e.g., the coupling of angular momenta of identical spins), and it is impossible to account for all experimental observations with excessively simple concepts. To illustrate this point further, many commonly used two-dimensional (2D) NMR experiments require multiple spin coherences to be produced and exploited. The relaxation of these coherences is invariably governed by the mathematical expressions that have evolved in the field of coupled spin relaxation. Several groups[12-21] have contributed extensively in recent years to the comprehension of these phenomena.

Some simplification of the material is made possible by limiting the cases to be treated to those that illustrate the relevant principles without being unnecessarily complicated. We make the following choices in the material to be presented:

(1) The simplest assumption of spin isolation leading to the Bloch equations obviously must be rejected to observe the effects of coupled spin relaxation.

(2) The X approximation will be assumed. *Second* order effects, present when scalar couplings are of the order of chemical shift differences, will not be considered.

(3) Only longitudinal or T_1 type processes are considered. This is accomplished by imposing a *secular approximation*, to separate the static, or at least slowly varying, components of the magnetization from rapidly oscillating components associated with precession in response to either static or rf (radio frequency) magnetic fields. The traditional Redfield density matrix development transforms the equation of motion to an interaction representation using the static or Zeeman Hamiltonian and representing the equation of motion in terms of eigenstates of this Hamiltonian. This leads to explicit oscillatory factors in terms of the eigenvalues for each element of the relaxation matrix.[22] When this oscillatory term has a frequency other than zero the corresponding relaxation matrix element is nonsecular and may be set to zero since it will have no influence on the behavior of the secular terms. In a totally equivalent development,[23] the density matrix may be expanded in a complete set of spin operators many of which correspond to experimental measurables. The secular approximation then consists of selecting the part of the relaxation matrix corresponding to those basis operators that commute with I_z. (See Mehring[24] for more details on commuting operators and secular approximations.)

(4) Our treatment focuses on spin $^1/_2$ nuclei that only quantize along the axis of the $\mathbf{B}_0$ field. This restriction eliminates consideration of quadrupolar nuclei that interact strongly with electric field gradients and that often quantize along axes other than that controlled by $\mathbf{B}_0$ in the Zeeman interaction.

(5) We make the so called *sudden approximation* which amounts to assuming that relaxation does not occur during the period a perturbing rf pulse is applied to the sample. For typical systems studied by high-resolution liquid NMR it is usually possible to accomplish the needed perturbations in a time short compared to all relaxation processes.

(6) When molecular tumbling motion in liquids is much more rapid than the nuclear precession or Larmor frequency, an *extreme narrowing approximation* provides significant mathematical simplification in the Fourier expansion of the spatial correlation function. Avoidance of the extreme narrowing condition is not very difficult and the totally general case is carried in this review until direct evaluation is required.

(7) We limit our consideration in this review to only isotropic fluids. Ensemble averaging of spatial correlation functions, expanded in spherical harmonics, is greatly simplified as all projections of the spherical harmonics behave identically in isotropic systems. Thus, the averaging need be done only for the simplest zero projection of each rank.

(8) Finally, we focus on relaxation mechanisms involving a composite first rank random field term and the second rank dipole–dipole interaction. In each rank, however, both auto-correlated and cross-correlated terms are included, but interfering cross terms between

the dipolar and random field mechanisms are absent. These many assumptions are compatible with data from many organic systems especially when taken at lower magnetic fields.

Workers have explored in considerable detail the consequences of deviations from several of the above simplifying assumptions and approximations. The following items are numbered to correspond to those given above. The literature on (1) isolated spins, (2) second-order effects, (3) transverse relaxation, and (4) quadrupolar nuclei is too large to include in this review. Treatments of (5) spin systems perturbed by rf pulses comparable in length with relaxation times and in noncompliance with the sudden approximation leads to extremely complicated expressions for the time development of the magnetization and even steady-state solutions are often not simple. However, some success has been achieved for very simple spin systems.[25-28] The literature on (7) ordered systems, e.g., liquid crystals and micelles, is now quite extensive, and the mathematical methods for analysis are largely in place.[9,29-42]

With the use of ever higher magnetic field strengths, chemical shielding anisotropy,[21,43-46] and cross-correlated terms between chemical shielding anisotropy and the dipolar mechanisms, thought to be an anomaly 10 years ago, are now being reported in ever increasing numbers.[16-18,20,21,47-55] These new interference terms fit nicely into the formalism of cross terms and coupled relaxation initially provided by Mackor and MacLean.[56] Pyper[57] and Blicharski et al.[58,59] clearly emphasized their theoretical importance 20 years ago. Werbelow and Grant[60] anticipated early their significance in multiplet relaxation modes, but only recently has experimental evidence, coming primarily from multidimensional NMR studies, indicated their general importance. Undoubtedly, with the rapid growth of multidimensional NMR at very high fields, we can expect to find even more cases of such interference phenomena that eliminate spin inversion symmetry of the relaxation Hamiltonian commonly exploited to simplify the equation of motion.

This review is organized along the following lines: The quantum mechanical density matrix formalism and associated theoretical developments[4-7] required in the treatment of coupled spin systems are presented briefly in section II.B. The dipolar mechanism is given in detail in section II.C, along with a brief summary of various other spin–lattice interactions.[10,57,61] The effect of spin inversion symmetry[8,62-66] is explained in section II.D. Detailed phenomenological equations for longitudinal relaxation in the AX and AX_2 cases are given in section III. The relationships existing between molecular diffusional motion and relaxation power densities or correlation functions are treated in section IV. Typical spin-coupled experiments are described in section V, and the interpretation of such relaxation data in terms of diffusional models for molecular reorientation is briefly explored for specific examples in section VI. Finally, section VII illustrates the type of information available when coupled spin relaxation data are interpreted with statistical mechanical models.

II. The Theory of Nuclear Spin Dynamics

A sample containing spin $^1/_2$ nuclei, when placed in a strong external magnetic field, $\mathbf{B}_0$, develops a bulk magnetization that is parallel to and proportional to the magnitude of $\mathbf{B}_0$, to the number of nuclei present, and to the magnetic moment of each nucleus. As the direction of $\mathbf{B}_0$ defines the spin quantization or z axis in the laboratory reference frame, it also specifies the longitudinal relaxation axis. Radio frequency magnetic fields are used to perturb the magnetization from thermal equilibrium, and then relaxation processes return the spins to equilibrium when the rf field is removed. These relaxation processes, described by a system of coupled linear differential equations, determine a variety of time independent relaxation parameters that contain information on the molecular structure and motion.

Spin perturbations normally are implemented with high intensity pulses of rf energy short compared with relaxation times. Under the sudden approximation negligible relaxation occurs during the pulse leaving the relaxation to develop only under the influence of $\mathbf{B}_0$. Spin–lattice relaxation studies, therefore, consist of applying pulses to a sample in thermal equilibrium, and then monitoring the magnetization as it returns to equilibrium. The relaxation parameters in the equations of motion are numerically adjusted until the solutions of the differential equations fit the experimental data as closely as possible using a least-squares criterion. These relaxation parameters then may be interpreted in terms of various models for molecular structure and reorientation dynamics. The mathematical basis for the equations of motion used in this review is only outlined, but the reader is referred to standard texts[6,12,22,67] for more details. The reviews by Werbelow and Grant,[8] Vold and Vold,[9] and Canet[10] provide a comprehensive overview of the theoretical developments in coupled spin relaxation and also a valuable compendium of equations for a variety of coupled spin cases.

A. Classical Treatment, The Bloch Equation

When nuclear spins do not interact significantly with one another, they may be considered to be isolated and the classical equations of motion due to Bloch[2,3] adequately describe the time evolution of the bulk magnetization. These equations may be cast in a frame rotating at an angular frequency, ω, about the laboratory z axis to yield

$$\begin{aligned}
\frac{dM_x}{dt} &= \left[M_y(\gamma B_0 - \omega) - M_z \gamma B_y\right] - \frac{M_x}{T_2} \\
\frac{dM_y}{dt} &= -\left[M_x(\gamma B_0 - \omega) - M_z \gamma B_x\right] - \frac{M_y}{T_2} \\
\frac{dM_z}{dt} &= \left(M_x \gamma B_y - M_y \gamma B_x\right) - \frac{M_z - M(\infty)}{T_1}
\end{aligned} \tag{1}$$

$\mathbf{M}(t)$ is the magnetization induced in the sample, and $M(\infty)$ is the thermal equilibrium magnetization, often designated as M_0. The time-dependent components $B_x(t)$ and $B_y(t)$ represent the applied rf field in the xy plane and the z component of the field is usually time independent with magnitude $B_0 - \omega/\gamma$ in the rotating frame. In the absence of rf fields and with $\omega_0 = \gamma B_0$, M_z approaches the thermal equilibrium value, $M(\infty)$, exponentially with the characteristic time, T_1. Such longitudinal spin–lattice parameters may be used to obtain information pertaining to molecular structure

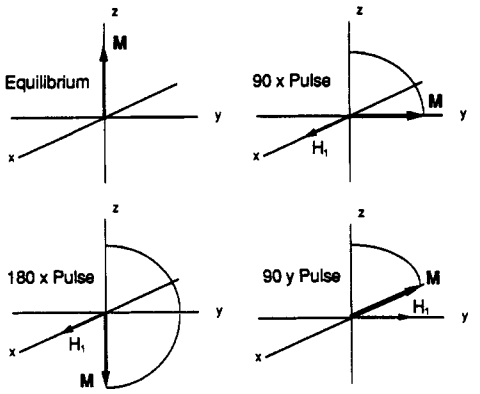

Figure 1. A rf pulse of stength, H_1, with phase and duration properly adjusted can produce any desired precession of the magnetization.

and dynamics. Components M_x and M_y also decay exponentially to zero but with a transverse time constant, T_2, but these equally important T_2 or spin–spin relaxation processes are not treated in this review. However, since z magnetization cannot be detected with an NMR spectrometer, it is necessary to access information on M_z through measurement of the xy magnetization. It is assumed that the measured xy magnetization can be made proportional to the desired z magnetization using an appropriate rf pulse.

In a NMR spectrometer with phase detection the signal produced is proportional to and has the same time dependence as the xy magnetization in the rotating frame. The precession frequency in the laboratory, $\omega_0 = \gamma B_0$, is normally on the order of hundreds of megahertz for modern spectrometers, but when the rotating frame frequency, ω, is selected to be comparable to ω_0, the Bloch equations become manageable. Pulses of rf field rotating at ω applied in the laboratory xy plane will, in the rotating coordinate frame, result in static fields about which the magnetization precesses. The magnetization can be rotated to any desired orientation in the rotating frame (see Figure 1) by adjusting the phase, amplitude and width of the rf pulse. To comply with the sudden approximation it is necessary to accomplish these nutations in a time short compared to the relaxation times.

B. Redfield Density Matrix Treatment

1. The Quantum Mechanical Hamiltonian

The physical basis for spin–lattice relaxation may be described quantum mechanically in terms of the Hamiltonian

$$\hat{H} = \hat{H}_l + \hat{H}_0 + \hat{H}_1(t) + \hat{V} \tag{2}$$

For the systems considered here the Hamiltonian, $\hat{H}$, is composed of dominant terms for the spins, $\hat{H}_0$, and the lattice, $\hat{H}_l$. The term, $\hat{H}_1(t)$, expresses the effect of rf fields applied by the spectrometer. This term has explicit time dependence because external fields will be treated classically. Finally, an interaction term, $\hat{V}$, coupling the spins to the lattice,[68] will contain the terms upon which we will concentrate to characterize the molecular dynamics. The "hat" will be used to indicate quantum mechanical operators. The spin-lattice terms, $\hat{V}$, may be written

$$\hat{V} = \sum_i \hat{U}_i \hat{T}_i \tag{3}$$

where the sum extends over all the interactions between the spins and the lattice. The set of operators, $\hat{T}_i$, associated with the spin system, is known in detail, but the exact form of the corresponding operators, $\hat{U}_i$, describing the liquid lattice is generally not known. However, it is often possible to model the effects of the lattice on the nuclear spins when it is desired to make measurements on the spins and not the lattice. If the Hamiltonian were known completely, it would be possible, at least in principle, to solve the time-dependent Schrödinger equation and to calculate the expectation value of any spin operator. Since this is normally not possible, one is obliged to employ simplifying approximations for $\hat{U}_i$ to make progress. Extensive details will be given in this review for the dipolar mechanism which often dominates the relaxation of spin $^1/_2$ nuclei and which has proven to be a rich source of structural and dynamical information. Under appropriate experimental conditions, the remaining spin–lattice interactions will be regarded as a composite external random field term. Canet[10] has provided detailed information on terms in $\hat{V}$ for several spin–lattice interactions.

2. The Equation of Motion—Basic Theory

In this section we will briefly outline the formalism required to proceed from the Hamiltonian (2) to an equation of motion that can be used to interpret experimental data. References are given to assist the reader desiring further details. The fundamental equation of motion for nuclear spins can be derived from the time-dependent Schrödinger equation:[22,69]

$$\frac{d\hat{\rho}}{dt} = -i\left[\hat{H}(t), \hat{\rho}(t)\right] \tag{4}$$

where $\hat{H}$ is the Hamiltonian given in (2) of the entire system (spins and lattice), and the density operator, $\hat{\rho}$, embodies all that can be known about the lattice and the ensemble of spins.

By using (2) the expanded equation of motion can be written as

$$\begin{aligned}\frac{d\hat{\rho}}{dt} &= -i\left[\hat{H}_l + \hat{H}_0 + \hat{H}_1(t) + \hat{V}, \hat{\rho}(t)\right] \\ &= -i\left\{\left[\hat{H}_l, \hat{\rho}(t)\right] + \left[\hat{H}_0, \hat{\rho}(t)\right] + \left[\hat{H}_1(t), \hat{\rho}(t)\right] + \left[\hat{V}, \hat{\rho}(t)\right]\right\}\end{aligned} \tag{5}$$

The first and second commutators produce rapid oscillations in the off diagonal elements of the density matrix (e.g., the precession of the magnetization due to $\mathbf{B}_0$) in a manner analogous to the classical Bloch equations given in (1). A unitary transformation may be defined as follows:

$$\hat{O}^{(r)}(t) = e^{i\left(\hat{H}_l + \hat{H}_0\right)t} \hat{O} e^{-i\left(\hat{H}_l + \hat{H}_0\right)t} \tag{6}$$

Equation 6 constitutes a transformation into an interaction representation. This is analogous to the rotating frame transformation used in the Bloch equations and reduces (5) to

$$\frac{d\hat{\rho}^{(r)}}{dt} = -i\left\{\left[\hat{H}_1^{(r)}(t), \hat{\rho}^{(r)}(t)\right] + \left[\hat{V}^{(r)}(t), \hat{\rho}^{(r)}(t)\right]\right\} \tag{7}$$

The formal solution of (7) in the absence of external

time-dependent fields is given by

$$\hat{\rho}^{(r)}(t) = \hat{\rho}^{(r)}(0) - i\int_0^t \mathrm{d}t' \left[\hat{V}^{(r)}(t'), \hat{\rho}^{(r)}(t')\right] \tag{8}$$

A first-order perturbation approximation allows one to substitute $\hat{\rho}^{(r)}(0)$ for $\hat{\rho}^{(r)}(t')$ in (8) to give

$$\hat{\rho}^{(r)}(t) \cong \hat{\rho}^{(r)}(0) - i\int_0^t \mathrm{d}t' \left[\hat{V}^{(r)}(t'), \hat{\rho}^{(r)}(0)\right] \tag{9}$$

Substitution of (9) back into (8) in a recursive manner provides the second-order perturbation solution to (7):

$$\begin{aligned}\hat{\rho}^{(r)}(t) \cong \hat{\rho}^{(r)}(0) &- i\int_0^t \mathrm{d}t' \left[\hat{V}^{(r)}(t'), \hat{\rho}^{(r)}(0)\right] \\ &- \int_0^t \mathrm{d}t' \int_0^{t'} \mathrm{d}t'' \left[\hat{V}^{(r)}(t'), \left[\hat{V}^{(r)}(t''), \hat{\rho}^{(r)}(0)\right]\right]\end{aligned} \tag{10}$$

The second term on the right is presumed to be zero since random fluctuations in relaxation are not expected to cause significant frequency shifts. Differentiating (10) gives

$$\frac{\mathrm{d}\hat{\rho}^{(r)}}{\mathrm{d}t} = -\int_0^t \mathrm{d}t' \left[\hat{V}^{(r)}(t), \left[\hat{V}^{(r)}(t'), \hat{\rho}^{(r)}(0)\right]\right] \tag{11}$$

Changing the variable to $t - t' = \tau$, resetting the initial time value from zero to t, and extending the upper limit of the integral to infinity allows one to write

$$\frac{\mathrm{d}\hat{\rho}^{(r)}}{\mathrm{d}t} = -\int_0^\infty \mathrm{d}\tau \left[\hat{V}^{(r)}(t), \left[\hat{V}^{(r)}(t-\tau), \hat{\rho}^{(r)}(t)\right]\right] \tag{12}$$

The justification for this step follows from the assumption that the fluctuations leading to relaxation are rapid compared with the evolution of the density operator. Thus, a time domain can be specified in which the value of the integrand falls to zero while the density operator only changes slightly from its initial value. These conditions normally obtain in nonviscous liquids where the fluctuating fields caused by molecular reorientation are in the nanosecond to picosecond range. In large macromolecules the reorientation rates are much slower and when they approach times comparable to the Larmor precession frequency these conditions may be violated. A reduced spin density operator, $\hat{\sigma}$, defined by performing a partial trace over the lattice degrees of freedom will simplify the above equations in $\hat{\rho}$, and is defined as follows:

$$\hat{\sigma}(t) = \mathrm{Tr}_l\{\hat{\rho}(t)\} \tag{13}$$

It should be apparent that the legitimacy of this operation depends on the separability of $\hat{\rho}$ into lattice and spin degrees of freedom. Using $\hat{\sigma}(t)$ from (13) the time-dependent expectation value, $\langle\hat{O}\rangle(t)$, of any spin operator, $\hat{O}$, corresponding to a measurable may be obtained from

$$\langle\hat{O}\rangle(t) = \mathrm{Tr}_s\{\hat{\sigma}(t)\hat{O}\} \tag{14}$$

3. The Redfield Formalism

By tracing over the lattice variables in (13) and collecting from (14) the expectation values of the various $\hat{V}(t)$ interaction terms, after a somewhat involved development,[4-7] (12) may be converted into the so-called Redfield equation

$$\frac{\mathrm{d}\sigma^{(r)}_{\kappa\kappa'}}{\mathrm{d}t} = \sum_{\lambda\lambda'} e^{+i(\kappa-\kappa'-\lambda+\lambda')t} R_{\kappa\kappa'\lambda\lambda'} \left[\sigma^{(r)}_{\lambda\lambda'}(t) - \sigma^{(r)}_{\lambda\lambda'}(\infty)\right] \tag{15}$$

In this form, (15) is given in terms of eigenstate matrix elements of the static spin Hamiltonian (i.e., κ and λ are eigenvalues as $\hat{H}_0|\kappa\rangle = \kappa|\kappa\rangle$). The matrix element of any general operator is, $\langle\kappa|\hat{O}|\lambda\rangle = O_{\kappa\lambda}$. Use of an eigenstate representation in (15) avoids the necessity of using super operators, and the secular approximation is explicitly embodied in the exponential term. Under the secular approximation the argument of the exponential term vanishes whereas the nonsecular or oscillating components have a non-zero exponential argument.

An expression, totally equivalent to (15), has been derived by Wang and Grant[23] using an irreducible spherical tensor basis and projection operator techniques. In this representation the secular approximations are preserved in the commutation properties of the angular momentum operators. The mathematical power of irreducible tensor bases is appreciable especially in the derivation of complex expressions, but the eigenstate representation is used in this review to accommodate nonspecialists more familiar with the traditional formulation. It is also common for practicing chemists to approach dynamical processes with an energy level representation where relaxation is characterized by transitional relaxation rate constants linking the eigenstates. Unfortunately, the presence of coherent rf fields is treated with considerably more difficulty in this historical eigenstate representation.

The time-dependent variations in the combined spin–lattice states are restricted to changes only in the spin-density matrix because of the overwhelming magnitude of the lattice heat capacity relative to that of the nuclear spins. Thus, the lattice may be presumed at all times to be in thermal equilibrium while the time-varying spin states, in the absence of a rf field, are driven to thermal equilibrium by the spin–lattice interactions. In a lattice at equilibrium the correlation of the temporal lattice fluctuations is independent of the origin of time making the various $R_{\kappa\kappa'\lambda\lambda'}$ constant over time. When the exponential argument $(\kappa - \kappa' - \lambda + \lambda')$ in (15) is significantly larger than the relaxation rate, the exponential term oscillates rapidly compared to the slow time evolution of the density matrix under relaxation thereby reducing the effective impact of these terms to zero. Under this so called secular approximation, many of the spin density matrix terms become irrelevant and the equations of motion are simplified accordingly. The exponential coefficients in front of $R_{\kappa\kappa\lambda\lambda}$ are clearly secular and may be identified with longitudinal transition probabilities between states κ and λ. These $R_{\kappa\kappa\lambda\lambda}$ parameters control the spin–lattice relaxation and are associated with the diagonal elements of the density matrix, $\sigma^{(r)}_{\kappa\kappa}(t)$, which specify the probability that the state κ is occupied.

In the eigenstate representation, Redfield terms of the form, $R_{\kappa\lambda\kappa\lambda}$, are associated with an exponential term that also is clearly secular, but these rates control the transverse or spin–spin relaxation processes. As long as the spectrum consists of clearly resolved transitions, all remaining $R_{\kappa\kappa'\lambda\lambda'}$ terms are associated with exponential coefficients that are nonsecular and may be omitted from consideration. Hence, for simple first

order spectra, secular arguments are able to uncouple the diagonal from the off-diagonal elements of the density matrix. Should two or more transitions overlap due to second order features in the spectrum, diagonal and off-diagonal elements in $\sigma_{\kappa\kappa'}$ may couple, and this case requires a more extensive mathematical analysis involving some of the fourth rank $R_{\kappa\kappa'\lambda\lambda'}$ terms. Highly second order spin systems generally have been neglected because of these secular problems in the mathematical analysis.

For spin systems containing two or more identical spins and consequently degenerate lines, it has been possible, at least for the simpler cases explored to date, to choose an eigenbasis that restricts to diagonal elements the type of Redfield terms required to account for longitudinal relaxation. Redfield terms that otherwise couple off-diagonal density matrix elements into the spin–lattice relaxation manifold, again become zero under the symmetry of the relevant eigenfunctions. Thus, in systems such as AX_2 and AX_3, spin–spin and spin–lattice relaxation processes may still be separated in the Redfield equation (15). Admittedly one may argue that this distinction is semantical as the elements of the so called off-diagonal Redfield terms associated with a spin product basis are subsumed into the new diagonal Redfield terms of the eigenstate representation.

The relaxation coefficient $R_{\kappa\kappa'\lambda\lambda'}$, involving the spin states κ, κ', λ, and λ', is given by

$$R_{\kappa\kappa'\lambda\lambda'} = K_{\kappa\lambda\kappa'\lambda'}(\omega_{\kappa\lambda}) + K_{\kappa\lambda\kappa'\lambda'}(\omega_{\kappa'\lambda'}) - \delta_{\kappa\lambda}\sum_{\gamma} K_{\gamma\kappa'\gamma\lambda'}(\omega_{\gamma\lambda'}) - \delta_{\kappa'\lambda'}\sum_{\gamma} K_{\gamma\lambda\gamma\kappa}(\omega_{\gamma\lambda}) \quad (16)$$

where the spectral density, $K_{\kappa\lambda\kappa'\lambda'}(\omega_{\kappa\lambda})$ is

$$K_{\kappa\lambda\kappa'\lambda'}(\omega_{\kappa\lambda}) = \int_0^\infty \mathrm{d}\tau\, V_{\kappa\lambda}(t) V_{\kappa'\lambda'}(t-\tau) e^{i\omega_{\kappa\lambda}\tau} \quad (17)$$

The $V_{\kappa\lambda}(t)$ are matrix elements in the eigenstate basis, and $\hat{V}(t)$ in the Hamiltonian may be expressed in spherical tensors to facilitate the dot product given in (3). Equation 18, equivalent to (3), expresses $\hat{V}(t)$ as a spherical tensor expansion:

$$\hat{V}(t) = \sum_{\mu}\sum_{l}\sum_{q=-l}^{l} (-1)^q U_{-q}^{(l)}(\mu,t)\hat{T}_q^{(l)}(\mu) \quad (18)$$

where the sum over μ spans all appropriate mechanisms, l and q are, respectively, the rank and projection indices associated with the spherical tensors representing a given mechanism. The $U_q^{(l)}(\mu,t)$ and $\hat{T}_q^{(l)}(\mu)$ are the spatial and spin tensors, respectively. The spin spectral density now becomes

$$K_{\kappa\lambda\kappa'\lambda'}(\omega_{\kappa\lambda}) = \sum_{\mu\mu'}\sum_{ll'}\sum_{qq'} (-1)^q T_{q,\kappa\lambda}^{(l)}(\mu) T_{q',\kappa'\lambda'}^{(l')}(\mu') J_{\kappa\lambda\kappa'\lambda'}^{\mu\mu' ll' qq'}(\omega_{\kappa\lambda}) \quad (19)$$

where the spatial power density is defined by

$$J_{\kappa\lambda\kappa'\lambda'}^{\mu\mu' ll' qq'}(\omega_{\kappa\lambda}) = \int_0^\infty (-1)^{q'} U_{-q,\kappa\lambda}^{(l)}(\mu,t) U_{q',\kappa'\lambda'}^{(l')}(\mu',t) e^{i\omega_{\kappa\lambda}\tau}\,\mathrm{d}\tau \quad (20)$$

It is apparent from (19) and (20) that power densities important in spin relaxation are of two general types; those with $\mu = \mu'$ giving an auto-correlation term in a single interaction μ and those with $\mu \neq \mu'$ requiring a cross-correlated or interference term in two different interactions. Section II.C treats the various types of interactions affecting relaxation.

When only longitudinal relaxation is considered the indices on the $R_{\kappa\kappa'\lambda\lambda'}$ are constrained by secular arguments and the important Redfield terms in the eigenstate representation are limited to the following types:

$$R_{\kappa\kappa\lambda\lambda} = 2K_{\kappa\lambda\kappa\lambda}(\omega_{\kappa\lambda})$$
$$R_{\kappa\kappa\kappa\kappa} = -\sum_{\gamma\neq\kappa} 2K_{\gamma\kappa\gamma\kappa}(\omega_{\gamma\kappa}) = -\sum_{\gamma\neq\kappa} R_{\gamma\gamma\kappa\kappa} \quad (21)$$

This greatly simplies the fourth-ranked expression given in (15), collapsing it to a second-rank equation to be discussed in section II.D.

C. Spectral Power Densities for Various Spin Interactions

1. General Comments on Important Spin Relaxation Mechanisms

The intramolecular dipole–dipole mechanism and a composite random field term encompassing several first-rank or pseudo-first-rank mechanisms are given below in sections II.C.2 and II.C.3, respectively. Canet[10] has presented a rather comprehensive treatment of a variety of other mechanisms, and we omit duplicating much of this detailed information.

An important second-rank relaxation interaction in the Hamiltonian arises from chemical shielding anisotropy (csa). The external magnetic field, $\mathbf{B}_0$, is chemically shielded by molecular electrons that reflect the electronic environment of the nucleus. These shielding fields depend on the orientation of the molecule with respect to $\mathbf{B}_0$, and the resulting anisotropy, if sufficiently large, can modulate with molecular tumbling the magnetic perturbations at the relaxing spin. This relaxation term becomes increasingly significant as NMR studies move to higher magnetic fields because the relaxation rate due to anisotropic shielding fields is proportional to the magnitude of $\mathbf{B}_0$ squared.[70] The nonlinear functionality of relaxation on $\mathbf{B}_0$ may be used to separate this contribution from that of the other relaxation mechanisms.[71,72]

The csa mechanism studied extensively by Farrar[21,43–46] may dominate, in its own right, the relaxation of nonproton-bearing nuclei, and these works on primarily phosphorus and fluorine nuclei offer seminal examples of such csa relaxation. More novel are the cross-correlated terms in coupled relaxation that become important when the csa interaction is comparable with the dipole–dipole mechanism.[21,47–54] The dipolar and csa mechanisms are both governed by the same molecular motion and have the same rotational correlation times. In general, cross terms between different interactions of the same rank will be effective when they conform to the same symmetry and have correlation times of comparable magnitudes. Interestingly, these interference terms destroy the inversion symmetry of the spin Hamiltonian[57] and can yield absolute signs of the scalar couplings that produce the multiplet structure. Workers will have to give increased attention to

csa–dipolar cross terms as higher magnetic fields are employed because favorable conditions will exist for such relaxation processes. Relaxation studies are one of the few ways to access the antisymmetric terms in the chemical shielding tensor.[73-75]

2. Intramolecular Dipole–Dipole Interactions

Each magnetic nucleus creates a magnetic field at other spin sites in a molecule, and the strength of these fields depends on the inverse cube of the distance between the interacting nuclei and the orientation of the internuclear vector relative to the external magnetic field. Thus, the fluctuating dipolar fields are modulated in time with molecular motion. By casting the rank two dipolar Hamiltonian in terms of irreducible spherical tensor operators, the full benefits of symmetry are achieved. By using (18) the dipole–dipole contribution to the Redfield terms is then given by

$$\hat{V}(dip,t) = \sum_{i<j} \sum_{q=-2}^{2} (-1)^q U_{-q}^{(2)}(ij,t) \hat{T}_q^{(2)}(ij) \tag{22}$$

where the first sum in i and j replaces the sum over μ in (18) and extends over all pairs of spins ij in the system. The sum in l is limited to $l = 2$ for the dipolar term and $q = -q'$ in order for the application of spin tensors to be nonvanishing. The normalized irreducible spin operators for the dipolar terms are given in standard angular momentum operator notation as follows:

$$\begin{aligned} \hat{T}_0^{(2)}(ij) &= \tfrac{1}{\sqrt{6}}\left(4\hat{I}_z^i\hat{I}_z^j - \hat{I}_+^i\hat{I}_-^j - \hat{I}_-^i\hat{I}_+^j\right) \\ \hat{T}_{\pm1}^{(2)}(ij) &= \mp\left(\hat{I}_\pm^i\hat{I}_z^j + \hat{I}_z^i\hat{I}_\pm^j\right) \\ \hat{T}_{\pm2}^{(2)}(ij) &= \hat{I}_\pm^i\hat{I}_\pm^j \end{aligned} \tag{23}$$

and the corresponding second-rank dipolar lattice functions for the qth projection are given by

$$U_q^{(2)}(ij,t) = -\xi_{ij} Y_q^{(2)}\left[\theta_{ij}(t),\phi_{ij}(t)\right] \tag{24}$$

Standard distances and constants are given by

$$\xi_{ij} = \sqrt{\frac{6\pi}{5}} \frac{\gamma_i\gamma_j\hbar}{r_{ij}^3} \tag{25}$$

where γ_i is the gyromagnetic ratio of the ith nucleus and r_{ij} is the i–j internuclear distance. The i and j labels designate the pair of interacting dipolar spins, and the normalized second rank spherical harmonics, $Y_q^{(2)}(\theta_{ij}(t), \phi_{ij}(t))$, specify the orientation of the internuclear vector in terms of the polar angles, θ and ϕ. To define the distances and angles, it is usually assumed that the part of the molecule bearing the coupled spins is rigid. While molecular vibrations alter internuclear distances, the frequencies involved are much higher than any of those associated with NMR and the vibrationally averaged $\langle r_{ij}^{-3}\rangle$ replaces r_{ij}^{-3}. Note, $\langle r_{ij}^{-3}\rangle$ is not $\langle r_{ij}\rangle^{-3}$.

Application of (19), (20), and (22), gives the dipole–dipole spectral densities as

$$\begin{aligned} K_{\kappa\lambda\kappa\lambda}(dip,\omega_{\kappa\lambda}) = &\sum_{i\neq j}\sum_{k\neq l}\sum_q (-1)^q \\ &\times \langle\kappa|\hat{T}_q^{(2)}(dip,ij)|\lambda\rangle\langle\lambda|\hat{T}_{-q}^{(2)}(dip,kl)|\kappa\rangle J_{ijkl}^q(\omega_{\kappa\lambda}) \end{aligned} \tag{26}$$

where $\omega_{\kappa\lambda}$ is the energy difference in frequency units between the κ and λ nuclear states and ij and kl represent pairs of interacting spins. The spatial dipolar power density is given by

$$J_{ijkl}^q(\omega_{\kappa\lambda}) = \xi_{ij}\xi_{kl}\int_0^\infty (-1)^q \left\langle Y_{-q}^{(2)}\left[\Omega_{ij}^{lab}(0)\right] Y_q^{(2)}\left[\Omega_{kl}^{lab}(t)\right]\right\rangle e^{i\omega_{\kappa\lambda}t}\,dt \tag{27}$$

where $Y_q^2[\Omega_{ij}^{lab}(t)]$ is the qth projection of the second-rank spherical harmonic. The angular function, $\Omega_{kl}^{lab}(t)$, is the corresponding polar angles $(\theta_{ij}^{lab}(t),\phi_{ij}^{lab}(t))$ for the r_{ij} dipole–dipole vector in the laboratory frame. Equation 27 is simplified considerably when the spatial order dies out rapidly before $e^{i\omega_\kappa t}$ changes. In this *extreme narrowing* limit, $\omega_{\kappa\lambda}t \approx 0$, and the integral in (27) is simplified greatly.

The presence of two independent sets of nuclear spins ij and kl indicates the importance of auto-correlated power densities when $ij = kl$, but also of cross-correlated dipolar terms when $ij \neq kl$. These cross dipole–dipole terms, contained in (19) and (20), introduce cross-correlated information directly into the relaxation power densities. As indicated above, the dipolar power densities become simpler when the extreme narrowing approximation obtains, i.e., $J_{ijkl}^q(\omega_{\kappa\lambda}) \cong J_{ijkl}^q(0)$, because (27) loses its dependence on $\omega_{\kappa\lambda}$. Furthermore, if the sample is not experiencing any preferential spatial ordering, the correlation function for different projections of $Y_q^2[\Omega_{ij}^{lab}(t)]$ are all the same (a condition that exists in an isotropically ordered liquid) and an additional simplification is realized. These two reductions in complexity allow contraction in notation for all values of q to give

two spin auto-correlation

$$J_{ijij}^q(\omega_{\kappa\lambda}) \cong J_{ijij}^o(0) \equiv J_{ij}$$

three spin cross-correlation

$$J_{ijjl}^q(\omega_{\kappa\lambda}) \cong J_{ijjl}^o(0) \equiv J_{ijl} \tag{28}$$

four spin cross-correlation

$$J_{ijkl}^q(\omega_{\kappa\lambda}) \cong J_{ijkl}^o(0) \equiv J_{ijkl}$$

Note, the two-spin auto-correlation term needs only two labels, while the three-spin cross term requires three indices. The nucleus that appears twice in the three-spin dipolar power density is placed at the middle index position in the simplified notation. The four-spin correlation term involves all four spins, and no compaction of spin notation is possible even though only the zero projection need be calculated for an isotropic fluid. It is obvious that the second-rank dipole–dipole interaction can only correlate a maximum of four coupled spins at least in the limit of second-order perturbation expressions.

Theoretical expressions for the dipolar spectral densities in anisotropic media such as liquid crystals have been presented for a number of simple coupled spin cases.[9,29-42,76] In these anisotropic media the correlation functions for the various projections of the spherical harmonic in (27) no longer equal one another and all of the projection terms in (27) must be retained in deriving expressions for the spectral densities. While relaxation in anisotropic media is not addressed further in this review, the references given here indicate these

studies are of considerable importance because anisotropic media remove some of the line degeneracies associated with symmetry thereby increasing the number of measurables in the spin system.

3. First-Rank, or Pseudo-First-Rank, Random Field Interactions

The composite first-rank, random field interaction energy for spin–lattice is given by

$$\hat{V}(rand,t) = \sum_i \sum_{q=-1}^{1} (-1)^q U_{-q}^{(1)}(i,t)\hat{T}_q^{(1)}(i) \tag{29}$$

where the normalized irreducible first-rank spin operators are

$$\hat{T}_0^{(1)}(i) = \sqrt{2}\hat{I}_z(i) \qquad \hat{T}_{\pm 1}^{(1)}(i) = \mp \hat{I}_{\pm}(i) \tag{30}$$

and the generalized first-rank spatial tensor at nucleus i is

$$U_q^{(1)}(i) = \gamma_i \sum_{\mu} B_q^{(1)}(\mu,i,t) \tag{31}$$

The time-dependent $B_q^{(1)}(\mu,i,t)$ is the qth component (in the spherical basis) of any fluctuating field from the μth interaction at the position of nucleus i. $B_q^{(1)}(\mu,i,t)$ in Cartesian form is given by

$$\begin{aligned} B_0^{(1)}(\mu,i,t) &= \frac{1}{\sqrt{2}} B_z(\mu,i,t) \\ B_{\pm 1}^{(1)}(\mu,i,t) &= \mp \frac{1}{2}\left\{B_x(\mu,i,t) \pm i\, B_y(\mu,i,t)\right\} \end{aligned} \tag{32}$$

By applying the irreducible interaction terms in (29) through (32) in (19) and (20), the random field spectral density becomes

$$K_{\kappa\lambda\kappa\lambda}(rand,\omega_{\kappa\lambda}) = \sum_q (-1)^q \langle \kappa|\hat{T}_q^{(1)}(i)|\lambda\rangle\langle\lambda|\hat{T}_{-q}^{(1)}(j)|\kappa\rangle j_{ij}^q(\omega_{\kappa\lambda}) \tag{33}$$

with

$$j_{ij}^q(\omega_{\kappa\lambda}) = \gamma_i\gamma_j \int_0^{\infty} (-1)^q \sum_{\mu,\mu'} \left[B_{-q}^{(1)}(\mu,i,0)B_q^{(1)}(\mu',j,t)\right] e^{i\omega_{\kappa\lambda}t}\, dt \tag{34}$$

The literature includes a variety of definitions for the random field power density that differ from (33) and (34) usually by factors of 2. These definitional diversities arise from the use of unnormalized $T_q^{(k)}$ and from integral limits in (34) of $-\infty$ to $+\infty$. Again, it is convenient to use a simpler compacted notation for these random field terms as follows:

single spin auto-correlation

$$j_{ii}^q(\omega_{\kappa\lambda}) \cong j_{ii}^0(0) \equiv j_i$$

two spin cross-correlation

$$j_{ij}^q(\omega_{\kappa\lambda}) \cong j_{ij}^0(0) \equiv j_{ij} \tag{35}$$

Note, two different types of cross terms exist in (34). There are the single $i = j$ and dual $i \neq j$ nuclear spin correlations given in (35), but one may also have auto and cross mechanistic correlations when $\mu = \mu'$ and $\mu \neq \mu'$, respectively. This latter type of cross mechanistic power density is possible in both j_i and j_{ij}.

Expressions for a variety of B_q are available for different interactions,[10] but it is often convenient in the absence of detailed information on these several terms to combine the various random field interactions into the composite single and cross nuclear correlation terms given in (35). These different interactions have varying impact on the relaxation of coupled nuclei but are not always easily identified and separated one from another. The fitting of relaxation data usually requires consideration of such terms to allow the better understood dipole–dipole terms to be extracted. The random terms[61,67,77–81] include the following: some intermolecular dipole–dipole interactions modulated by not only rotational but also translational diffusion,[82–84] spin–rotation interactions,[61,85–88] scalar coupling of the first and second kind,[70] free electron and paramagnetic impurities such as oxygen,[89] etc. All of these types of interactions are assumed to transform under the symmetry of first-rank tensors in accordance with (31) and (32), but to be completely precise some of the interactions should be considered as only *pseudo*-first-rank random field terms. It needs to be recognized that random field terms, of any rank, may affect the density matrix of the designated spin subsystem as first rank projections, and therefore may be included in the class of power densities discussed in this section. Interference between all the various random field interactions potentially may exist, but fortunately the various mechanisms often have very different correlation times and therefore do not form compatible mechanistic cross terms.

When the random field assumption breaks down special attention must be given to the explicit effect of the offending mechanism on the relaxation process. Intermolecular dipole–dipole interactions modeled as random field terms likely present the greatest hazard to the random field assumption. They often do not behave as even pseudo-first-order terms, if the motion of the perturbing intermolecular dipole is highly correlated to that of the spin system under study. Of course, if the spin system under study is not sufficiently dilute in the liquid lattice, the assumption of isolated spin systems breaks down, and equations upon which the analysis of relaxation data is based may not be valid. The early work of Khazanovich and Zitsermann[90] and of Simon and Vold[91] on the relative importance of inter- and intramolecular dipole–dipole relaxation illustrates the situation where a more complete relaxation treatment is needed. Spin relaxation in dilute solutions using aprotic solvents has been the typical way to avoid serious intermolecular dipolar interferences between intermolecular protons. Thus, those employing random field simplifications should do so with some care as it is essential that one always investigate the possibility of fatal errors being introduced into the analysis.

D. Symmetry Mode Analysis of Spin–Lattice Relaxation

As noted in (21) in section II.B only a limited number of Redfield terms are significant when longitudinal relaxation is considered in the eigenstate representation. In addition, the indices on the density matrix are also collapsed to include only the diagonal elements that give the state populations, i.e., $\sigma_{\lambda\lambda} = N_\lambda$. In this form,

the Redfield terms may be considered to be simple transition probabilities, i.e., $R_{\kappa\kappa\lambda\lambda} = W_{\kappa\lambda}$, linking the populations of the various spin eigenstates. Under these conditions, (15) and (21) yield a set of differential equations for tracking changes in the various state populations as follows:

$$\frac{dN_\kappa}{dt} = \sum_\lambda W_{\kappa\lambda}[N_\lambda - N_\lambda(\infty)] \tag{36}$$

where N_κ spans (κ = 1 to 2^n) all eigenstate populations. Writing (36) in matrix notation gives

$$\frac{d\mathbf{N}}{dt} = \mathbf{W}[\mathbf{N} - \mathbf{N}(\infty)] \tag{37}$$

In a two-spin AX system, four spin eigenstates exist and a four by four **W** transition matrix is obtained from this Redfield formalism. For an AX_2 spin system, eight eigenstates produce an eight by eight **W** transition matrix, and larger coupled spin systems require correspondingly larger transition matrices which scale as 2^n when n is the number of coupled spins. In each case **W** is the special Redfield matrix given by (16) and (21) for longitudinal relaxation.

In high-resolution multiplet NMR experiments, not only the total magnetization of each nuclear spin but also the intensity of each multiplet line is measurable as a function of time. These line intensities, $L_{\kappa\lambda}$, become the relaxation *measurables* for monitoring time changes in the spin states and are proportional to $\Delta N_{\kappa\lambda} = (N_\kappa - N_\lambda)$. By transforming (37) into appropriate linear combinations of N_κ, the equations of motion are cast into measurable NMR variables. Use of inversion symmetry, normally present in the Hamiltonian,[8,62-66] allows the size of the transition matrices to be subdivided accordingly. These approrpriately selected linear combinations of spin-state populations, corresponding to measurable NMR line intensities, specify a set of dynamical variables or magnetization modes, υ, of the system as follows:

$$\upsilon_\kappa = \sum_\lambda a_{\kappa\lambda} N_\lambda \quad \text{or} \quad \boldsymbol{\upsilon} = \mathbf{T}\cdot\mathbf{N} \tag{38}$$

where $T_{\kappa\lambda} = a_{\kappa\lambda}$.

Applying the transformations given by (38) in (37) yields

$$\frac{d\boldsymbol{\upsilon}}{dt} = \boldsymbol{\Gamma}[\boldsymbol{\upsilon} - \boldsymbol{\upsilon}(\infty)] \tag{39}$$

where $\boldsymbol{\Gamma} = \mathbf{TWT}^{-1}$ becomes the relaxation matrix in a given magnetization mode basis, and $\upsilon(\infty)$ is the magnetization mode vector of equilibrium values. If the inversion symmetry of the Hamiltonian is preserved in **T**, the coupled differential equations in the measurable magnetization modes reduce in complexity as the Γ matrix is factored into symmetrical and antisymmetrical parts of equal size. To be precise the inversion symmetry exchanges the frequencies of symmetry related lines that vary from one another by only an infinitesimal difference in their corresponding Boltzmann factors. The permutations of such line assignments, therefore, can not be recognized from intensity measurements in the experimental spectrum. Construction of these various magnetization mode vectors, υ, then reflects the symmetry under spin inversion and factors the appropriate transition matrix into two components.

The completely symmetric linear combinations of state populations always include the combination, $\upsilon_T = \sum_\kappa N_\kappa$, representing the total spin population. This magnetization variable will remain invariant (i.e., $d\upsilon_T/dt = 0$) with time due to the conservation of nuclear particles in a closed system. The effect of spin conservation is to reduce by one the number of differential equations in the symmetric manifold. Illustrations of the use of inversion symmetry and its consequence will be discussed in more detail in section III where specific individual cases are considered.

III. Symmetry Equations for Simple Spin Systems

The complexity of the spin–lattice equations of motion may be appreciable even for fairly simple spin systems. As indicated above, there are 2^n coupled equations for n spin $^1/_2$ nuclei but considerable simplification can be achieved with the inversion symmetry discussed in section II.D. These manageable calculations can be used to extract the values of the corresponding spectral densities from the experimental data. We treat in detail the AX spin case, because of its relative simplicity, as a way to illustrate the recipe for setting up the coupled differential equations. The more complex AX_2 spin case, a principal emphasis in this review, is then treated with matrix methods to provide mathematical expressions for this useful and commonly encountered coupled spin system. The reader is referred to important discussions of AB,[92] A_3,[93-95] homonuclear AX_2,[96-99] AX_3,[52,100-102] ABX,[103,104] AMX,[105-108] and AMX_2[49] cases given elsewhere in considerable detail.

A. The AX Spin System

1. The Equations of Motion and the Relaxation Matrix

The coupled AX two-spin system may be discussed in terms of lines L_1 and L_2 in the spectral region of the A spin and of L_3 and L_4 in the X spin region (see Figure 2). The interlevel transition probabilities are given by the W rates with the $\kappa\lambda$ designation indicated by the nuclear species A or X and by the net change in spin quantum number specified in Figure 2. With these definitions[65] a set of coupled differential equations for the AX spin system is obtained as follows:

$$\frac{d}{dt}\begin{pmatrix} N_1 \\ N_2 \\ N_3 \\ N_4 \end{pmatrix} = \begin{pmatrix} -W_a & W_{1A} & W_{1X} & W_2 \\ W_{1A} & -W_b & W_0 & W_{1X} \\ W_{1X} & W_0 & -W_b & W_{1A} \\ W_2 & W_{1X} & W_{1A} & -W_a \end{pmatrix}\begin{pmatrix} N_1 - N_1(\infty) \\ N_2 - N_2(\infty) \\ N_3 - N_3(\infty) \\ N_4 - N_4(\infty) \end{pmatrix} \tag{40}$$

where (21) defines the diagonal elements as

$$\begin{aligned} W_a &= W_{1A} + W_{1X} + W_2 \\ W_b &= W_{1A} + W_{1X} + W_0 \end{aligned} \tag{41}$$

Appropriate linear combinations of L_i specify the multiplet magnetization modes and capitalize on the

inversion symmetry property of the spin system to give

$$\upsilon_A = N_1 - N_2 + N_3 - N_4 = (L_1 + L_2)/k_A = 2\,\mathrm{tr}\left[\hat{T}_0^{(1)}(A)\hat{T}_0^{(0)}(X)\hat{\sigma}\right] = 2\,\mathrm{tr}\left[\hat{I}_z(A)\hat{\sigma}\right] \quad (42a)$$

$$\upsilon_X = N_1 + N_2 - N_3 - N_4 = (L_3 + L_4)/k_X = 2\,\mathrm{tr}\left[\hat{T}_0^{(0)}(A)\hat{T}_0^{(1)}(X)\hat{\sigma}\right] = 2\,\mathrm{tr}\left[\hat{I}_z(X)\hat{\sigma}\right] \quad (42b)$$

$$\upsilon_\Delta = N_1 - N_2 - N_3 + N_4 = (L_1 - L_2)/k_A = (L_3 - L_4)/k_X = 2\,\mathrm{tr}\left[\hat{T}_0^{(1)}(A)\hat{T}_0^{(1)}(X)\hat{\sigma}\right] = 4\,\mathrm{tr}\left[\hat{I}_z(A)\hat{I}_z(X)\hat{\sigma}\right] \quad (42c)$$

$$\upsilon_T = N_1 + N_2 + N_3 + N_4 = 2\,\mathrm{tr}\left[\hat{T}_0^{(0)}(A)\hat{T}_0^{(0)}(X)\hat{\sigma}\right] = \mathrm{tr}\left[\hat{E}\hat{\sigma}\right] \quad (42d)$$

This equation defines the magnetization modes in terms of the measurables of the system, L_i, and the state populations of the system, N_κ. The N_κ eigenstate representation also provides a conceptual link between the irreducible spherical tensor operators[23] and the experimentally defined modes in line intensities. The normalized irreducible tensor operators for two coupled heteronuclear AX spins are $\hat{T}_0^{(0)}(A) = \hat{T}_0^{(0)}(X) = \hat{E}/\sqrt{2}$, $\hat{T}_0^{(1)}(A) = \sqrt{2}\hat{I}_z(A)$ and $\hat{T}_0^{(1)}(X) = \sqrt{2}\hat{I}_z(X)$. Also given in (42) are the expressions for the various magnetization modes in terms of standard $\hat{I}_z(i)$ spin operators and the identity operator, $\hat{E}$.

Multiplet magnetization modes have the following meanings. The total number of spins is υ_T. The z magnetization measured for either the A or X spins becomes υ_A or υ_X, respectively. Finally, a multiplet difference mode, $\upsilon_{i\Delta}$, may be recognized in either the A or X spectrum as the difference between either the A or X doublets, respectively. These magnetizations modes each have quantum mechanic operators that may be evaluated in any representation by tracing with the spin-density matrix the appropriate zero projection angular momentum operator indicated in (42). The coefficients in front of the traces of (42) bring the operators into correspondence with the measurables of the system. The k_i scaling factors in (42) depend on spectrometer parameters and carry no molecular significance. They are essential in the fitting program, however, as a way to adjust for instrumental variations between experiments (see section V.B.1).

The transformation given by (42) may be put in matrix form, **T**, as follows

$$\mathbf{T} = \begin{pmatrix} +1 & -1 & +1 & -1 \\ +1 & +1 & -1 & -1 \\ +1 & -1 & -1 & +1 \\ +1 & +1 & +1 & +1 \end{pmatrix} \quad \mathbf{T}^{-1} = \tfrac{1}{4}\begin{pmatrix} +1 & +1 & +1 & +1 \\ -1 & +1 & -1 & +1 \\ +1 & -1 & -1 & +1 \\ -1 & -1 & +1 & +1 \end{pmatrix} \quad (43)$$

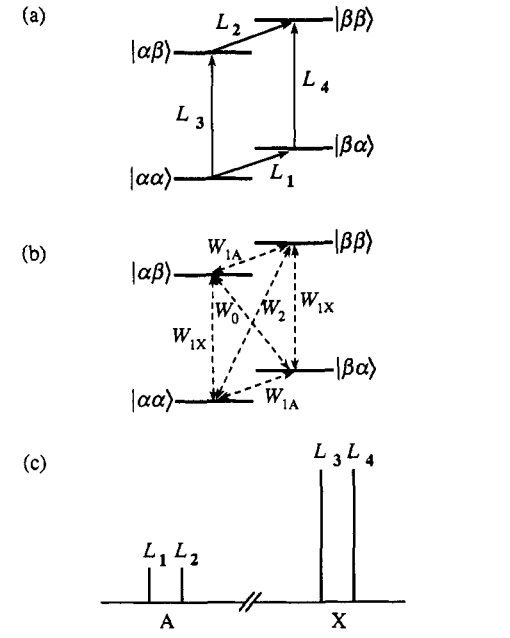

Figure 2. For a ^{13}CH (AX) spin system, part a shows the energy level diagram labeled by the eigenstates of the static Hamiltonian, $\hat{H}_0$. (The first label gives the state of the carbon spin and the second that of the proton.) The L_i indicate the allowed (i.e., single quantum) transitions that appear similarly labeled in the schematic spectrum (c). The interlevel relaxation rates are shown in part b. Note that W_0 and W_2 correspond to zero and two quantum processes, respectively, and produce relaxation between levels where no allowed transitions producing spectral lines exist.

to be used in converting (40) into simultaneous equations of the type specified by (39) as follows:

$$\frac{d}{dt}\begin{bmatrix} \upsilon_A \\ \upsilon_X \\ \upsilon_\Delta \\ \upsilon_T \end{bmatrix} = -\begin{bmatrix} \begin{pmatrix} \rho_A & \sigma \\ \sigma & \rho_X \end{pmatrix} & 0 & 0 \\ 0 & 0 & \mu & 0 \\ 0 & 0 & 0 & 0 \end{bmatrix}\begin{bmatrix} \upsilon_A - \upsilon_A(\infty) \\ \upsilon_X - \upsilon_X(\infty) \\ \upsilon_\Delta - \upsilon_\Delta(\infty) \\ \upsilon_T - \upsilon_T(\infty) \end{bmatrix} \quad (44)$$

where the magnetization mode relaxation matrix, $\mathbf{\Gamma} = \mathbf{TWT}^{-1}$, given explicitly in (44) has been partially block diagonalized. The value for $\upsilon_\Delta(\infty)$ is zero. Thus, the four coupled differential equations have been condensed into two coupled equations in υ_A and υ_X and single differential equations in υ_Δ and υ_T as follows:

$$\frac{d\upsilon_A}{dt} = -\rho_A[\upsilon_A - \upsilon_A(\infty)] - \sigma[\upsilon_X - \upsilon_X(\infty)]$$
$$\frac{d\upsilon_X}{dt} = -\sigma[\upsilon_A - \upsilon_A(\infty)] - \rho_X[\upsilon_X - \upsilon_X(\infty)] \quad (45)$$

$$\frac{d\upsilon_\Delta}{dt} = -\mu\upsilon_\Delta \quad (46)$$

$$\frac{d\upsilon_T}{dt} = 0 \quad (47)$$

Equation 47 specifies the conservation of spins and therefore does not couple with the remaining equations. The composite relaxation parameters are related to the interlevel transition probabilities and given by

$$\rho_A = \tfrac{1}{T_{1A}} = W_2 + 2W_{1A} + W_0$$
$$\rho_X = \tfrac{1}{T_{1X}} = W_2 + 2W_{1X} + W_0$$
$$\sigma = \tfrac{1}{T_{1AX}} = W_2 - W_0$$
$$\mu = \tfrac{1}{T_{1\Delta}} = 2(W_{1A} + W_{1X}) \quad (48)$$

where the T_{1A} and T_{1X} designations refer to A and X relaxation times, respectively, and T_{1AX} is a cross relaxation time. The T_{1AX} relaxation parameter is referred to as the cross relaxation time, not to be confused with cross relaxation power densities, as it couples the υ_A and υ_X modes. These quantities govern the coupled differential equations in (45) first derived by Solomon.[109]

In (48) the $T_{1\Delta}$ parameter is a relaxation time associated with the multiplet difference magnetization and was discussed by Shimizu and Fujiwara[110] and by Mackor and MacLean.[56,111,112] More recent literautre is also helpful.[65,113] While (45) requires a double exponential general solution, (46) has a single exponential solution in the $T_{1\Delta}$ relaxation time.

When relaxation due to anisotropy of chemical shielding is comparable to the dipole–dipole mechanism, (19) allows for the possibility of correlated terms between the two mechanisms. For the AX case this correlation is manifest in nonvanishing Γ matrix elements connecting the υ_Δ in the symmetric manifold to υ_A and υ_X in the antisymmetric manifold. Thus, this coupling of the symmetric and antisymmetric modes invalidates the assumption of inversion symmetry in the spin Hamiltonian. This results in the observation that, for a system prepared in a state with only the antisymmetric modes populated, magnetization may be seen to flow into the symmetric modes. Indeed, this has been observed in a number of systems.[21,44,47,48,50,53,55,114]

Working with (26) through (28) and (33) through (35) provides the following relationships linking the terms in **W** to the following dipolar and random field power densities:

$$\begin{aligned} W_0 &= K^{(0)}_{AX}(dip,\omega_X-\omega_A) && \cong \tfrac{1}{3}J_{AX} \\ W_2 &= K^{(2)}_{AX}(dip,\omega_X+\omega_A) && \cong 2J_{AX} \\ W_{1A} &= K^{(1)}_{AX}(dip,\omega_A)+K_A(rand,\omega_A) && \cong \tfrac{1}{2}J_{AX}+2j_A \\ W_{1X} &= K^{(1)}_{AX}(dip,\omega_X)+K_X(rand,\omega_X) && \cong \tfrac{1}{2}J_{AX}+2j_X \end{aligned} \tag{49}$$

The extreme narrowing dipolar and random field power densities given in (49) may be related to the symmetry transition parameters as follows:

$$\begin{aligned} \rho_A &= 2J^{(2)}_{AX}(\omega_X+\omega_A)+J^{(1)}_{AX}(\omega_A)+\tfrac{1}{3}J^{(0)}_{AX}(\omega_X-\omega_A) \\ &\quad +4j^{(1)}_A(\omega_A) \\ &\cong \tfrac{10}{3}J_{AX}+4j_A \\ \rho_X &= 2J^{(2)}_{AX}(\omega_X+\omega_A)+J^{(1)}_{AX}(\omega_X)+\tfrac{1}{3}J^{(0)}_{AX}(\omega_X-\omega_A) \\ &\quad +4j^{(1)}_X(\omega_X) \\ &\cong \tfrac{10}{3}J_{AX}+4j_X \\ \sigma &= 2J^{(2)}_{AX}(\omega_X+\omega_A)-\tfrac{1}{3}J^{(0)}_{AX}(\omega_X-\omega_A) \\ &\cong \tfrac{5}{3}J_{AX} \\ \mu &= J^{(1)}_{AX}(\omega_A)+J^{(1)}_{AX}(\omega_X)+4j^{(1)}_A(\omega_A)+4j^{(1)}_X(\omega_X) \\ &\cong 2J_{AX}+4j_A+4j_X \end{aligned} \tag{50}$$

Both the general and extreme narrowing limits for the symmetry relaxation parameters are given in (50).

2. Nuclear Overhauser Enhancement

The Solomon equation given in (45) also describes the very important nuclear Overhauser enhancement (NOE) experiment where A is observed while decoupling X. An extensive literature through 1971 on this valuable experiment is given in the comprehensive book by Noggle and Schirmer[115] along with a theoretical treatment of the effect. In the classical AX treatment of NOE, υ_X is locked to zero under a strong saturating rf field and (45) becomes

$$\begin{aligned} \frac{d\upsilon_A}{dt} &= -\rho_A[\upsilon_A-\upsilon_A(\infty)]+\sigma\upsilon_X(\infty) \\ &= -\rho_A\left[\upsilon_A-\left(1+\eta_{A\{X\}}\right)\upsilon_A(\infty)\right] \end{aligned} \tag{51}$$

with

$$\eta_{A\{X\}} = \frac{\sigma\upsilon_X(\infty)}{\rho_A\upsilon_A(\infty)} = \frac{\sigma\gamma_X}{\rho_A\gamma_A} \tag{52}$$

Equation 51 has a single exponential solution with a characteristic relaxation rate, $\rho_A = 1/T_{1A}$, and its steady state solution (i.e., $d\upsilon_A/dt = 0$) gives the following for υ_A^{ss}:

$$\frac{\upsilon_A^{ss}}{\upsilon_A(\infty)} = \left(1+\eta_{A\{X\}}\right) = \text{NOE} \tag{53}$$

The explicit dependence of the NOE upon the dipolar and random field power densities is obtained from (50), (52), and (53) as

$$\begin{aligned} \eta_{A\{X\}} &= \left(\frac{\gamma_X}{\gamma_A}\right) \\ &\quad \frac{2J^{(2)}_{AX}(\omega_X+\omega_A)-\frac{1}{3}J^{(0)}_{AX}(\omega_X-\omega_A)}{2J^{(2)}_{AX}(\omega_X+\omega_A)+J^{(1)}_{AX}(\omega_A)+\frac{1}{3}J^{(0)}_{AX}(\omega_X-\omega_A)+4j^{(1)}_A(\omega_A)} \\ &\cong \left(\frac{\gamma_X}{\gamma_A}\right)\frac{5J_{AX}}{10J_{AX}+12j_A} \end{aligned} \tag{54}$$

Thus, $\eta_{A\{X\}} = \gamma_X/2\gamma_A$ in the limit where $J_{AX} \gg j_A$, but $\eta_{A\{X\}} = 0$ if $j_A \gg J_{AX}$.

B. The AX_2 Spin System

Equations of motion for the AX_2 spin system have appeared in numerous places that treat the Γ transition matrix in a number of different ways.[10,30,64,66,82,100,101,116] The diversity in these treatments reflects evolving concepts on how to maximize the magnetization mode definitions, and at other times have reflected an attempt to provide a type of normalization that leaves the Γ matrix symmetrical. When the equation of motion is expressed in modes that are traces of normalized irreducible operators a symmetrical Γ matrix is obtained, but attempts to keep the modes in a one to one correspondence with normalized irreducible spherical operators defeat the purpose of finding operators that will describe a given set of measurables. The merits of using orthonormal sets of operators to derive the equation of motion in an operator basis are obvious to all familiar with these developments. However, having derived the equations, simple transformations into an optimal mode set are then required if the equations are to reflect directly the experimental quantities. Or-

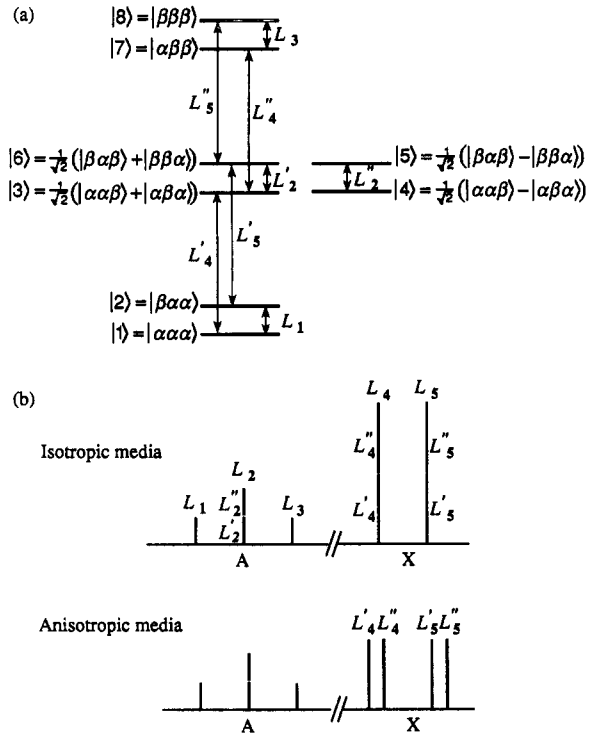

Figure 3. For a $^{13}CH_2$ (AX_2) spin system, part a shows the energy level diagram labeled by the eigenstates of the static Hamiltonian, $\hat{H}_0$. (The first label gives the state of the carbon spin and the second and third that of the two identical protons.) The L_i indicate the allowed (i.e., single quantum) transitions that appear similarly labeled in the schematic spectrum (b). Note that in an isotropic fluid L_2, L_4, and L_5 are each composed of two transitions having the same frequency, but in an anisotropic medium (e.g., a nematic liquid crystal) a doublet of doublets appears and each of the four transitions composing L_4 and L_5 is resolved.

thogonality arguments cease to be of any great relevance if they create problems in the fitting procedures (i.e., give unequal statistical weight to otherwise equivalent measurements). Thus, we conform to only two requirements. First, the maximum number of measurables must appear within the mode set, and, second, we continue to employ the inversion symmetry, when appropriate, of the Hamiltonian to achieve the greatest amount of factoring in Γ. There is no importance in maintaining a symmetrical Γ matrix if it compromises one of these requirements.

Should the fitting be done in a mode set that weights the various line intensities or boundary conditions in a biased way, the statistical assessment of the data analysis will be distorted as the independent experimental measurements should be given equal weight. Some of the mode sets in the literature have given more consideration to normalization conditions than to the numerical fitting methods required to extract the relaxation parameters. When a degree of arbitrariness exists in the choice of any specific mode, then we select modes that are orthogonal to the required set and most closely related to one of the irreducible spherical tensor operators.[23] With availability of data on molecules in anisotropic media, came the recognition that the AX_2 case can provide up to six independent measurables when the X doublet breaks into a quartet in the presence of non-zero dipolar couplings.[30] Partially oriented molecules dissolved in anisotropic media exhibit XX dipolar couplings that change the appearance of the X spectrum accordingly (see Figure 3). Spin inversion in the AX_2 spin system, when not destroyed by interference terms, again factors the relaxation matrix into four by four antisymmetric and three by three symmetric matrices.

In this review we have selected AX_2 magnetization modes that are very similar to those of Werbelow et al.[30] These modes are directly defined with experimental line intensities thereby maintaining the intuitive physical interpretations that may be ascribed to each mode. Six of the seven selected modes correspond to the six potentially available measurables. The AX_2 set is given as follows:

$$\begin{aligned}
{}^a\upsilon_A &= \tfrac{1}{k_A}(L_1 + L_2 + L_3) \\
&= N_1 - N_2 + N_3 + N_4 - N_5 - N_6 + N_7 - N_8 \\
{}^a\upsilon_X &= \tfrac{1}{k_X}(L_4 + L_5) \\
&= N_1 + N_2 - N_7 - N_8 \\
{}^a\upsilon_{+-+} &= \tfrac{1}{k_A}(L_1 - L_2 + L_3) \\
&= N_1 - N_2 - N_3 - N_4 + N_5 + N_6 + N_7 - N_8 \\
{}^a\upsilon_{\pm\mp} &= \tfrac{1}{k_X}(L'_4 - L''_4 - L'_5 + L''_5) \\
&= N_1 - N_2 - 2N_3 + 2N_6 + N_7 - N_8
\end{aligned} \tag{55a}$$

$$\begin{aligned}
{}^s\upsilon_{+o-} &= \tfrac{1}{k_A}(L_1 - L_3) = \tfrac{1}{k_X}(L_4 - L_5) \\
&= N_1 - N_2 - N_7 + N_8 \\
{}^s\upsilon_{\pm\pm} &= \tfrac{1}{k_X}(L'_4 - L''_4 + L'_5 - L''_5) \\
&= N_1 + N_2 - 2N_3 - 2N_6 + N_7 + N_8 \\
{}^s\upsilon_{t-3s} &= (N_{\text{triplet}} - 3N_{\text{singlet}}) \\
&= N_1 + N_2 + N_3 - 3N_4 - 3N_5 + N_6 + N_7 + N_8 \\
{}^s\upsilon_T &= N_{\text{total}} \\
&= N_1 + N_2 + N_3 + N_4 + N_5 + N_6 + N_7 + N_8
\end{aligned} \tag{55b}$$

where the lines, L_i, are given in Figure 3 in terms of the energy level diagram for AX_2. This figure also designates the corresponding labels for the eigenstate populations, N_i, used in (55). The k_A and k_X scaling parameters were discussed above for the AX case and retain their same meanings.

The standard set of zero projection irreducible tensor operators for the AX_2 case may be formed[23] from the direct products of the corresponding irreducible tensor operators for the A spin as

$$\hat{T}_0^{(0)}(A) = \hat{E}/\sqrt{2}$$
$$\hat{T}_0^{(1)}(A) = \sqrt{2}\,\hat{I}_z(A)$$

and for the degenerate X spins as

$$\hat{T}_{0E}^{(0)}(X_2) = \hat{E}/2$$
$$\hat{T}_{0X}^{(0)}(X_2) = 2\hat{\mathbf{I}}(X)\cdot\hat{\mathbf{I}}(X')/\sqrt{3}$$
$$\hat{T}_0^{(1)}(X_2) = \{\hat{I}_z(X) + \hat{I}_z(X')\}/\sqrt{2}$$
$$\hat{T}_0^{(2)}(X_2) = \sqrt{2}\{3\hat{I}_z(X)\hat{I}_z(X') - \hat{\mathbf{I}}(X)\cdot\hat{\mathbf{I}}(X')\}/\sqrt{3}$$

These direct products form a natural set of quantum

mechanical operators that define the magnetization modes as follows:

$$
\begin{aligned}
{}^{a}\upsilon_A &= \sqrt{8}\,\mathrm{tr}\left[\hat{T}_0^{(1)}(A)\hat{T}_{0E}^{(0)}(X_2)\,\hat{\sigma}\right] \\
&= 2\,\mathrm{tr}\left[\hat{I}_z(A)\,\hat{\sigma}\right] \\
{}^{a}\upsilon_X &= 2\,\mathrm{tr}\left[\hat{T}_0^{(0)}(A)\hat{T}_0^{(1)}(X_2)\,\hat{\sigma}\right] \\
&= \mathrm{tr}\left[\left\{\hat{I}_z(X)+\hat{I}_z(X')\right\}\hat{\sigma}\right] \qquad (56a) \\
{}^{a}\upsilon_{+-+} &= \tfrac{4}{\sqrt{3}}\,\mathrm{tr}\left[\hat{T}_0^{(1)}(A)\left\{\hat{T}_0^{(2)}(X_2)+\tfrac{1}{\sqrt{2}}\hat{T}_{0X}^{(0)}(X_2)\right\}\hat{\sigma}\right] \\
&= 8\,\mathrm{tr}\left[\hat{I}_z(A)\hat{I}_z(X)\hat{I}_z(X')\,\hat{\sigma}\right] \\
{}^{a}\upsilon_{\pm\mp} &= 2\sqrt{3}\,\mathrm{tr}\left[\hat{T}_0^{(1)}(A)\hat{T}_0^{(2)}(X_2)\,\hat{\sigma}\right] \\
&= 4\,\mathrm{tr}\left[\hat{I}_z(A)\left\{3\hat{I}_z(X)\hat{I}_z(X')-\hat{\mathbf{I}}(X)\cdot\hat{\mathbf{I}}(X')\right\}\hat{\sigma}\right]
\end{aligned}
$$

$$
\begin{aligned}
{}^{s}\upsilon_{+o-} &= 2\,\mathrm{tr}\left[\hat{T}_0^{(1)}(A)\hat{T}_0^{(1)}(X_2)\,\hat{\sigma}\right] \\
&= 2\,\mathrm{tr}\left[\hat{I}_z(A)\left\{\hat{I}_z(X)+\hat{I}_z(X')\right\}\hat{\sigma}\right] \\
{}^{s}\upsilon_{\pm\pm} &= 2\sqrt{3}\,\mathrm{tr}\left[\hat{T}_0^{(0)}(A)\hat{T}_0^{(2)}(X_2)\,\hat{\sigma}\right] \\
&= 2\,\mathrm{tr}\left[\left\{3\hat{I}_z(X)\hat{I}_z(X')-\hat{\mathbf{I}}(X)\cdot\hat{\mathbf{I}}(X')\right\}\hat{\sigma}\right] \qquad (56b) \\
{}^{s}\upsilon_{t-3s} &= 2\sqrt{6}\,\mathrm{tr}\left[\hat{T}_0^{(0)}(A)\hat{T}_{0X}^{(0)}(X_2)\,\hat{\sigma}\right] \\
&= 4\,\mathrm{tr}\left[\hat{\mathbf{I}}(X)\cdot\hat{\mathbf{I}}(X')\,\hat{\sigma}\right] \\
{}^{s}\upsilon_T &= \sqrt{8}\,\mathrm{tr}\left[\hat{T}_0^{(0)}(A)\hat{T}_{0E}^{(0)}(X_2)\,\hat{\sigma}\right] \\
&= \mathrm{tr}\left[\hat{E}\,\hat{\sigma}\right]
\end{aligned}
$$

The coefficients on the rhs of (56) are selected to give the correct linear combination of line intensities specified in (55) along with the corresponding combination of state populations, N_i's. Thus, the magnetization modes in (56) are expressed in terms of both irreducible tensor operators and standard single spin angular momentum operators.

Note, ${}^{s}\upsilon_T$ again specifies the total spin population that is conserved and again decouples from the remaining equations. Six of the remaining seven coupled magnetization modes or dynamical variables in (55) and (56) are potentially measurable if one employs the benefit of anisotropic media to order the AX_2 molecule. In isotropic media only four of the dynamical modes correspond to direct measurables. They are ${}^{a}\upsilon_A$, the total A magnetization; ${}^{a}\upsilon_X$, the total X magnetization; ${}^{a}\upsilon_{+-+}$, the difference in intensity between the outer two lines and the inner line of the A triplet; and ${}^{s}\upsilon_{+o-}$, the difference in intensity between either the two lines of the X doublet or between the outer two lines of the A triplet. Two other modes have clear meanings and can be measured in anisotropic media. These include the antisymmetric, ${}^{a}\upsilon_{\pm\mp}$, mode that gives the differences specified by (55) between the lines of the X quartet in an anisotropic media. Similarly, the related ${}^{s}\upsilon_{\pm\pm}$ mode in the symmetric manifold also gives a different combination of these four lines within the X quartet. The line degeneracy of L'_4, L''_4 and of L'_5, L''_5 in isotropic fluids renders the ${}^{a}\upsilon_{\pm\mp}$ and ${}^{s}\upsilon_{\pm\pm}$ modes unobservable.

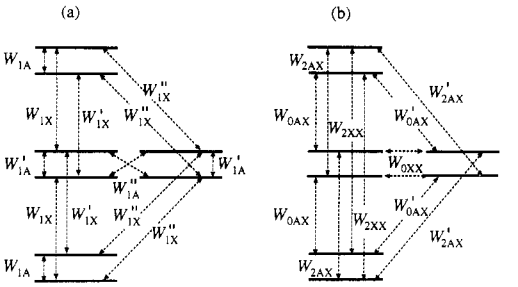

Figure 4. The interlevel relaxation rates corresponding to allowed transitions in the AX_2 case are shown in part a, while those corresponding to zero and two quantum relaxation processes are shown in part b.

Both of these modes may, in principle, be measured in anisotropic media as preferential ordering removes the degeneracies in the isotropic X doublet given by $(L'_4 + L''_4)$ and $(L'_5 + L''_5)$. Thus, it is convenient to construct a set of modes and general Γ matrix that can be used in both cases. The final mode ${}^{s}\upsilon_{t-3s}$ differs from that given originally[30] even though it corresponds to an irreducible tensor operator. Like ${}^{s}\upsilon_T$, it has no interpretation in terms of line magnetizations, but it does have an interesting meaning. The ${}^{s}\upsilon_{t-3s}$ mode tracks the populations of the six states with a triplet X spin multiplicity less three times the population of the two states with singlet X character. In the AX_2 case, rf-induced transitions between these two manifolds are symmetry forbidden, and thus selection rules prevent direct observation of the mode. It is interesting, however, that information on the excitation of ${}^{s}\upsilon_{t-3s}$ may be obtained in the dynamical fitting of relaxation data. The superscript labels the linear combinations of the populations as being either symmetric (s) or antisymmetric (a) under the operation of spin inversion.

Figure 4 defines the elements that appear in the Redfield matrix, **W**, as

$$
\mathbf{W} = \left[\begin{array}{cccc|cccc}
-W_a & W_{1A} & W_{1X} & W''_{1X} & W'_{2AX} & W_{2AX} & W_{2XX} & 0 \\
W_{1A} & -W_b & W_{0AX} & W'_{0AX} & W''_{1X} & W'_{1X} & 0 & W_{2XX} \\
W_{1X} & W_{0AX} & -W_c & W_{0XX} & W''_{1A} & W'_{1A} & W'_{1X} & W_{2AX} \\
W''_{1X} & W'_{0AX} & W_{0XX} & -W_d & W'_{1A} & W''_{1A} & W''_{1X} & W'_{2AX} \\
\hline
W'_{2AX} & W''_{1X} & W''_{1A} & W'_{1A} & -W_d & W_{0XX} & W'_{0AX} & W''_{1X} \\
W_{2AX} & W'_{1X} & W'_{1A} & W''_{1A} & W_{0XX} & -W_c & W_{0AX} & W_{1X} \\
W_{2XX} & 0 & W'_{1X} & W''_{1X} & W'_{0AX} & W_{0AX} & -W_b & W_{1A} \\
0 & W_{2XX} & W_{2AX} & W'_{2AX} & W''_{1X} & W_{1X} & W_{1A} & -W_a
\end{array}\right] \qquad (57)
$$

where

$$
\begin{aligned}
W_a &= W_{1A} + W_{1X} + W''_{1X} + W_{2AX} + W'_{2AX} + W_{2XX} \\
W_b &= W_{1A} + W'_{1X} + W''_{1X} + W_{0AX} + W'_{0AX} + W_{2XX} \\
W_c &= W'_{1A} + W''_{1A} + W_{1X} + W'_{1X} + W_{0AX} + W_{2AX} + W_{0XX} \\
W_d &= W'_{1A} + W''_{1A} + 2W''_{1X} + W'_{0AX} + W'_{2AX} + W_{0XX}
\end{aligned} \qquad (58)
$$

Note, this **W** matrix is symmetric about both the diagonal axis and the antidiagonal axis (a property that reflects the inversion symmetry) and may be transformed into a partially diagonalized Γ matrix using the information in (55) to obtain the following **T** matrix and its inverse, $\mathbf{T}^{-1}$:

$$\mathbf{T} = \begin{bmatrix} 1 & -1 & 1 & 1 & -1 & -1 & 1 & -1 \\ 1 & 1 & 0 & 0 & 0 & 0 & -1 & -1 \\ 1 & -1 & -1 & -1 & 1 & 1 & 1 & -1 \\ 1 & -1 & -2 & 0 & 0 & 2 & 1 & -1 \\ 1 & -1 & 0 & 0 & 0 & 0 & -1 & 1 \\ 1 & 1 & -2 & 0 & 0 & -2 & 1 & 1 \\ 1 & 1 & 1 & -3 & -3 & 1 & 1 & 1 \\ 1 & 1 & 1 & 1 & 1 & 1 & 1 & 1 \end{bmatrix} \tag{59a}$$

$$\mathbf{T}^{-1} = \frac{1}{24}\begin{bmatrix} 3 & 6 & 3 & 0 & 6 & 2 & 1 & 3 \\ -3 & 6 & -3 & 0 & -6 & 2 & 1 & 3 \\ 3 & 0 & +3 & -6 & 0 & -4 & 1 & 3 \\ 3 & 0 & -9 & 6 & 0 & 0 & -3 & 3 \\ -3 & 0 & 9 & -6 & 0 & 0 & -3 & 3 \\ -3 & 0 & -3 & 6 & 0 & -4 & 1 & 3 \\ 3 & -6 & 3 & 0 & -6 & 2 & 1 & 3 \\ -3 & -6 & -3 & 0 & 6 & 2 & 1 & 3 \end{bmatrix} \tag{59b}$$

The resulting partially diagonal Γ matrix and corresponding differential equations become

$$\frac{d}{dt}\begin{bmatrix} {}^a\mathbf{v} \\ {}^s\mathbf{v} \end{bmatrix} = \begin{bmatrix} {}^a\Gamma & 0 \\ 0 & {}^s\Gamma \end{bmatrix}\begin{bmatrix} {}^a\mathbf{v} - {}^a\mathbf{v}(\infty) \\ {}^s\mathbf{v} - {}^s\mathbf{v}(\infty) \end{bmatrix} \tag{60}$$

with $d^s v_T/dt = 0$. The antisymmetric component of the Γ matrix is given in (61) and the symmetric component is in (62) (Chart I). The expressions for the various W's in terms of the dipolar and random field power densities are

$$\begin{aligned}
W_{1A} &= J^{(1)}_{AX}(\omega_A) + J^{(1)}_{XAX}(\omega_A) + 2j^{(1)}_{A}(\omega_A) \\
W'_{1A} &= 2j^{(1)}_{A}(\omega_A) \\
W''_{1A} &= J^{(1)}_{AX}(\omega_A) - J^{(1)}_{XAX}(\omega_A) \\
W_{1X} &= \tfrac{1}{2}J^{(1)}_{AX}(\omega_X) + \tfrac{1}{2}J^{(1)}_{XAX}(\omega_X) + J^{(1)}_{XX}(\omega_X) \\
&\quad + 2J^{(1)}_{AXX}(\omega_X) + 2j^{(1)}_{X}(\omega_X) + 2j^{(1)}_{XX}(\omega_X) \\
W'_{1X} &= \tfrac{1}{2}J^{(1)}_{AX}(\omega_X) + \tfrac{1}{2}J^{(1)}_{XAX}(\omega_X) + J^{(1)}_{XX}(\omega_X) \\
&\quad - 2J^{(1)}_{AXX}(\omega_X) + 2j^{(1)}_{X}(\omega_X) + 2j^{(1)}_{XX}(\omega_X) \\
W''_{1X} &= \tfrac{1}{2}J^{(1)}_{AX}(\omega_X) - \tfrac{1}{2}J^{(1)}_{XAX}(\omega_X) \\
&\quad + 2j^{(1)}_{X}(\omega_X) - 2j^{(1)}_{XX}(\omega_X)
\end{aligned} \tag{63a}$$

$$\begin{aligned}
W_{0AX} &= \tfrac{1}{3}J^{(0)}_{AX}(\omega_X - \omega_A) + \tfrac{1}{3}J^{(0)}_{XAX}(\omega_X - \omega_A) \\
W'_{0AX} &= \tfrac{1}{3}J^{(0)}_{AX}(\omega_X - \omega_A) - \tfrac{1}{3}J^{(0)}_{XAX}(\omega_X - \omega_A) \\
W_{0XX} &= \tfrac{2}{3}J^{(0)}_{AX}(0) - \tfrac{2}{3}J^{(0)}_{XAX}(0) + 2j^{(0)}_{X}(0) - 2j^{(0)}_{XX}(0) \\
W_{2AX} &= 2J^{(2)}_{AX}(\omega_X + \omega_A) + 2J^{(2)}_{XAX}(\omega_X + \omega_A) \\
W'_{2AX} &= 2J^{(2)}_{AX}(\omega_X + \omega_A) - 2J^{(2)}_{XAX}(\omega_X + \omega_A) \\
W_{2XX} &= 2J^{(2)}_{XX}(2\omega_X)
\end{aligned} \tag{63b}$$

By using (63) in (61) and (62) the antisymmetric part of Γ given for power densities in extreme narrowing is given in (64) and the symmetric part of Γ is in (65) (Chart II).

IV. Motional Diffusion Models

A. General Historical Background

The effect of molecular motion on nuclear spin relaxation has been treated in one of two ways. For a rigid molecule with three degrees of motional freedom, explicit expressions have been derived which relate the dipolar power densities to rotational diffusion parameters and the molecular geometry. Large flexible molecules, however, undergo overall diffusion as well as internal segmental motion. Coupling between overall diffusional motion and various internal motions prevents the derivation of closed expressions relating the molecular dynamics directly to the NMR relaxation parameters. In this instance the NMR power densities are converted into standard Cartesian correlation times and compared with molecular mechanics calculations based on various approximations to the Langevin equation. Molecular potential functions which govern the segmental motion and frictional coefficients that control the diffusional liquid dynamics are then introduced in the molecular mechanics to simulate the correlation times obtained from the spin relaxation studies. The extent of agreement depends upon the approximations used in the Langevin equations and upon the suitability of the parameters that control the motional features.

Early theories of rotational Brownian motion were proposed by Debye[117] and by Perrin.[118,119] These or similar methods have been used by a number of workers[120-126] to discuss the anisotropic motional dependence of single nuclear spin relaxation times. Woessner's expressions[120,123] for the dependence of $1/T_1$ upon anisotropic molecular diffusion (i.e., spherical, symmetrical, and asymmetrical) can be especially useful as they indicate the relative importance of various rotational modes upon single parameter spin relaxation.[48,61,78,79,127-130] The manner in which very rapid motion about a single axis (e.g., the principal axis of a methyl top) suppresses relaxation is clearly indicated in Woessner's work. Hubbard's[131,132] evaluation of spherical harmonic correlation functions was helpful in developing expressions for treating the dipole–dipole interaction. However, the asymmetrical rotational diffusion expected for an AX_2 methylene spin moiety requires multiplet relaxation parameters to have sufficient information to characterize the anisotropic motional features. Using these concepts developed for general asymmetric diffusional motion, expressions for coupled spin relaxation parameters have been given by Grant and Werbelow.[8,133]

B. Favro Diffusion Equation and Rigid Molecules

To evaluate the spherical harmonic correlation function in (30) it must be first transformed into the molecular frame using the following standard expansion:

$$\left\langle Y^{(2)}_q\left(\Omega^{lab}_{ij}(0)\right) Y^{(2)}_{q'}\left(\Omega^{lab}_{kl}(t)\right)\right\rangle = \sum_{nn'}\left\langle D^{(2)}_{nq}(\Omega(0))\, D^{(2)}_{n'q'}(\Omega(t))\right\rangle Y^{(2)}_n\left(\Omega^{mol}_{ij}\right) Y^{(2)}_{n'}\left(\Omega^{mol}_{kl}\right) \tag{66}$$

where the Wigner rotation matrices, $D^{(2)}_{nq}[\Omega(0)]$, are as

CHART I

$$
{}^{a}\Gamma = -\begin{bmatrix}
W_{2AX}+W'_{2AX}+W_{0AX}+W'_{0AX}+W_{1A}+W'_{1A}+W''_{1A} & +W_{2AX}+W'_{2AX}-W_{0AX}-W'_{0AX} & W_{2AX}-W'_{2AX}+W_{0AX}-W'_{0AX}+W_{1A}-W'_{1A}-W''_{1A} & -W_{2AX}+W'_{2AX}-W_{0AX}+W'_{0AX} \\
\tfrac{1}{2}(W_{2AX}+W'_{2AX}-W_{0AX}-W'_{0AX}) & \tfrac{1}{2}(W_{2AX}+W'_{2AX}+W_{0AX}+W'_{0AX}+W_{1X}+W'_{1X}+2W''_{1X}+4W_{2XX}) & \tfrac{1}{2}(W_{2AX}-W'_{2AX}-W_{0AX}+W'_{0AX}) & \tfrac{1}{2}(-W_{2AX}+W'_{2AX}+W_{0AX}-W'_{0AX}+W_{1X}-W'_{1X}) \\
W_{1A}-W'_{1A}-W''_{1A} & W_{1X}-W'_{1X} & W_{1A}+W'_{1A}+W''_{1A}+4W''_{1X} & W_{1X}+W'_{1X}-2W''_{1X} \\
\tfrac{1}{2}(-W_{2AX}+W'_{2AX}-W_{0AX}+W'_{0AX}+2W_{1A}-2W'_{1A}-2W''_{1A}) & \tfrac{1}{2}(-W_{2AX}+W'_{2AX}+W_{0AX}-W'_{0AX}+3W_{1X}-3W'_{1X}) & -\tfrac{1}{2}W_{2AX}-\tfrac{1}{2}W'_{2AX}-\tfrac{1}{2}W_{0AX}-\tfrac{1}{2}W'_{0AX}+W_{1A}-W'_{1A}+W''_{1A}+2W''_{1X}-2W_{0XX} & \tfrac{1}{2}(W_{2AX}+W'_{2AX}+W_{0AX}+W'_{0AX}+4W'_{1A}+3W_{1X}+3W'_{1X}-2W''_{1X}+4W_{0XX})
\end{bmatrix} \tag{61}
$$

$$
{}^{s}\Gamma = -\begin{bmatrix}
\tfrac{1}{2}(W_{2AX}+W'_{2AX}+W_{0AX}+W'_{0AX}+4W_{1A}+W_{1X}+W'_{1X}+2W''_{1X}+4W_{2XX}) & \tfrac{1}{6}(3W_{2AX}+W'_{2AX}-3W_{0AX}-W'_{0AX}+3W_{1X}-3W'_{1X}) & \tfrac{1}{3}(W'_{2AX}-W'_{0AX}) & 0 \\
\tfrac{1}{2}(3W_{2AX}+W'_{2AX}-3W_{0AX}-W'_{0AX}+3W_{1X}-3W'_{1X}) & \tfrac{1}{6}(9W_{2AX}+W'_{2AX}+9W_{0AX}+W'_{0AX}+4W''_{1A}+9W_{1X}+9W'_{1X}+2W''_{1X}+4W_{0XX}) & \tfrac{1}{3}(W'_{2AX}+W'_{0AX}-2W''_{1A}+2W''_{1X}-2W_{0XX}) & 0 \\
2W'_{2AX}-2W'_{0AX} & \tfrac{1}{3}(2W'_{2AX}+2W'_{0AX}-4W''_{1A}+4W''_{1X}-4W_{0XX}) & \tfrac{1}{3}(4W'_{2AX}+4W'_{0AX}+4W''_{1A}+8W''_{1X}+4W_{0XX}) & 0 \\
0 & 0 & 0 & 0
\end{bmatrix} \tag{62}
$$

given by Rose.[11] In (66) the molecular geometry is incorporated in the time-independent terms, $Y_n^{(2)}(\Omega_{ij}^{mol})\,Y_n^{(2)}(\Omega_{kl}^{mol})$. The time dependence is found solely in the correlation function given by the $\langle D_{nq}^{(2)}[\Omega(0)]D_{n'q'}^{(2)}[\Omega(t)]\rangle$ correlation function that may be expanded in a conditional probability expression as follows:

$$
\left\langle D_{nq}^{(2)}(\Omega(0))D_{n'q'}^{(2)}(\Omega(t))\right\rangle = \iint P(\Omega_0)D_{nq}^{(2)}(\Omega_0)P(\Omega_0|\Omega,t)D_{n'q'}^{(2)}(\Omega)d\Omega_0 d\Omega \tag{67}
$$

$P(\Omega_0)$ is a normalizing term that also is the probability of the molecule occupying the orientation Ω_0 at time zero. $P(\Omega_0|\Omega,t)$ is a conditional probability that the molecule will have the orientation Ω at time t given that at time zero it had the orientation Ω_0. Favro[134] developed a method for obtaining $P(\Omega_0|\Omega,t)$ from the following wave equation:

$$
\frac{\partial P(\Omega_0|\Omega,t)}{\partial t} = \sum_{k=x,y,z} L_k \cdot R_{kk} \cdot L_k \; P(\Omega_0|\Omega,t) \tag{68}
$$

where L_k is the angular momentum operator about the kth axis and R_{kk} is the kth component of the diagonalized rotational diffusion tensor. Because (68) is analogous to the wave equation for the three-dimensional rigid rotor,[135] its solution may be cast into the following form:[8,133]

$$
P(\Omega_0|\Omega,t) = \sum_{\nu} \Psi_\nu^*(\Omega_0)\,\Psi_\nu(\Omega)e^{-b_\nu t} \tag{69}
$$

CHART II

$$
{}^{a}\Gamma = -\begin{bmatrix}
\frac{20}{3}J_{AX}+4j_A & \frac{10}{3}J_{AX} & \frac{20}{3}J_{XAX} & -\frac{14}{3}J_{XAX} \\
\frac{5}{3}J_{AX} & \frac{10}{3}J_{AX}+5J_{XX}+4j_X & \frac{5}{3}J_{XAX} & -\frac{5}{3}J_{XAX}+2J_{AXX} \\
2J_{XAX} & 4J_{AXX} & 4J_{AX}-2J_{XAX}+4j_A+8j_X-8j_{XX} & 2J_{XAX}+2J_{XX}+8j_{XX} \\
-\frac{1}{3}J_{XAX} & -\frac{5}{3}J_{XAX}+6J_{AXX} & -\frac{2}{3}J_{AX}+\frac{1}{3}J_{XAX} & \frac{14}{3}J_{AX}+\frac{2}{3}J_{XAX}+3J_{XX}+4j_A+8j_X+4j_{XX}
\end{bmatrix} \tag{64}
$$

$$
{}^{s}\Gamma = -\begin{bmatrix}
\frac{16}{3}J_{AX}+5J_{XX}+2J_{XAX}+4j_A+4j_X & \frac{10}{9}J_{AX}+\frac{5}{9}J_{XAX}+2J_{AXX} & \frac{5}{9}J_{AX}-\frac{5}{9}J_{XAX} & 0 \\
\frac{10}{3}J_{AX}+\frac{5}{3}J_{XAX}+6J_{AXX} & +\frac{20}{3}J_{AX}+3J_{XX}+\frac{10}{3}J_{XAX}+8j_X+4j_{XX} & 0 & 0 \\
\frac{10}{3}J_{AX}-\frac{10}{3}J_{XAX} & 0 & \frac{20}{3}J_{AX}-\frac{20}{3}J_{XAX}+8j_X-8j_{XX} & 0 \\
0 & 0 & 0 & 0
\end{bmatrix} \tag{65}
$$

where the b_ν are the eigenvalues of (68) and the eigenfunctions are expansions of $D^{(\ell)}_{\mu,k}(\Omega)$:

$$\Psi_{\ell,\mu,\eta}(\Omega) = \sum_k a_{\eta,k} D^{(\ell)}_{\mu,k}(\Omega) \tag{70}$$

Note, it is known that the $D^{(\ell)}_{\mu,k}(\Omega)$ are the natural solutions for the problem of the three-dimensional rigid rotor just as the $Y^{(\ell)}_q(\Omega)$ are the solutions for the two-dimensional rigid rotor. Using (70) in the set of equations (69) back through (66) gives explicit expressions for the spherical harmonic correlation function found for $J^q_{ijkl}(\omega_{\kappa\lambda})$ in (27). This exercise is more than a trivial step, and the reader is referred to the literature[8,133] for further details. Use is made of the angular momentum properties of $D^{(\ell)}_{\mu,k}(\Omega)$ wherein these functions are simultaneously eigenfunctions of L^2, L_z^{mol}, and L_z^{lab}. The orthogonality properties of $D^{(\ell)}_{\mu,k}(\Omega)$ also greatly facilitate the evaluation of (67). The final set of expressions derived by this approach of Favro[134] for the various dipolar power densities in terms of the molecular structure and the associated rotational diffusion constants are given for the following three cases:

1. Spherical Top Molecule

$$J_{ijkl}(\omega) = \frac{\xi_{ij}\xi_{kl}}{8\pi}\left\{3\left(l_{ij}l_{kl}+m_{ij}m_{kl}+n_{ij}n_{kl}\right)-1\right\}\frac{6R}{(6R)^2+\omega^2} \tag{71}$$

Remember that

$$\xi_{ij} = \sqrt{\frac{6\pi}{5}}\frac{\gamma_i\gamma_j\hbar}{r_{ij}^3} \tag{25}$$

The auto-correlation terms in (70) have $ij = kl$ and $(l_{ij}l_{kl} + m_{ij}m_{kl} + n_{ij}n_{kl}) = 1$ for all internuclear vectors making the auto-correlated terms such as J_{AX} independent of the molecular geometry. However, when $ij \neq kl$ the cross terms, such as J_{XAX}, will depend upon the angle θ between ij and kl in spherical top molecules because $(l_{ij}l_{kl} + m_{ij}m_{kl} + n_{ij}n_{kl}) = \cos\theta$.

2. Symmetric Top Molecule

$$J_{ijkl}(\omega) = \frac{\xi_{ij}\xi_{kl}}{16\pi}\left\{A_{ijkl}\frac{6R_\perp}{(6R_\perp)^2+\omega^2} + B_{ijkl}\frac{5R_\perp+R_\parallel}{(5R_\perp+R_\parallel)^2+\omega^2} + C_{ijkl}\frac{2R_\perp+4R_\parallel}{(2R_\perp+4R_\parallel)^2+\omega^2}\right\} \tag{72}$$

The $R_\parallel$ and $R_\perp$ are, respectively, the parallel and perpendicular rotational diffusion constants. The coefficients A, B, and C contain the directional cosines l, m, and n (relative to the x, y, and z axes, respectively) for the ij and kl internuclear vectors and specify the molecular geometry as follows:

$$A_{ijkl} = \left(3n_{ij}^2 - 1\right)\left(3n_{kl}^2 - 1\right)$$
$$B_{ijkl} = 12\left(l_{ij}l_{kl} + m_{ij}m_{kl}\right)n_{ij}n_{kl} \quad (73)$$
$$C_{ijkl} = 3\left[\left(l_{ij}l_{kl} + m_{ij}m_{kl}\right)^2 - \left(l_{ij}m_{kl} - m_{ij}l_{kl}\right)^2\right]$$

A consideration of (72) and (73) indicates that auto- and cross-correlated power densities will depend upon how molecular geometry relates to the axes prescribed by the two unique rotational diffusion constants.

3. Asymmetric Top Molecule

$$J_{ijkl}(\omega) = \frac{\xi_{ij}\xi_{kl}}{16\pi}\left\{c_1\frac{b_1}{b_1^2+\omega^2} + c_2\frac{b_2}{b_2^2+\omega^2} + c_3\frac{b_3}{b_3^2+\omega^2} + c_4\frac{b_4}{b_4^2+\omega^2} + c_5\frac{b_5}{b_5^2+\omega^2}\right\} \quad (74)$$

The b_i terms are eigenvalues of (66) and contain the rotational diffusion information as follows:

$$b_1 = 4R_{xx} + R_{yy} + R_{zz}$$
$$b_2 = R_{xx} + 4R_{yy} + R_{zz}$$
$$b_3 = R_{xx} + R_{yy} + 4R_{zz} \quad (75)$$
$$b_4 = 6R + 6\sqrt{R^2 - \Re^2}$$
$$b_5 = 6R - 6\sqrt{R^2 - \Re^2}$$

The following compacted rotational diffusion terms are needed to evaluate (75):

$$R = \tfrac{1}{3}\left(R_{xx} + R_{yy} + R_{zz}\right)$$
$$\Re^2 = \tfrac{1}{3}\left(R_{xx}R_{yy} + R_{xx}R_{zz} + R_{yy}R_{zz}\right) \quad (76)$$
$$\left(R^2 - \Re^2\right) = \tfrac{1}{9}\left(R_{xx}^2 + R_{yy}^2 + R_{zz}^2 - R_{xx}R_{yy} - R_{xx}R_{zz} - R_{yy}R_{zz}\right)$$

It is often helpful to use reduced variables for the rotational diffusion constants and for the eigenvalues:

$$\rho_q = \frac{R_{qq}}{R_{zz}} \qquad \beta_i = \frac{b_i}{R_{zz}}, \quad (77)$$
$$\rho = \frac{R}{R_{zz}} \qquad \zeta = \frac{\Re}{R_{zz}}$$

In these reduced variables, (75) and (76) become

$$\beta_1 = 4\rho_x + \rho_y + 1$$
$$\beta_2 = \rho_x + 4\rho_y + 1$$
$$\beta_3 = \rho_x + \rho_y + 4 \quad (78)$$
$$\beta_4 = 6\rho + 6\sqrt{\rho^2 - \zeta^2}$$
$$\beta_5 = 6\rho - 6\sqrt{\rho^2 - \zeta^2}$$

where

$$\rho = \tfrac{1}{3}\left(\rho_x + \rho_y + 1\right)$$
$$\left(\rho^2 - \zeta^2\right) = \tfrac{1}{9}\left(\rho_x^2 + \rho_y^2 - \rho_x\rho_y - \rho_x - \rho_y + 1\right) \quad (79)$$

TABLE I. Geometrical Orientation of AX, AX′, and XX′ Bond Vectors

bond vector	l_{ij}	m_{ij}	n_{ij}
AX	α	β	0
AX′	α	$-\beta$	0
XX′	0	1	0

Finally, the various c_i coefficients in (74) are given by

$$c_1 = 12m_{ij}m_{kl}n_{ij}n_{kl}$$
$$c_2 = 12l_{ij}l_{kl}n_{ij}n_{kl}$$
$$c_3 = 12l_{ij}l_{kl}m_{ij}m_{kl} \quad (80)$$
$$c_4 = d + e\cos\chi + f\sqrt{3}\sin\chi$$
$$c_5 = d - e\cos\chi - f\sqrt{3}\sin\chi$$

with

$$d = 3\left(l_{ij}^2l_{kl}^2 + m_{ij}^2m_{kl}^2 + n_{ij}^2n_{kl}^2\right) - 1$$
$$e = 1 - 3\left(l_{ij}^2m_{kl}^2 + l_{kl}^2m_{ij}^2 + n_{ij}^2n_{kl}^2\right) \quad (81)$$
$$f = \left(3m_{ij}^2m_{kl}^2 - 3l_{ij}^2l_{kl}^2 - m_{ij}^2 - m_{kl}^2 + l_{ij}^2 + l_{kl}^2\right)$$

and

$$\cos\chi = \frac{\left(2R_{zz} - R_{xx} - R_{yy}\right)}{6\sqrt{R^2 - \Re^2}} = \frac{\left(2 - \rho_x - \rho_y\right)}{6\sqrt{\rho^2 - \zeta^2}}$$
$$\sin\chi = \frac{\sqrt{3}\left(R_{xx} - R_{yy}\right)}{6\sqrt{R^2 - \Re^2}} = \frac{\sqrt{3}\left(\rho_x - \rho_y\right)}{6\sqrt{\rho^2 - \zeta^2}} \quad (82)$$

Note, c_1, c_2, c_3, d, e, and f specify only geometrical parameters of the spin systems, but c_4 and c_5 require a mix of geometrical parameters and the ρ_x and ρ_y reduced rotational diffusion terms.

4. AX_2 Asymmetric Top Molecule

By selecting a specific spin case with the internuclear orientations in the molecule the directional cosines of (80) and (81) are specified, and explicit expressions may be obtained for the dipolar power densities. The cosines corresponding to the structure of an AX_2 methylene group are given in Table I for $\alpha = \cos(\theta/2)$ and $\beta = \sin(\theta/2)$ with θ the XAX′ angle. The remaining AX_2 geometric constants appearing in (79) and (80) are given in Table II with $a_\pm = (1 \pm \cos\theta)/2$. Note, explicit expressions in θ are $4a_+a_- = \sin^2\theta$; $(a_- - a_+) = -\cos\theta$; and $(a_+^2 + a_-^2) = (1 + \cos^2\theta)/2$. As $c_1 = c_2 = 0$ two of the five terms in (74) are eliminated for the AX_2 symmetry. Further simplification is also achieved in the extreme narrowing limit where $b_i \gg \omega$. The general AX_2 expression for the dipolar power density under these constraints is

$$J_{ijkl}\left(K,\theta,\rho_x,\rho_y\right) = \frac{\xi_{ij}\xi_{kl}}{16\pi R_{zz}}\left\{\frac{c_3(\theta)}{\beta_3\left(\rho_x,\rho_y\right)} + \frac{c_4\left(\theta,\rho_x,\rho_y\right)}{\beta_4\left(\rho_x,\rho_y\right)} + \frac{c_5\left(\theta,\rho_x,\rho_y\right)}{\beta_5\left(\rho_x,\rho_y\right)}\right\} \quad (83)$$

where $K = (r_{ij}^3r_{kl}^3R_{zz})^{-1}$ arises from the $\xi_{ij}\xi_{kl}/R_{zz}$ term, and the reduced rotational diffusion constants, ρ_x and ρ_y, are given in (77).

A careful consideration of (83) along with Tables I and II indicates that the dipolar power densities are

TABLE II. Geometrical Parameters for Asymmetric Top Molecules

	c_1	c_2	c_3	d	e	f
J_{AX}	0	0	$12a_+a_-$	$3(a_+^2 + a_-^2) - 1$	$1 - 6a_+a_-$	$a_- - a_+$
$J_{XX'}$	0	0	0	2	1	1
$J_{XAX'}$	0	0	$-12a_+a_-$	$3(a_+^2 + a_-^2) - 1$	$1 - 6a_+a_-$	$a_- - a_+$
$J_{AXX'}$	0	0	0	$3a_- - 1$	$1 - 3a_+$	a_-

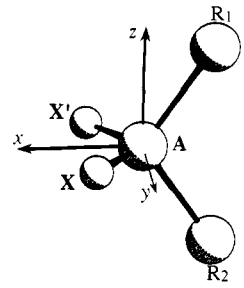

Figure 5. The molecule fixed coordinate system used in defining the reorientational parameters for an AX_2 spin system is shown. The symbols, R_1 and R_2, represent arbitraryfunctionalities free of spins that couple appreciably to the AX_2 system of interest.

expressed in terms of six parameters: three rotational diffusion parameters, ρ_x, ρ_y, and R_{zz}, and the three molecular structural parameters, r_{CH}, r_{HH}, and θ. Unfortunately, only four independent dipolar J's are available to evaluate these terms. The law of cosines provides a relation between r_{CH} and r_{HH} (i.e., $r_{HH}^2 = 4a_-r_{CH}^2$) no further relationships exist to reduce the number of parameters to four. However, careful inspection of (83) reveals that the sixth power of the internuclear distances always appears as a product with R_{zz} and only K may be determined from the experimental spectral densities. Both R_{zz} and r_{ij} can never be independently determined from the experimental spectral densities. Independent information on r_{CH} is required to obtain all three rotational diffusion constants, R_{xx}, R_{yy}, and R_{zz}. The fourth and final item of information may be either θ or the ratio of internuclear distances, r_{HH}/r_{CH}. Thus, only the uniquely selected diffusion constant, R_{zz}, scaled by r_{CH}^6; the HCH' angle, θ; and ratios ρ_x and ρ_y can be measured independently. Expressions relating the four power densities and the molecular structure and diffusion parameter, K, θ, ρ_x, and ρ_y, are readily obtained from (83) and Table II.

C. Flexible Molecules and Segmental Motion

In flexible molecular chains, coupling of various motional degrees of freedom invalidates the rigid rotational diffusion model. This difficulty is overcome in part by transforming the dipolar correlation functions into Cartesian correlation functions, and the results then compared with sophisticated molecular motional calculations using an approximate Langevin equation. In this approach the dipolar spectral densities are first transformed into standard Cartesian spectral densities where the symmetry axes of the AX_2 group, given in Figure 5, serve as the reference frame.

The normalized Cartesian correlation time, τ_i, is defined[136] as

$$\tau_{qq'} = \int_0^\infty dt \frac{\langle T_{qq'} \cdot T_{qq'}(t) \rangle}{\langle T_{qq'} \cdot T_{qq'} \rangle} = \frac{J_{q,q'}}{\langle T_{qq'} \cdot T_{qq'} \rangle} \tag{84}$$

where the $J_{q,q'}$ is a power density of the correlation function in the irreducible Cartesian tensor, $T_{qq'}$, at zero frequency, and $\langle T_{qq'} T_{qq'} \rangle$ is a normalizing term that is $^2/_3$ when qq' is equal to xx, yy, and zz and is $^1/_2$ for qq' equal to xy, xz, and yz. The four dipole spectral densities may also be expressed in terms of these Cartesian power densities[136] as follows:

$$\begin{aligned}
J_{AX} &= \frac{3\xi_{AX}^2}{8\pi} \\
&\quad \left\{a_+^2 J_{xx,xx} + a_-^2 J_{yy,yy} + 2a_+a_- J_{xx,yy} + 4a_+a_- J_{xy,xy}\right\} \\
J_{XX'} &= \frac{3\xi_{XX}^2}{8\pi}\left\{J_{yy,yy}\right\} \\
J_{XAX'} &= \frac{3\xi_{AX}^2}{8\pi} \\
&\quad \left\{a_+^2 J_{xx,xx} + a_-^2 J_{yy,yy} + 2a_+a_- J_{xx,yy} - 4a_+a_- J_{xy,xy}\right\} \\
J_{AXX'} &= \frac{3\xi_{AX}\xi_{XX}}{8\pi}\left\{a_+ J_{xx,yy} + a_- J_{yy,yy}\right\}
\end{aligned} \tag{85}$$

where again $a_\pm = {}^1/_2(1 \pm \cos\theta)$ with θ the XAX' angle. These equations are obtained by projecting the spin–spin vectors $\boldsymbol{r}_{ij}$ and $\boldsymbol{r}_{kl}$ (where ij and kl represent the AX, AX', and XX' nuclear pairs) along the directions of unit Cartesian vectors ($\boldsymbol{e}_x$, $\boldsymbol{e}_y$, and $\boldsymbol{e}_z$) using the irreducible tensor notation given in (84). The only cross term, $J_{xx,yy}$, in (85) may be eliminated by expressing it as a linear combination of auto-correlation functions[136] as follows:

$$2J_{xx,yy} = J_{zz,zz} - J_{xx,xx} - J_{yy,yy} \tag{86}$$

One may now obtain an expression for the four auto-correlation $J_{qq',qq'}$, including the $J_{zz,zz}$ of (86), in terms of the dipolar power densities by obtaining the inverse of the transformation given in (85). Note, at this point in the derivation all the Cartesian power densities are in an auto-correlation form, and it is convenient to drop the redundant indices. Applying the normalization condition in (84) to the J_{qq}'s yields the normalized Cartesian correlation times in the measured dipolar power densities as follows:

$$\begin{aligned}
\tau_{xx} &= \frac{4\pi}{a_+^2}\left\{\frac{J_{AX} + J_{XAX'}}{2\xi_{AX}^2} + \frac{a_-^2 J_{XX'}}{\xi_{XX}^2} - \frac{2a_- J_{AXX'}}{\xi_{AX}\xi_{XX}}\right\} \\
\tau_{yy} &= 4\pi\left\{\frac{J_{XX'}}{\xi_{XX}^2}\right\} \\
\tau_{xy} &= \frac{2\pi}{3a_+a_-}\left\{\frac{J_{AX}}{\xi_{AX}^2} - \frac{J_{XAX'}}{\xi_{AX}^2}\right\} \\
\tau_{zz} &= \frac{4\pi}{a_+^2} \\
&\quad \left\{\frac{J_{AX} + J_{XAX'}}{2\xi_{AX}^2} + \frac{(a_+ - a_-)^2 J_{XX'}}{\xi_{XX}^2} + \frac{2(a_+ - a_-)J_{AXX'}}{\xi_{AX}\xi_{XX}}\right\}
\end{aligned} \tag{87}$$

The dipolar spectral densities are thus transformed into Cartesian correlation times (τ_{xx}, τ_{yy}, τ_{zz}, and τ_{xy}) and may be compared with standard statistical mechanical correlation times obtained from molecular mechanics. From the definition of τ_{qq}, rotations about the q axis do not contribute to the relaxation of the diagonal modes (i.e., τ_{xx}, τ_{yy}, and τ_{zz}). Rather, these three modes relax by a rotational reorientation about either of the two directions orthogonal to the q axis.

Reorientational motion about all axes affects τ_{xy}. Fuson et al.[136] discuss this feature in some detail with attention given to the physical interpretation of these quantities. As auto-correlation times are generally easier to conceptualize, the four Cartesian correlation times are more readily interpreted than the two auto- and two cross-correlated dipolar NMR terms obtained experimentally from AX_2 relaxation measurements.

V. Coupled Relaxation Experiments

In this section a few examples of multiplet relaxation, taken from the authors' work, are given to illustrate the nature of the experiments and types of longitudinal relaxation data that are obtained. The various ways in which the spin systems may be perturbed and a brief summary of the computer fitting programs are presented.

A. Spin Preparation Steps

A variety of initial spin perturbations are typically used in $^{13}CH_2$ multiplet relaxation studies to displace the spin system from equilibrium. Following each of these initial spin preparations, the system is allowed to evolve for a time, D_2, followed by a 90° observe pulse in the ^{13}C domain. The resulting free induction decay, FID, is then collected and Fourier transformed to yield the partially relaxed line intensities. The proton decoupler channel, which remains off during the FID in all experiments, is used in many of the experiments as a proton pulse generator during the spin preparation period.

Five different types of spin preparations are illustrated for 1-decanol-1-^{13}C dissolved in perdeuterated diglyme at 273 K, as follows: (1) ^{13}C hard pulse, (2) ^1H hard pulse, (3) ^1H soft pulse, and two closely related multiple pulse perturbations (4) ^+J pulse and (5) ^-J pulse. Magnetizations are expressed in units of the total carbon magnetization at thermal equilibrium. The experimental points in each experiment are compared with the least-square fits obtained by adjusting the parameters of the coupled relaxation equations (see section V.B.). It is important to note that all five of these data sets are regressed simultaneously to accurately determine all the parameters in the relaxation model. When one does fit all five experiments simultaneously, the difference between the experimental points and calculated fit lines seldom exceeds 1% of the total carbon magnetization. Each experiment is designed to perturb significantly one or more of the several magnetization modes, so that, overall, a significant amount of magnetization is caused to flow through as many available relaxation pathways as possible.

1. Carbon Hard Pulse

In the ^{13}C coupled inversion recovery experiment, shown in Figure 6, a carbon 180° pulse inverts all three lines of the carbon triplet. The overall ^{13}C magnetization mode, $^a\upsilon_C$, negated under the pulse, then returns to equilibrium. Because the $^a\upsilon_C$ mode is coupled to three other modes in (60), the decay is, in principle, multiexponential; but the 1:2:1 equilibrium ratio of relative intensities of the $^{13}CH_2$ multiplet is only minimally perturbed as the inverted multiplet relaxes to equilibrium. As illustrated by these data, it is often the

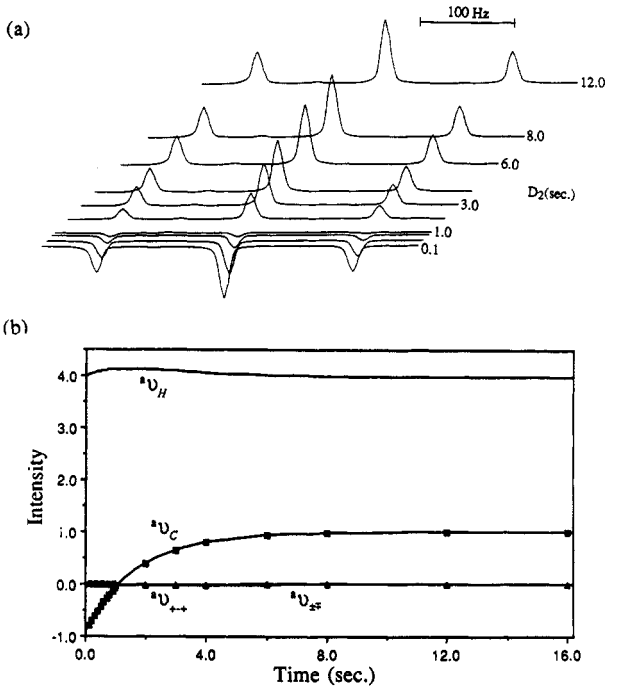

Figure 6. (a) A series of partially relaxed ^{13}C spectra obtained at vaious times, D_2, after application of a nonselective pulse to invert the triplet of the labeled carbon of $CH_3(CH_2)_8{}^{13}CH_2OH$. The data were obtained in deuterated diglyme at 273 K. (b) Experimental values of magnetization modes taken from these spectra compared to the values predicted by the nonlinear least-squares fit of the relaxation model discussed in the text. The symmetric manifold is not observably perturbed in this experiment and is not shown.

case that the traditional ^{13}C inversion recovery experiment can be rather accurately approximated by a single effective T_1 relaxation parameter. However, considered in the context of the overall equations of motion, the observation that appreciable magnetization does not accumulate in the other measured modes under this perturbation places significant constraints on the values of all elements of the Γ matrix but accurately fixes the value of $^a\Gamma_{11}$ and makes significant inferences regarding the value of $^a\Gamma_{13}$.

The boundary conditions at $t = 0$ and $t = \infty$ which are used for the $^a\upsilon$ and $^s\upsilon$ magnetization vectors in this experiment are given by

$$^a\mathbf{\upsilon}(0) = \begin{bmatrix} -\alpha_{11} \\ G \\ \delta_{11} \\ \delta_{11} \end{bmatrix} \qquad ^a\mathbf{\upsilon}(\infty) = \begin{bmatrix} 1 \\ G \\ \delta_{11} \\ \delta_{11} \end{bmatrix}$$

$$^s\mathbf{\upsilon}(0) = \begin{bmatrix} \Delta\alpha_{11} + \delta_{12} \\ 0 \\ 0 \\ 0 \end{bmatrix} \qquad ^s\mathbf{\upsilon}(\infty) = \begin{bmatrix} \delta_{12} \\ 0 \\ 0 \\ 0 \end{bmatrix} \tag{88}$$

where $G = \gamma_H/\gamma_C$ and the efficiency of the overall magnetization inversion used in this experiment to perturb the spins from equilibrium is α_{11}. A well-executed experiment would yield a α_{11} value that approaches unity. The $\Delta\alpha_{11}$ parameter models a differential pulse efficiency for the $^s\upsilon_{+0-}$ mode that can occur if the two outer lines of the triplet are not equally perturbed. The δ_{11} and δ_{12} parameters reflect the fact

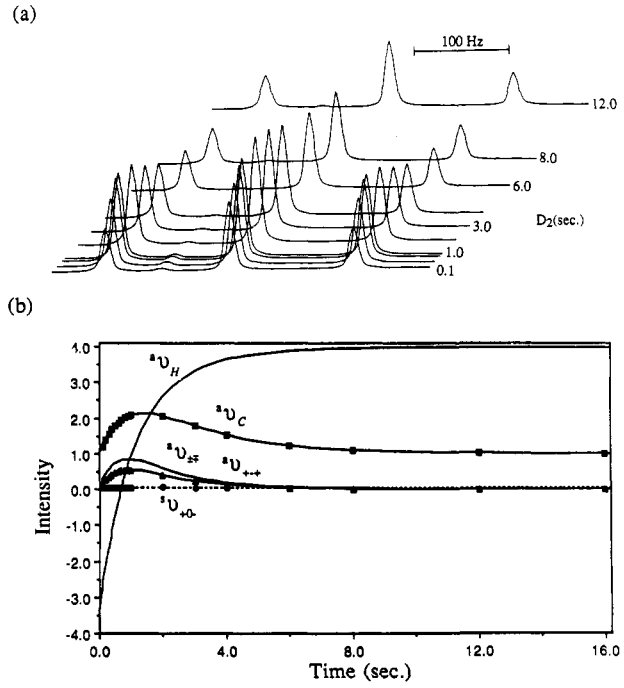

Figure 7. (a) A series of partially relaxed ^{13}C spectra obtained at various times, D_2, after application of a nonselective pulse to invert both of the lines corresponding to the protons attached to the labeled carbon of $CH_3(CH_2)_8{}^{13}CH_2OH$. The data were obtained in deuterated diglyme at 273 K. (b) Experimental values of magnetization modes taken from these spectra compared to the values predicted by the nonlinear least-squares fit of the relaxation model discussed in the text.

that the spectrometer receiver system may not have constant gain across the spectral width leading to small distortions of the multiplet. This in turn causes the magnetization modes that would otherwise relax to zero to retain a small but finite value at equilibrium. Distortion of the center line relative to the average of the outer two lines of the triplet affects ${}^a\upsilon_{+-+}$ and is given by δ_{11}, and the corresponding distortion between the two outer lines of the triplet affects ${}^s\upsilon_{+0-}$ and is given by δ_{12}. In a well-executed experiment, both δ_{11} and δ_{12} should approach zero. When δ_{12} is close to zero and when no significant contribution of $\Delta\alpha_{11}$ to ${}^s\upsilon_{+0-}$ is introduced by the carbon hard pulse, a condition easily monitored in this experiment, the inclusion of ${}^s\upsilon$ data becomes irrelevant to the fitting process and there is no need to employ either the $\Delta\alpha_{11}$ or the δ_{12} parameters. In fact, any of these parameters associated with artifacts of the measurement process may be set to some predetermined value and not iterated in the fitting process if they are known a priori. However, failure to recognize their influence on the fitting process has been found to lead to significant systematic trends in the residuals. Additional discussion of these issues is included in section V.B.

2. Proton Hard Pulse

In the proton hard pulse experiment, a nonselective, high power 180° proton pulse is applied at the middle of the proton doublet to invert simultaneously both proton lines. Initially the ^{13}C multiplet has its thermal equilibrium structure and intensity, but the complete $^{13}CH_2$ spin system is now far from equilibrium with the lattice. As the spins return to equilibrium, shown in Figure 7, the two observable ^{13}C antisymmetric magnetization modes that appear in the equation of motion are first populated and then depopulated. During this process, the original 1:2:1 ^{13}C multiplet undergoes significant distortion as the ${}^a\upsilon_{+-+}$ mode develops in time. This case is quite novel as the original ^{13}C triplet has the same 1:2:1 structure at $t = 0$ and at $t = \infty$ but passes through a variety of other intensity patterns for intermediate values of t. None of the other experiments exhibit the importance of coupled relaxation involving multiple exponential recovery more clearly than this one. The pattern never develops significant unequal intensities for the outer lines of the triplet indicating (1) that the proton pulse was well executed and no significant ${}^s\upsilon_{+0-}$ magnetization is introduced and (2) that the symmetric and antisymmetric magnetization modes are indeed not coupled. If cross-correlation terms between dipole–dipole and chemical shielding anisotropy were important, one might detect a break in the inversion symmetry and a coupling of the two manifolds.

The boundary conditions for the proton hard pulse experiment are given by

$$ {}^a\boldsymbol{\upsilon}(0) = \begin{bmatrix} 1 \\ -G\alpha_{21} \\ \delta_{21} \\ \delta_{21} \end{bmatrix} \qquad {}^a\boldsymbol{\upsilon}(\infty) = \begin{bmatrix} 1 \\ G \\ \delta_{21} \\ \delta_{21} \end{bmatrix} $$

$$ {}^s\boldsymbol{\upsilon}(0) = \begin{bmatrix} G\Delta\alpha_{21} + \delta_{22} \\ 0 \\ 0 \\ 0 \end{bmatrix} \qquad {}^s\boldsymbol{\upsilon}(\infty) = \begin{bmatrix} \delta_{22} \\ 0 \\ 0 \\ 0 \end{bmatrix} \tag{89} $$

The overall pulse efficiency is given by α_{21} while δ_{21} and δ_{22} have the same meaning as δ_{11} and δ_{12}, respectively, from the carbon hard pulse experiment. The first subscript designates the experiment and the second is a serial index within the experiment. As before, if the experiment is well executed, $\Delta\alpha_{21}$ is close to zero, the ${}^s\upsilon_{+0-}$ is left unpopulated, and the fitting of the symmetric manifold becomes unnecessary. However, if any asymmetry is introduced into the proton doublet by the pulse, it will be manifested in ${}^s\upsilon_{+0-}$ as measured in the carbon spectrum magnified by a factor of G. In those cases where the symmetric manifold is included in the fit, values for both $\Delta\alpha_{21}$ and δ_{22} must be obtained.

3. Proton Soft Pulse

In the ^1H soft pulse experiment a low-power proton pulse is used to selectively invert one of the two proton lines, and the effect on the ^{13}C multiplet may be observed in Figure 8. This perturbation affects the ^{13}C multiplet due to a ^1H to ^{13}C polarization transfer (discussed initially by Jakobson[137]). The width, amplitude, and frequency of the pulse are adjusted to yield the ideal 9:2:−7 carbon multiplet magnetization response expected for this polarization transfer. The instrumental adjustments involve striking a compromise between the low power required to focus the spin perturbation only on one proton line while maintaining sufficient power to complete the spin preparation in a time short compared with the spin relaxation processes. Reasonably short relaxation times encountered for alkyl chain molecules require intermediate power (soft)

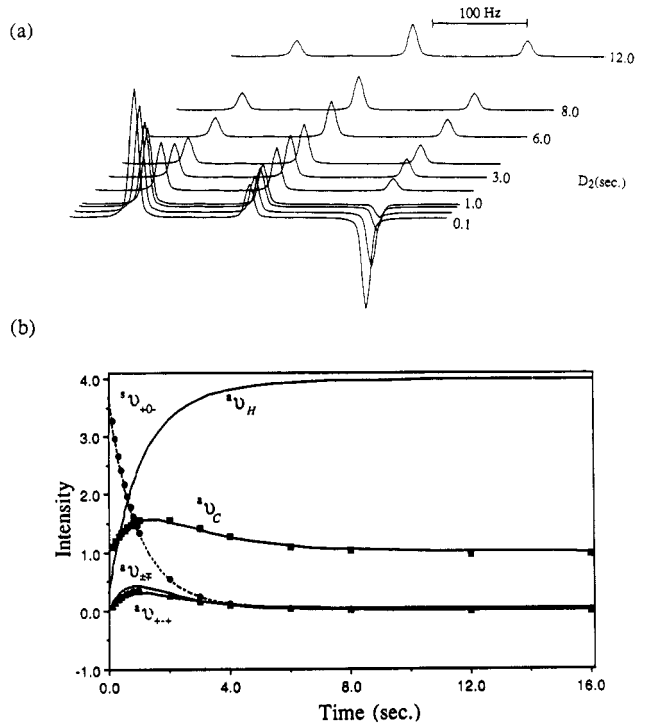

Figure 8. (a) A series of partially relaxed ^{13}C spectra obtained at various times, D_2, after application of a selective pulse to invert one of the lines corresponding to the protons attached to the labeled carbon of $CH_3(CH_2)_6{}^{13}CH_2OH$. The data were obtained in deuterated diglyme at 273 K. (b) Experimental values of magnetization modes taken from these spectra compared to the values predicted by the nonlinear least-squares fit of the relaxation model discussed in the text.

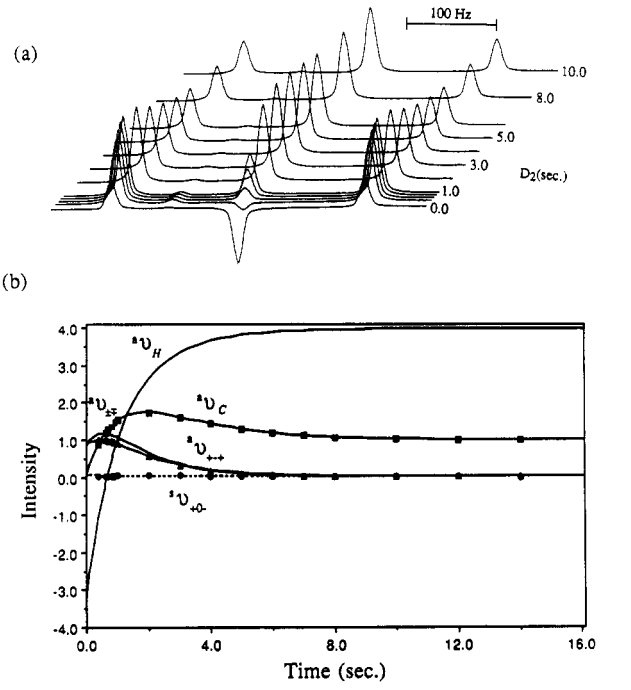

Figure 9. (a) A series of partially relaxed ^{13}C spectra obtained at various times, D_2, after application of the ^{+}J pulse sequence shown in Figure 11 to the labeled carbon of $CH_3(CH_2)_6{}^{13}CH_2OH$. The data were obtained in deuterated diglyme at 273 K. (b) Experimental values of magneitzation modes taken from these spectra compared to the values predicted by the nonlinear least-squares fit of the relaxation model discussed in the text.

pulses.[138] Even these soft pulses have bandwidths that, unfortunately may spread over more than one line of a multiplet.

To deal with this problem effectively, perturbing rf fields are often used that affect significantly both lines of the proton doublet. By applying the pulse exactly on resonance for one line of the doublet and tailoring the amplitude of the perturbing pulse to the value of the carbon–proton scalar coupling constant so that $\gamma B_2 = J_{CH}/\sqrt{3}$, the decoupling power can produce a 360° pulse on the off-resonance proton line, returning it to its original position, while rotating the on-resonance line through only 180°. Another, perhaps simpler, way to state this condition is that the amplitude of the proton rf field must be adjusted to produce a 180° pulse on-resonance in a time equal to $\sqrt{3}/(2J_{CH})$. A related though not identical initial condition could be achieved by using the familiar INEPT pulse sequence to perturb the symmetric manifold.

The boundary conditions for the proton soft pulse experiment are

$$ {}^{a}\mathbf{v}(0) = \begin{bmatrix} 1 \\ -G\Delta\alpha_{31} \\ \delta_{31} \\ \delta_{31} \end{bmatrix} \qquad {}^{a}\mathbf{v}(\infty) = \begin{bmatrix} 1 \\ G \\ \delta_{31} \\ \delta_{31} \end{bmatrix} $$

$$ {}^{s}\mathbf{v}(0) = \begin{bmatrix} G\alpha_{31} + \delta_{32} \\ 0 \\ 0 \\ 0 \end{bmatrix} \qquad {}^{s}\mathbf{v}(\infty) = \begin{bmatrix} \delta_{32} \\ 0 \\ 0 \\ 0 \end{bmatrix} \tag{90} $$

The α's and δ's have analogous definitions to those in the two previous experiments. If one assumes that the preparation pulse leaves the sum of ${}^{a}v_H$ and ${}^{s}v_{+0-}$ invariant in spite of any small imperfections, then $\Delta\alpha_{31} = 1 - \alpha_{31}$. Interestingly, all three measurable ^{13}C modes vary significantly in this experiment as both the ${}^{s}v_{+0-}$ and the ${}^{a}v_H$ modes are displaced appreciably from their thermal equilibrium values in the spin preparation phase of the experiment. Thus, both the antisymmetric and symmetric manifolds are significantly stimulated by this pulse; none of the other pulse preparations produce such extensive excursions in both the antisymmetric and symmetric manifolds.

4. *J* Pulse Excitation

This class of experiments involves a pulse sequence similar to that used for 2D J spectroscopy.[139] Shown in Figure 9 is the inversion of the center peak of the ^{13}C triplet by a ^{+}J pulse while the outer peaks are left unperturbed. In Figure 10 the outer peaks are inverted by a ^{-}J pulse without disturbing the center peak.[140,141] Both of these perturbations leave the ${}^{a}v_{+-+}$ and ${}^{a}v_{\pm\mp}$ mode far from equilibrium in contrast to the first three experiments discussed above.

The pulse sequence for the $^{\pm}J$ pulse experiment is given in Figure 11. During the preparation period, a $(\pi/2)_{+x}$ pulse tips the carbon magnetization along the $+y$ axis in the rotating frame. At time $\tau = 1/(4J_{CH})$ the three vectors corresponding to a carbon triplet are 90° out of phase. Simultaneous application of π_{+y} pulses to both the carbon and proton spins refocuses the chemical shift and field inhomogeneity, but the spin system continues to evolve under scalar coupling. When the refocusing is completed, after another τ period, the

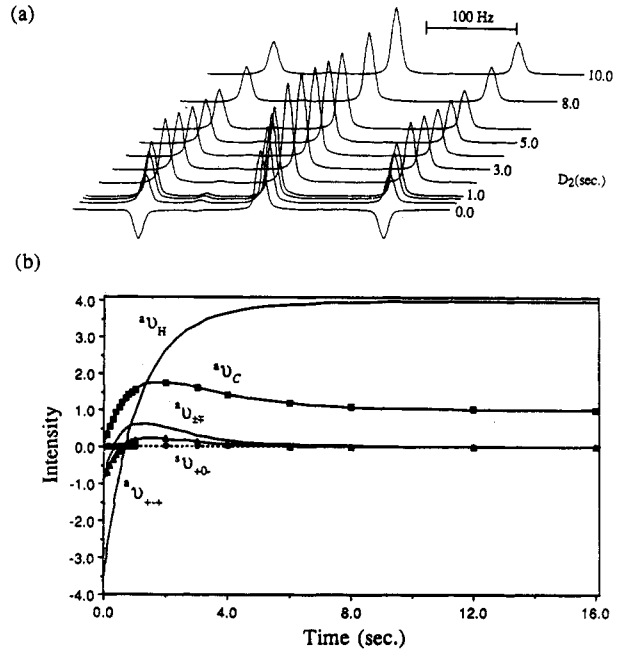

Figure 10. (a) A series of partially relaxed ^{13}C spectra obtained at various times, D_2, after application of the ^{-}J pulse sequence shown in Figure 11 to the labeled carbon of $CH_3(CH_2)_8{}^{13}CH_2OH$. The data were obtained in deuterated diglyme at 273 K. (b) Experimental values of magnetization modes taken from these spectra compared to the values predicted by the nonlinear least-squares fit of the relaxation model discussed in the text.

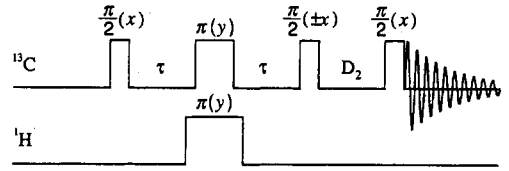

Figure 11. The J pulse sequence used to obtain maximum initial excitation of $^{a}v_{+-+}$. The ^{+}J and ^{-}J forms of the experiments are determined by setting the phase of the second $\pi/2$ carbon pulse to $+x$ or $-x$, respectively, $\tau = 1/(4J_{CH})$, and D_2 is arrayed so as to monitor the relaxation process.

multiplet magnetization vectors have evolved to an antiphase configuration along the y axis (i.e., the inner and outer lines are 180° out of phase). A $(\pi/2)_{+x}$ pulse for the ^{+}J pulse or a $(\pi/2)_{-x}$ pulse for the ^{-}J pulse then rotates the carbon magnetization to the z direction. At this point the system is allowed to relax for a time, D_2, after which a final $(\pi/2)_{+x}$ carbon observation pulse is applied to convert the resulting longitudinal magnetization into transverse magnetization to obtain the FID. An array of D_2 values monitors the time-dependent return of the magnetization to thermal equilibrium. To minimize the accumulation of systematic errors, the preparation and read pulses along with the receiver phase are independently cycled through the four quadrature phases to produce a 16-step phase cycle. The two J spectral experiments, though related, yield $^{a}v_{+-+}$ magnetizations that are opposite in sign (compare Figures 9 and 10). It is noteworthy that the $^{a}v_{+-+}$ in the ^{-}J pulse experiment goes through a positive excursion before decaying back to zero. Similar dramatic multiple exponential behavior is also exhibited by $^{a}v_C$.

The boundary conditions for these two J pulse experiments can be summarized together as follows:

$$
{}^{a}\mathbf{v}(0) = \begin{bmatrix} \Delta\alpha_{\pm1} \\ -G\alpha_{\pm2} \\ \pm\alpha_{\pm1} + \delta_{\pm1} \\ \pm\alpha_{\pm1} + \delta_{\pm1} \end{bmatrix} \quad {}^{a}\mathbf{v}(\infty) = \begin{bmatrix} 1 \\ G \\ \delta_{\pm1} \\ \delta_{\pm1} \end{bmatrix}
$$

$$
{}^{s}\mathbf{v}(0) = \begin{bmatrix} \Delta\alpha_{\pm2} + \delta_{\pm2} \\ 0 \\ 0 \\ 0 \end{bmatrix} \quad {}^{s}\mathbf{v}(\infty) = \begin{bmatrix} \delta_{\pm2} \\ 0 \\ 0 \\ 0 \end{bmatrix} \tag{91}
$$

The $\alpha_{\pm2}$ represents the efficiency of the proton 180° refocusing pulse, $\alpha_{\pm1}$ is the overall efficiency with which the J pulse sequence generates the magnetization observed in the carbon spectrum. The other parameters are defined analogously to the previous experiments. Again, if $\Delta\alpha_{\pm2}$ affecting $^{s}v_{+0-}$ is zero in an optimal experiment, then only the antisymmetric manifold will be relevant to the fitting. All four antisymmetric modes in this set of experiments are displaced significantly from their equilibrium values and, therefore, should reveal information on all significant relaxation pathways. The symmetric manifold shows no perturbation in either Figure 9 or 10 indicating that the J spectral pulses are effective only in the antisymmetrical manifold. While this information is important in assessing the quality of the experiment it is not used in the fitting program.

5. The Importance of Diverse Spin Perturbations

The accuracy with which the various spectral densities can be measured from the above set of experiments is obviously limited by the overall signal-to-noise in the various ^{13}C spectra from which the line intensities are determined. However, the accuracy of any given power density can be further enhanced or degraded by the nature of the experiments used to perturb the spin system from equilibrium. Failure to adequately perturb a given mode may leave some of the relaxation channels unutilized. If certain spectral densities appear only in the relaxation matrix elements corresponding to these poorly utilized channels, they also will be poorly determined. In early AX_2 studies only three experiments (namely, the proton soft pulse, the proton hard pulse, and the standard ^{13}C inversion-recovery experiments) were used to perturb the spin system from thermal equilibrium (see for example Mayne et al.[66]). As a consequence a maximum perturbation is created for the $^{a}v_C$, $^{a}v_H$, and $^{s}v_{+0-}$ modes. However, considerable benefit can be realized in perturbing the $^{a}v_{+-+}$ mode from its thermal equilibrium state using the $^{\pm}J$ pulse sequence discussed above. Significant improvement in the accuracy of determining the relaxation parameters was achieved by adding data from the $^{\pm}J$ pulse experiments,[140] and the marginal standard deviations for $J_{HH'}$ and j_H are reduced accordingly. These improvements are realized because unfavorable correlations between the pairs $(J_{HH'}, j_{HH'})$ and $(j_H, j_{HH'})$ are reduced. Inclusion of $^{\pm}J$ pulse data also results in more rapid convergence of the computer fitting procedure. The perturbation created for the $^{a}v_{+-+}$ and $^{a}v_{\pm\mp}$ modes with the $^{\pm}J$ pulses, particularly at short times, emphasizes relaxation channels in the coupled differential equations with a stronger dependence on j_H and $j_{HH'}$ as may be

noted in (64). Further improvement in the determination of the proton power densities would likely follow from the availability of proton magnetization data. Unfortunately, the strong proton resonances due to ^{12}C molecules usually interfere with the direct use of proton multiplet data.

B. The Computer Fitting Programs

The problem of extracting values for the spectral densities from the relaxation data consists of, first, solving the differential equations under the appropriate boundary conditions for the experiments performed and, second, using nonlinear regression techniques to fit these solutions to the experimental data. Both of these steps must be accomplished numerically, and a fairly powerful digital computer is required to complete the task in a reasonable time. In order for the regression analysis to fix the values of all the relevant spectral densities, experiments using a variety of boundary conditions must be regressed simultaneously. The results shown in Figures 6–10 were obtained by regressing all the data shown simultaneously. Decatur et al.[46] have explored this complication of coupled relaxation in some detail for some of the two spin cases involved in their work. The regression analysis produces a covariance matrix giving an estimate of the errors in the values of the parameters. One must also examine the residuals, i.e., the differences between the computed and the experimental values of the data, for systematic errors indicating aspects of the data not explained by the relaxation equations. Certain practical considerations require the introduction of additional parameters to reduce these systematic errors to acceptable levels. Our normal criterion is that the systematic component of the residuals must be less than or at least not much greater than the random component.

1. Instrumental Fitting Parameters

A variety of parameters other than the spectral densities are incorporated into the fitting routines to accommodate the instrumental imperfections in the experiments. For example, each separate experiment included in the fitting procedure must have its own intensity scaling parameter, k_i, given, for example, in (42) and (56) to model the effects of amplifier gain and the other arbitrary variations in the instrumental measurements. Imperfections in the perturbing pulse also need to be introduced in the boundary conditions for the several experiments discussed in section V.A. For example, the limitations on creating an idealized 180° spin inversion are parameterized with an α_i. These values, which approach unity for perfect spin preparations, should be at least above 0.9 for a well-executed experiment. The $\Delta\alpha_i$ are also pulse imperfection parameters normally taken to be zero and often associated with the symmetric manifold when the symmetric modes are unintentionally perturbed from equilibrium. They are given in (88) to (91) to allow for inclusion of data from slightly less than optimized experiments. When the $\Delta\alpha_i$ become appreciable this indicates that serious problems exist in the experiment and may indicate that such data should be excluded from the fitting procedure. Finally, a set of parameters, δ_i, is introduced to account for the instrumental distortions of the various triplet lines that appear even in the equilibrium multiplet structures. For example, when one measures the thermal equilibrium carbon spectrum of a $^{13}CH_2$ group, the intensities may differ by a few percent from the expected 1:2:1 ratio, and this imperfection will produce clearly discernible systematic errors in the residuals. In a perfect experiment the δ_i would be zero, and, therefore, these parameters also must be small if the instrument is operating under favorable conditions.

2. Historical Evolution of the Fitting Programs

It is appropriate to summarize briefly the development of computer programs used in the fitting procedures. The sophistication of these codes evolved as newer concepts emerged and improved experimental methods provided better data. The initial AX_2 fitting program, recorded in Mayne's thesis,[142] was written in the early 1970's. This code, which is no longer extant, ignored the random field cross terms given in (34) and (35). It also incorporated only an approximate treatment for the observation of the ^{13}C inversion recovery under proton decoupling.[66] The decoupling approximation worked well in this simple decoupled inversion recovery experiment because only the Γ_{11} and Γ_{12} terms tend to influence the recovery of $^{a}\nu_C$ under NOE steady-state condition. This initial code was similar to a program prepared in the late 1970's by Prestegard and Fuson,[143] and the two codes gave comparable fits on the same data.

The second Utah code, referred to as the line intensity fitting (LIF) routine, was prepared towards the end of the 1970's and described by Chenon et al.[144] The LIF code treated individual line intensities rather than magnetization modes as the dependent variables of the equation of motion and, differing appreciably in its structure from the initial fitting programs, it was used as an independent confirmation of the accuracy of other existing codes. The manner in which boundary conditions are incorporated in the LIF is different, and an alternative set of library routines for matrix manipulation was used.

A new code, entitled the magnetization mode fitting (MMF) routine was created in the late 1970's using REDUCE, a computer program for doing symbolic mathematical manipulations, to derive the relaxation equations and boundary conditions with decoupling. The output of REDUCE included FORTRAN codes for the MMF program. The MMF program, compared in the work of Chenon et al.[144] with the results of the LIF method, exhibited satisfactory agreement between the two programs. The discrepancies between the MMF and LIF program in the $^{13}CH_2Cl_2$ work were sufficiently minor that they were attributed to rounding errors. The sets of parameters obtained from the two programs generally agreed within their estimated marginal standard deviations. The MMF routine uses the magnetization modes of (55) and (56) and may therefore be used to fit molecules dissolved in either isotropic or anisotropic fluids.

VI. Diffusion in Rigid and Flexible Chain Molecules

Carbon-13 magnetic resonance (CMR) relaxation methods, historically, have provided a powerful technique for studying molecular dynamics in organic com-

pounds,[145] but coupled spin methods have greatly enhanced the motional information available from such studies. A reasonably good variety of small to medium molecules have now been studied in low viscosity liquids, including $^{13}CH_2(CN)_2$,[84] $^{13}CH_2I_2$,[65] $^{13}CH_2Cl_2$,[83,144,146] various chlorobenzenes,[96-99,147] cyclopropane,[148] cyclopropanone,[55] nonane,[149] and 1-decanol.[140,141] Coupled spin relaxation measurements also have exhibited very high promise in solutions of biomolecules,[150,151] and other macromolecular systems.[152-154] In these larger molecules internal degrees of motional freedom are very important to an adequate discussion of the molecular dynamics and, hence, to spin relaxation. Molecules dissolved in anisotropic media such as nematic phases exhibit more resolved transitions for simple spin systems due to the incompletely averaged first order dipole–dipole couplings. Motional constraints imposed by this anisotropic lattice provide very interesting systems for dynamic studies, and a number of workers have explored such systems.[29,34,35,155-157] Relaxation measurements in anisotropic media provide correlation information on both spatial and orientational relationships affecting the molecular motion. Data on rigid methylene halides and the flexible chain molecules, nonane and 1-decanol, illustrate the types of molecular dynamical information that is available in coupled spin studies.

A. Rigid Methylene Halide Molecules

The first extensive longitudinal relaxation study of a coupled AX_2 system involved the measurement of magnetization modes as a function of time for methylene iodide, $^{13}CH_2I_2$.[66] Following the prescription outlined above, values for the four dipolar spectral densities (J_{CH}, J_{HH}, J_{CHH}, J_{HCH}) and two random field terms, (j_C and $j_H = j_{HH}$) under extreme narrowing conditions were extracted from the time development of the magnetization modes. The spin system was prepared using the carbon hard pulse, proton hard pulse, and proton soft pulse. Data under full proton decoupling for a standard inversion recovery experiment and for an evolution of the system from thermal equilibrium to a fully developed NOE were also included in the least-squares analysis in the methylene iodide study. When this work was done in the early 1970's, equipment capable of gating the decoupler on and off during various parts of the pulse sequence was generally unavailable, so only the total carbon magnetization was obtained from the latter two experiments. Under these conditions the transient behavior of the $^a\nu_C$ mode is essentially controlled by Γ_{11}. Later, data on $^{13}CH_2Cl_2$ were obtained under similar conditions to those of $^{13}CH_2I_2$ except that instrumental development by this time allowed gated decoupling data to be acquired.[144,146] Both methylene halides had a ^{13}C spin enrichment of about 90%, and their concentration is 13.5 mol % for $^{13}CH_2I_2$ in perdeuterobenzene and is 8.3 mol % for $^{13}CH_2Cl_2$ in carbon disulfide solution. Typical values of the dipolar power densities for these two methylene halides are contained in Table III.

At the time the data in Table III were taken, the auto-correlated, j_H, and cross-correlated, j_{HH}, random field terms were treated as equal, i.e., random fields at the positions of the two protons were assumed to be fully correlated. Therefore, only a single value for j_H and j_{HH} is reported. This locking of the two terms together produced no apparent systematic discrepancies in the fits. Several trends may be noted in the data of Table III. First, the power densities for the $^{13}CH_2I_2$ molecule are larger than $^{13}CH_2Cl_2$ at the same temperature as might be expected for a molecule with larger moments of inertia and a larger cross-section for interaction with the solvent. Besides larger dipolar J's in $^{13}CH_2I_2$, the relative magnitudes of the four dipolar J's form a reasonably consistent pattern for both $^{13}CH_2I_2$ and $^{13}CH_2Cl_2$. For example, the ratios of J_{CH}:J_{HH}:J_{CHH}:J_{HCH} are quite similar for $^{13}CH_2I_2$ (4.71:3.43:2.86:1) and $^{13}CH_2Cl_2$ (3.45:3.24:2.43:1) even though the overall magnitudes for the $^{13}CH_2I_2$ dipolar J's are 3 to 4 times larger than those for $^{13}CH_2Cl_2$. One must lower the temperature on $^{13}CH_2Cl_2$ by about 80 degrees to have comparable motional regimes for the chlorine molecule relative to that of the iodine. This difference will be influenced by changes in the solvent due to variations in viscosity and the extent of slip versus stick boundary conditions governing the hydrodynamics.

TABLE III. Methylene Halide Spectral Power Densities[a]

power densities[a]	$^{13}CH_2Cl_2$[b] 193 K	233 K	272 K	309 K	$^{13}CH_2I_2$:[c] 300 K
J_{CH}	15.6	7.4	4.4	3.3	10.0
$J_{HCH'}$	4.1	1.6	1.0	0.7	2.0
$J_{HH'}$	13.1	6.1	3.4	2.4	9.4
$j_{CHH'}$	10.1	4.8	2.8	2.0	6.8
j_C	~0	~0	1.3	2.0	15.1
$j_H - j_{HH'}$	3.2	1.4	1.2	1.1	3.4

[a] All values of J are given in ks^{-1}. To obtain units of s^{-1} multiply all values for J's by 10^{-3}. [b] Chenon, Bernassau, Mayne, and Grant (ref 144). [c] Mayne, Alderman, and Grant (ref 66).

The significant values measured for the two cross-correlated power densities, J_{CHH} and J_{HCH}, clearly indicate the importance of multispin cross terms in the spatial correlation functions used in coupled spin systems and documents the inadequacies of traditional relaxation studies that ignore these terms. Thus, the historically prominent proton decoupled carbon inversion recovery experiments leave most of the relaxation information undetermined.

The random field terms also show significantly larger values for $^{13}CH_2I_2$ relative to $^{13}CH_2Cl_2$, i.e., $j_C(^{13}CH_2I_2)/j_C(^{13}CH_2Cl_2) = 7.5$. Two possible explanations for this difference are that the spin-rotation relaxation is more efficient in $^{13}CH_2I_2$ because the R_{zz} reorientational motion about the I–I or z axis is more persistent thereby increasing the spin-rotation correlation time, τ_{sr}. This change in τ_{sr} would increase the spin-rotation contribution. Spin rotation in methyl groups has been studied in a variety of systems and the principles are discussed in these works.[85-87,158-160] Also, it is known that the scalar coupling between ^{13}C and the quadrupolar ^{127}I provides a more efficient relaxation mechanism than does that between ^{13}C and the quadrupolar Cl magnetic isotopes. The decline of j_C as the temperature is lowered in $^{13}CH_2Cl_2$ further indicates the importance at higher temperatures of the spin-rotation mechanism in $^{13}CH_2Cl_2$. Note, at the two lowest temperatures $j_C \approx 0$ and the relaxation of the ^{13}C nuclide is dominated totally by dipolar relaxation terms. Recently, Chenon, Coupry and Bernassau[83] have studied $^{13}CH_2Cl_2$ in deuterated and protonated solvents to de-

TABLE IV. Rotational Diffusion Constants in Methylene Halides

rotational diffusion constant[a]	$^{13}CH_2Cl_2$[b]				$^{13}CH_2I_2$:[c]
	193 K	233 K	272 K	309 K	300 K
R_{xx}	0.03	0.06	0.12	0.17	0.06
R_{yy}	0.03	0.07	0.11	0.15	0.02–0.04
R_{zz}	0.18	0.34	0.59	0.76	0.29
ρ_x	0.17	0.18	0.20	0.22	0.21
ρ_y	0.17	0.21	0.19	0.20	0.08

[a] All values of R are given in units of ps^{-1}. To obtain units of s^{-1} multiply all values by 10^{12}. [b] r_{CH} in $^{13}CH_2Cl_2$ is 1.08 Å. Relative errors are about $\Delta R_{xx} \approx 6\%$; $\Delta R_{yy} \approx 15\%$; $\Delta R_{zz} \approx 3\%$. [c] r_{CH} in $^{13}CH_2I_2$ is 1.09 Å. Relative errors are about $\Delta R_{xx} \approx 20\%$; $\Delta R_{yy} \approx 60\%$; $\Delta R_{zz} \approx 6\%$.

termine the relative importance of the intra- and intermolecular dipolar mechanisms for this molecule. They conclude that the coupled relaxation experiments yield the same values for the dynamical parameters in either case.

The small increase of j_H in $^{13}CH_2Cl_2$ as the temperature decreases argues against the dominance of spin-rotation interactions for the ^1H nuclei; this is not too surprising with the lack of p orbitals centered on the hydrogens. Instead, the increase of j_H with decreasing temperature indicates the dominance of those mechanisms that are enhanced by the slower motions occurring at lower temperatures, i.e., random intermolecular dipole–dipole interactions and proton–iodine dipolar–quadrupolar terms. The exact mechanism for j_H has not been determined, but evidently different mechanisms are required to explain the temperature dependence of j_H and j_C in $^{13}CH_2Cl_2$, as these two terms move in opposite directions with changes in temperature. Intermolecular dipole–dipole interactions from other $^{13}CH_2Cl_2$ molecules (concentration is 8–12 mol %) may relax the protons at the periphery of the molecule, but not the carbon nucleus that is at the center of the molecule. The larger gyromagnetic ratio for protons would also contribute to a more favorable random field proton–proton intermolecular interaction. The data of Table III and (83) are used to obtain the molecular dynamical parameters presented in Table IV. R_{zz} may be extracted from $(r_{CH}^6 R_{zz})$ by employing the microwave value of $r_{CH} = 1.082$[161] for $^{13}CH_2Cl_2$ and the reasonable value of $r_{CH} = 1.09$ for $^{13}CH_2I_2$. The HCH geminal angle is 111° for $^{13}CH_2Cl_2$ and 104° for $^{13}CH_2I_2$. The smaller angle for the iodine compound may be explained by repulsive effects between the bulky iodines compressing the HCH angle. The values for R_{xx}, R_{yy}, and R_{zz} and the corresponding values for ρ_x and ρ_y are given in Table IV.

A slower motional regime is clearly exhibited for $^{13}CH_2I_2$ by all three rotational diffusion constants, with consistent ratios of about 3 to 4 observed between the corresponding rotational diffusion constants in $^{13}CH_2Cl_2$ over $^{13}CH_2I_2$. Of considerable interest, is the rotational diffusion anisotropy measured by ρ_x and ρ_y, see (77). In $^{13}CH_2Cl_2$ the molecule diffuses as an effective symmetrical top with an anisotropy of about 1:5 for rotation about the perpendicular versus the parallel axis defined as the Cl–Cl internuclear vector. Errors for ρ_x and ρ_y in $^{13}CH_2Cl_2$ are sufficiently large that minor differences in these quantities can not be reliably differentiated. Chenon et al.[144] give careful attention to a discussion of the statistical significance of the several rotational diffusion parameters. While there appears to be a break in the symmetry of ρ_x and ρ_y in $^{13}CH_2I_2$ the statistical measures indicate some ill-conditioning for either R_{yy} or ρ_y that prevents a stronger statement from being made about the relative magnitudes of R_{xx} and R_{yy}. However, it is possible to measure reliably the value for R_{zz} and the large 5:1 anisotropy noted between the parallel and two perpendicular modes. The overall anisotropy of diffusional motion for both halides is remarkably similar and has an inverse dependence, at least qualitatively, with the moments of inertia for $^{13}CH_2Cl_2$ ($I_{xx} = 2.53 \times 10^{-45}$ kg m^2; $I_{yy} = 2.74 \times 10^{-45}$ kg m^2, and $I_{zz} = 2.62 \times 10^{-46}$ kg m^2)[162] and for $^{13}CH_2I_2$ ($I_{xx} = 1.22 \times 10^{-44}$ kg m^2; $I_{yy} = 1.25 \times 10^{-44}$ kg m^2, and $I_{zz} = 4.14 \times 10^{-46}$ kg m^2).[163] The relatively low moments of inertia about the z axis allow for the emergence of spin-rotation at higher temperatures.

Chenon et al.[144] explored the general validity of the small step rotational diffusion model of Favro[134] that was developed in section IV.B and then used it to obtain the diffusional parameters given in Table IV. They concluded that "inertia effects make a large but not major contribution to the motion at higher temperatures; however, inertial influence can be considered negligible" at lower temperatures, thereby justifying the small step diffusion assumptions used in the formulation of the Favro equation. These workers also discussed several aspects of the Stokes–Einstein hydrodynamic theories used to characterize the frictional drag associated with the molecular rotational diffusion. They concluded that only modest amounts of stick versus pure slip interfacial interaction is needed to explain the data.

Knauss, Evans, and Grant[164] used Brownian dynamics, BD, simulations based on a simple Langevin equation and on the Stokes friction law to estimate the rotational diffusion of methylene halides. (This work[164] contains additional relevant background literature.) For $^{13}CH_2Cl_2$ this approach underestimates R_{zz} slightly but overestimates by a comparable amount the values of R_{xx} and R_{yy}. The cancellation of these two deviations gives a reasonable theoretical estimate for the average rotational diffusion constant. The estimates of the anisotropies, ρ_x and ρ_y, are reasonable but somewhat smaller than the experimental values of Table IV. The theoretical BD results are in somewhat better agreement with the $^{13}CH_2I_2$ rotational diffusion anisotropies. Considering the rather crude approximations and simplified molecular mechanics used in the simulations, one is left with the conclusion that many of the essential elements of the hydrodynamics must have been captured by these simulations. The success of these theoretical efforts provided encouragement that reorientational motional features could be theoretically treated in flexible chain molecules where relaxation arising from segmental motion associated with internal degree of freedom is present. This initial effort provided a theoretical foundation for the work on nonane and 1-decanol to be briefly reviewed in the next section.

B. Flexible Aliphatic Chain Molecules

1. Labeled n-Nonane, n-Heneicosane, and 1-Decanol

Spin–lattice relaxation in a chain molecule may result both from overall rotation of the molecule as a rigid body and from internal segmental motion involving only

TABLE V. Methylene Spectral Densities in Alkyl Chains

power densities	1-decanol (273 K) C-1	C-5	C-9	nonane (273 K) C-2	C-5	nonane (313 K): C-5	heneicosane (313 K): C-11
J_{CH}	93	117	59	49	63	26	110
$J_{HH'}$	85	100	66	45	65	28	98
$J_{HCH'}$	−1.3	27	4	7	22	9	40
$J_{CHH'}$	54	79	36	34	47	19	82
j_C	~0	~0	~0	~0	~0	~0	~0
$j_H = j_{HH'}$	43	94	27	19	5	2	15

a limited number of atoms in the chain. For short chain molecules like butane, the overall rotational diffusion is sufficiently rapid according to BD simulations that it dominates internal motions. For medium-size molecules like *n*-nonane and 1-decanol, the conformational flexibility of the chain is rich enough to allow local segmental motion to be comparable with overall motion in its effect on the spin–lattice relaxation. Thus, both the overall and internal motions become important in these molecules. In very long chain molecules (e.g., polymers), the overall molecular tumbling motion becomes very much slower and usually totally ineffective in the relaxation process. There is, of course, the question of whether one may even consider overall motion independent of developing segmental motions in polymers because the various Cartesian motional modes[136] do not appear to be influenced by the molecular weight once the systems reach a critical size.[153,154] In intermediate-size molecules, spin-relaxation measurements are affected both by overall rotational diffusion and segmental motion and have a sufficiently large dynamic range, fortunately, to address information obtained over extended time regimes. As motion shifts from rotational diffusion in small molecules to segmental motion in long chain molecules the values of the spectral power densities respond accordingly.

Table V contains dipolar and random field power densities for a labeled $^{13}CH_2$ spin moiety placed at the middle of the chains and at the penultimate atom near each end of the molecule for *n*-nonane and 1-decanol. The labeled methylene in heneicosane was in the middle position of the 21 carbon linear chain. Selected data at 273 and 313 K are merely representative of extensive information acquired by Brown et al.[149] and by Liu et al.[165] on the two alkanes and 1-decanol, respectively. In each case the j_C was found to be negligible and the j_H and j_{HH} tended to be both small and equal in the two hydrocarbons. A possible explanation for the considerably larger *j*'s in the alcohol is the possible existence of minor complexation with paramagnetic metal impurities. The fitting programs found evidence only for $j_H \cong j_{HH}$.

One cannot help noting the similarity of dipolar terms at C-2 in nonane and C-9 in 1-decanol. Both methylenes appear next to the end of a reasonably long alkyl chain and exhibit almost identical dipolar power density profiles even though their random field terms differ significantly. Apparently the effect of the hydroxyl group is essentially fully attenuated by a continuous chain of nine aliphatic carbon atoms. Comparison of the three mid position carbons reveals variations in the magnitudes of spectral densities at C-5 in nonane, C-5 in 1-decanol, and C-11 in heneicosane. The anchoring effect of the hydroxyl group in 1-decanol increases all the *J*'s at C-5 relative to those at C-5 in nonane. Likewise, the effect of higher molecular weights in heneicosane is to increase markedly the four dipolar *J*'s at C-11. Perhaps in a molecule such as heneicosane the concept of local order[32] may be relevant, but the necessary frequency-dependent data on heneicosane that could address this possibility is still unavailable. The molecular mechanics, however, contained in section VII does implicitly include such concepts of local order. Nonane C-5 is recorded twice in Table V at 273 and 313 K to provide comparisons both with the 1-decanol and heneicosane samples, respectively. The differing physical properties of heneicosane and 1-decanol make accessible temperature ranges different for the two molecules. It is somewhat interesting that the 40-degree difference between the data for C-11 in heneicosane and for C-5 in 1-decanol leave the profiles of these two sets of values almost the same. Finally, the profile of power densities for C-1 in 1-decanol appears to be uniquely different from any of the other molecules studied. This uniqueness is attributed to the anchoring effect of the hydroxyl group as it participates in hydrogen bonding.

The dipolar spectral densities transformed into Cartesian power densities provide a set of standard second rank auto-correlation times. These times defined by (87) are linked to the experimental power densities that are given in Table VI. The ill-conditioned τ_{xx} values may be expected to be similar to τ_{yy} and are averaged with τ_{yy} or omitted if inordinately large errors are indicated (e.g., τ_{xx} for C-2 in nonane) to give a $\tau_\perp$. As slower motions or longer τ values tend to enhance the dipolar mechanism these correlation times describe the anisotropic motional features of dipolar spin relaxation. In each instance the values follow the pattern $\tau_{zz} > \tau_\perp(\overline{\tau_{xx},\tau_{yy}}) > \tau_{xy}$. Thus, it is the longtime τ_{zz} correlation time that is of greatest interest in dipolar relaxation. This correlation function characterizes the reorientation of the *z* axis lying generally along the longer axis of the alkyl chain and perpendicular to the HCH plane.

Motions related to the R_{xx} and R_{yy} rotational diffusional motions impact τ_{zz}. Likewise, rotational reorientation related to R_{zz} about the *z* axis influences τ_{xx}, τ_{yy}, and τ_{xy}. Only τ_{xy} is affected by reorientation about all three Cartesian axes. Therefore, its correlation time is the shortest. Ratios of $\tau_{zz}:\tau_\perp(\overline{\tau_{xx},\tau_{yy}}):\tau_{xy}$ are given in the last row of Table VI. Note, the middle carbons (C-5 in 1-decanol; C-5 in nonane; C-11 in heneicosane) all exhibit similar respective profiles (i.e., 3.9:1.5:1; 4.9:2.2:1; 5.1:2.2:1). Thus, the relative τ values defining motional

TABLE VI. Cartesian Correlation Functions for Alkyl Chains

correlation times	1-decanol (273 K) C-1	C-5	C-9	nonane (273 K) C-2	C-5	nonane (313 K): C-5	heneicosane (313 K): C-11
τ_{xy}	13	12	8	6	6	2.3	9
$\tau_\perp$	19	18	16	9	13	6	17
τ_{zz}	31	47	20	16	28	13	48
$\tau_{zz}:\tau_\perp:\tau_{xy}$	2.4:1.5:1	3.9:1.5:1	2.5:2.0:1	2.9:1.7:1	4.9:2.2:1	5.6:2.6:1	5.1:2.2:1

anisotropies establish patterns that are remarkably similar even though overall motion varies by 2- or 3-fold between the different molecules. Likewise, for C-9 in 1-decanol and C-2 in nonane a similar pattern (i.e., 2.5:2.0:1 versus 2.9:1.7:1, respectively) is found for these two related carbon atoms. The final pattern (2.4:1.5:1) for C-1 in 1-decanol again is similar to C-9 in decanol and C-2 in nonane, but the overall magnitudes of the correlation times are unique for C-1, indicating the importance of hydrogen bond formation. It would appear that overall rotational diffusion controls the magnitude of the J's with overall motion restricted both by hydrogen bonding and molecular bulk. Furthermore, the local anisotropies measured by the ratios of $\tau_{zz}:\tau_{\perp}(\tau_{xx},\tau_{yy}):\tau_{xy}$ would seem to be controlled by internal segmental motions as these ratios are often similar even when the magnitudes vary appreciably. As Table VI involves only limited amounts of temperature data for a single solvent, the reader is referred to recent literature[149,165] for a full discussion of both of these effects.

A comparison of the complete nonane and 1-decanol relaxation data illustrates the importance of solvent–solute interactions. The hydroxyl group in 1-decanol can form hydrogen bonds with oxygen-containing solvent molecules such as diglyme but cannot do so in other nonpolar solvents.[165] The variation in the anchoring effect of a terminal hydrogen bond upon different carbons along the chain provides information that can be used to address the structurally dependent features of both segmental and overall motions.

The dipolar spectral densities normally decrease as the temperature increases. Even so, for typical temperature ranges used in $^{13}CH_2$ coupled relaxation studies, the dipole–dipole interactions either dominate or are at least one of the principal mechanism for spin relaxation. For higher temperatures, however, the types and rates of various molecular motions increase, quenching the efficiency of the dipolar interactions and reducing the magnitude of the dipolar spectral densities. The intrinsic measurement errors appear to remain at about the same level with changes of temperature making the dipolar measurements relatively more accurate at lower temperatures. Unfortunately, the solubility of many compounds places a lower limit on the experimental temperatures that can be achieved. In many analyses of chain molecules, it is possible to lock j_C to zero since its fitted value seldom exceeds one marginal standard deviation from zero. This supports the obvious conclusion for chain molecules that ^{13}C spin-rotation contributions are unimportant, unlike the methylene halides. As tetrahedral carbons never appear at the periphery of a paraffin molecule, one also would not anticipate significant intermolecular dipolar contributions to j_C. The csa of paraffin carbons is also low making contributions from this mechanism small, at least at the fields used to date.

If only overall molecular motion contributes to the relaxation of the local modes, Cartesian correlation times at different chain positions should remain the same. However, the correlation times at the center carbons (C-5 in *n*-nonane and C-5 in 1-decanol) are always larger than for the penultimate carbons (C-2 or C-8 in nonane and C-9 in 1-decanol). Apparently these latter carbons enjoy greater motional freedom. For the motion of hydrocarbon chains in solution, two major factors affect the rate-determining processes. One is the energy barriers restricting conformational isomerization, and the other is the frictional force exerted by the surrounding solvent. The larger the volume that is needed to accommodate the motion of a solute molecule, the larger will be the effect of friction due to solvent molecules that must rearrange to accommodate the molecular motion of the solute. Based on this argument, smaller groups (i.e., –OH or $-CH_3$) attached at C-1 or C-9, respectively, can reorient relatively more easily than the longer chain segments attached to C-5. The experimental results are consistent with this intuitive steric concept, although the relative importance of the steric effect versus the hydrogen bond anchoring effect requires additional experimental information.

In 1-decanol, the relation, τ(C-5) > τ(C-1) > τ(C-9), exists for most of the Cartesian modes except that of C-1 in the solvent ethanol where an extensive hydrogen-bond network at the –OH group more firmly anchors this $^{13}CH_2$ group. The hydrogen-bonding network increases the rigidity of the C-1 carbon in 1-decanol due to increased solvent packing around the hydroxyl end of the 1-decanol chain. These effects result in significant changes in the correlation times for certain Cartesian modes. The deviation between τ(C-1) and τ(C-9) may be rationalized from the hydroxyl anchoring effect at C-1 and the different torsional potentials for C–C–C–C and C–C–C–OH linkages.

A study of Table VI indicates that the carbons at the middle of these chain molecules exhibit a higher anisotropy than do the end carbons. Preferential rotation around the long axis of an all-trans conformation of these molecules does not require large displacements of the backbone or of the solvent molecules with the attendant high frictional drag. At the penultimate carbon, local isomerization between conformations plays a more important role in the relaxation processes.

As noted earlier, very small chains are dominated by overall rotational diffusion. The flexibility of longer chains becomes pronounced due to the rapidly increasing number of conformations, and local segmental motion plays an even more important role in the relaxation processes. Therefore, there are significant differences in the motional processes as the degree of conformational freedom changes between small molecules and polymers. The conformational transition about a single bond can take place more readily in either small molecules or near the ends of long molecular chains. A carbon atom near the center of a long chain molecule will tend to reorient with isomerization transitions involving more than one C–C bond. Concerted motion with adjacent bonds is required otherwise central segments of the chain, if held rigid, could only undergo large motional displacements, and even in a relatively low viscosity solvent, an enormous frictional resistance would be exerted by the solvent on the solute. Such exceedingly slow motion, with a rate dependence on molecular size, is in contradiction to existing experimental results. Intuitively, it is therefore easy to see that most long chain conformational transitions should be cooperative, involving conformational changes in several proximate carbon–carbon bonds.

One way to avoid large displacements of the long chains attached to the rotating bond is to have neigh-

boring bonds undergo compensating transitions within a relatively short time interval of each other. The "crankshaft" model, proposed by Schatzki,[166] allows terminal groups on both ends of a long chain molecule to remain at roughly their same positions while bonds in the internal parts of the molecule undergo concerted conformational transitions. Neither translational nor rotational motion is required by this mechanism for the terminal groups. The crankshaft motion discussed by Jelinski et al.[167] involves correlated motion of five bonds and six atoms. This type of transition was shown to be important in polyesters containing butanediol. The other two types of "crank-like" conformational transitions, proposed by Helfand,[168–170] include gauche migration ($g^+tt \leftrightarrow ttg^-$) and pair gauche production ($ttt \leftrightarrow g^+tg^+$), and involve cooperative motions of three bonds. The counter rotation about parallel bonds of nearest neighbors does not require large-scale displacement of the remainder of the chain.

To extract the full value from the extensive correlation information, both magnitudes and anisotropies, it is necessary to make theoretical simulations of these motion-dependent parameters using standard molecular mechanics. In this way valuable insights into the potential functions controlling chain conformations and structures may be obtained on otherwise complex molecular systems. Information on the appropriate fluid frictional laws of Stokes also are contained in such simulations. Finally, successful modeling of 1-decanol requires critical information on the degree of intermolecular associations arising from hydrogen bonding. The following section presents relatively early work on molecular modeling of these features and how they affect nuclear spin relaxation.

VII. Statistical Mechanical Modeling of Chain Motion

A. Brownian Dynamics—Langevin Equations

Several classes of generalized Langevin equations, GLE, have been rigorously derived[171] to describe the motion of an interacting many-body system, $\boldsymbol{S}$, in a heat bath, $\boldsymbol{L}$. The fundamental assumption in deriving these GLE's is that the total interaction energy, $\boldsymbol{H}_{SL}$, between $\boldsymbol{S}$ and $\boldsymbol{L}$ is a scalar c number that is a function of time only. The constrained molecular dynamics (CMD) simulations[172] are found to produce structural and dynamical properties in liquids in good agreement with the exact MD method as long as the number of particles in $\boldsymbol{S}$ is not very small (i.e., greater than about 10). This condition is met by nonane and 1-decanol. In a dilute solution, the GLEs for a *single* solute molecule with $N + 1$ interacting beads can be written as[171]

$$\frac{d\mathbf{r}_i(t)}{dt} = \mathbf{v}_i \tag{92}$$

$$m_i \frac{d\mathbf{v}_i(t)}{dt} = \mathbf{P}_i(t) + \mathbf{F}_i(t) + \mathbf{R}_i(t) \quad i = 1,2,\cdots,N+1 \tag{93}$$

where $\mathbf{r}_i$ and $\mathbf{v}_i$ are the Cartesian displacements and velocities of bead i in a laboratory-fixed frame, $\mathbf{R}_i(t)$ is a random force with vanishing mean, and $\mathbf{P}_i(t)$ is the mutual potential forces between bead i and all the other molecular beads. It may incorporate potentials of mean force due to the static interaction with the solvent.[171] The friction force $\mathbf{F}_i(t)$ is given by

$$\mathbf{F}_i(t) = -\int_0^t d\tau \xi_i(\tau) m_i \mathbf{v}_i(t-\tau) \tag{94}$$

In the ordinary Langevin equation (OLE) description, a Dirac δ-function is used for the memory kernel, $\xi_i(t) = \xi_{i0}\delta(t)$.

B. Fluctuation–Dissipation Processes

Upon neglecting the correlation between $\mathbf{P}_i$ and $\mathbf{R}_i$ the memory kernel in (94) has the following dissipation–fluctuation relation:[171]

$$6m_i k_B T \xi_i(\tau) = \langle \mathbf{R}_i(0) | \mathbf{R}_i(\tau) \rangle \tag{95}$$

The frequency-dependent friction function is obtained from the classical hydrodynamic theory[173,174] of an incompressible viscous medium. This approach works well even at the molecular level. For a sphere with radius r, the friction function for the slip boundary conditions is given by a Stokes-like relation

$$\xi(s) = 4\pi\eta_s(s) r_e \tag{96}$$

where the effective hydrodynamic radius r_e is

$$r_e = \frac{r}{1 + \frac{\eta_s}{3\eta_l}} \tag{97}$$

In (97) η_s and η_l are, respectively, zero-frequency shear and longitudinal viscosities.

The solvent viscoelastic response is dependent on a variety of relaxation mechanisms.[175] One simple model[176] considers mode relaxations as independent processes; thus, the solvent shear viscosity can be decomposed into separate terms:

$$\eta_s(s) = G_\infty \sum_j \frac{C_{js}}{\omega_{js} + s} \tag{98}$$

where G_∞ is the infinite frequency shear modulus, C_{js} and ω_{js} are, respectively, the normalized relaxation amplitude and the relaxation frequency associated with mode j. For a solvent with internal motion, the relaxation modes include overall molecular reorientation, r, cooperative isomerization, i, structural relaxation, s, and vibrational relaxation, v. Each process evolves on a distinct time scale justifying the assumption of mode independence. Depending on the interval of the dynamic processes, the memory effects of various solvent relaxation modes are manifested differently in the motion of solute molecules. In the case of trans-gauche isomerization the barrier frequency of a torsional potential, e.g., Rychaert–Bellemans (R–B) potential[177] is on the order of 10^{13} s^{-1}. This value is comparable to that of structural relaxation rates, one order of magnitude smaller than that of vibrational relaxation rates, and 1 or 2 orders of magnitude larger than rates ascribed to rotational relaxation or cooperative conformation changes. These observations are reasonable if the structural relaxation of a hydrocarbon chain solvent is determined by the local torsional motion of the solvent.

The frequency dependence of the friction function may be approximated if picosecond dynamic processes are characterized by the following function:

$$\xi(s) = 4\pi r_e G_\infty \left\{ \frac{C_{is} + C_{rs}}{s} + \frac{C_{ss}}{\omega_{ss} + s} + \frac{C_{vs}}{\omega_{vs}} \right\} \tag{99}$$

A four-parameter empirical function similar to (99) was proposed by Zhu et al.[178] based on the analysis of MD simulations.[179,180] Our derivation is based solely on the continuum fluid dynamics. The parameters in (99) depend only on the properties of the solvent and can be estimated from experimental measurements such as ultrasonic absorption and Brillouin and depolarized Rayleigh scattering.

To evaluate the dynamical parameters in (99), Sceat's formulation[176] of viscoelastic properties of *n*-alkane liquids is used in the following ansatz:

$$C_{ss} \approx 1.0 \tag{100}$$

$$\frac{C_{vs}}{\omega_{vs}} = 0.0 \tag{101}$$

$$\frac{C_{is}}{\omega_{is}} + \frac{C_{rs}}{\omega_{rs}} = 0.5\frac{C_{ss}}{\omega_{ss}} \tag{102}$$

$$C_{is} + C_{rs} \ll 1 \tag{103}$$

Equations 100–103 assume that the structural relaxation is the dominant channel in determining the frequency-dependent shear viscosity.

The random force on bead i, $\mathbf{R}_i(t)$, is composed of n parts:

$$\mathbf{R}_i(t) = \sum_{j=1}^{n} \mathbf{R}_{ij}(t) \tag{104}$$

where $\mathbf{R}_{ij}(t)$ is the force component due to the solvent relaxation mode j. As different relaxation modes are assumed to be uncoupled

$$6m_i kT\xi_{ij}(t) = \langle \mathbf{R}_{ij}(0)\cdot\mathbf{R}_{ij}(t)\rangle \tag{105}$$

where

$$\xi_{ij}(t) = \omega_{js}\,\xi_{0,ij}\,e^{-\omega_{js}t} \quad t \geq 0 \tag{106}$$

The friction coefficient $\xi_{0,ij}$ is equal to $4\pi r_e G_\infty C_{js}\omega_{js}^{-1}$. Equation 106 suggests that $\mathbf{R}_{ij}(t)$ is a wide-sense stationary stochastic process. If nonlinear couplings arise from the superimposition of a large number of weak van der Waals collisions, a Gaussian distribution for $\mathbf{R}_{ij}(t)$ is a good approximation in keeping with the so-called central limit theorem.

C. Molecular Model

A flexible-chain model, employed in the computer simulations, keep the bond lengths and geminal angles near their equilibrium positions with harmonic potentials. Various conformational states[181] are described by a set of torsional angles, ϕ_i, and governed by the R–B potential[177] for a C–C–C–C linkage and a Jorgensen potential[182,183] for a C–C–C–O linkage.[165] Exclusive volume is imposed with a Lennard-Jones 6-12 potential between beads separated further than the third nearest neighbors. The definitions of these dynamic variables are given in Figure 12.

Methylene, methyl, and hydroxyl groups are modeled as spherical beads with radius, r, deduced from the slip boundary conditions by setting the normal force to zero in the Lennard-Jones 6-12 potential with $r = (\sqrt[6]{2})\sigma$. As the spheres have radii greater than either the C–C or C–O bond lengths a considerable portion of the surface area of each bead is buried by its neighbors. These van der Waals spheres may be represented by a set of equivalent nonoverlapping spheres with smaller radii whose surface areas equal the exposed surfaces of the original van der Waals spheres.[184,185]

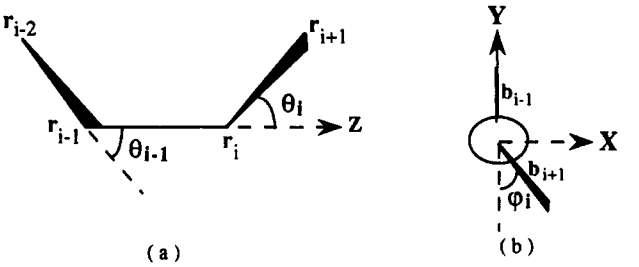

Figure 12. Schematic drawings of a portion of a chain molecule illustrating the definitions of the coordinate variables.

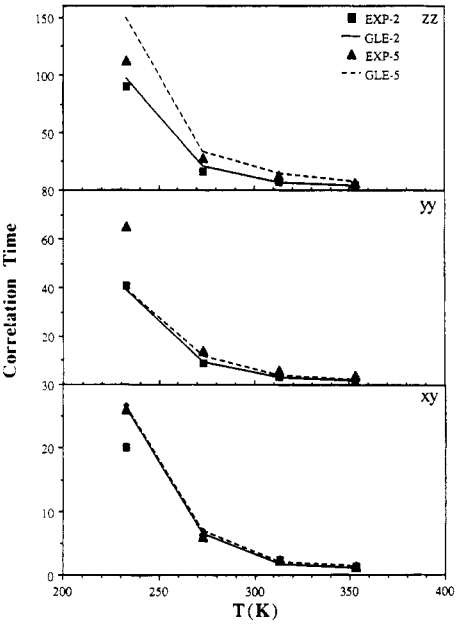

Figure 13. Comparison of the NMR experimental results with the GLE simulations at various temperatures for *n*-nonane dissolved in deuterated diglyme.

D. Comparison with NMR Experiments

Figures 13 and 14 show, respectively, the Cartesian correlation times for *n*-nonane and 1-decanol dissolved in diglyme at several temperatures. Positions C-2 and C-5 are given for nonane and C-1, C-5, and C-9 for 1-decanol. The experimental values[141,149] are compared with simulations of the Brownian motion using the approach of Xiang et al.[185] The GLE simulations give correlation times in reasonable agreement with the NMR measurements except at very low temperatures. This suggests that the coupling of the motions in the solute and solvent, which gives significantly reduced friction forces, has a measurable effect on the segmental motion of the chain molecule. As shown in a previous study,[185] the Cartesian correlation times are sensitive to changes in the solvent relaxation frequency ω_s. Therefore the NMR-coupled relaxation experiments in combination with dynamics simulations provide a useful method to determine solvent relaxation rates.

The relatively large deviation of the GLE simulation with single solvent relaxation mode for τ_{zz} = 150 ps at the central bead in nonane from the experimental re-

TABLE VII. Apparent Activation Energies for the Cartesian Modes and End-to-End Correlation Times for Nonane[a]

	method	e-t-e	*xx*	*yy*	*zz*	*xy*
overall molecule	GLE[b]	0.64 (0.18)				
	OLE[c]	0.83 (0.12)				
carbon-2	GLE[b]		1.38 (0.08)[b]	1.32 (0.14)	1.33 (0.16)	1.68 (0.27)
	OLE[c]		1.13 (0.12)[c]	0.97 (0.20)	1.16 (0.21)	0.99 (0.28)
carbon-5	GLE[b]		0.96 (0.09)	0.99 (0.12)	1.10 (0.16)	1.27 (0.19)
	OLE[c]		0.93 (0.18)	0.84 (0.21)	1.34 (0.26)	0.74 (0.29)

[a] The solvent viscosity is fixed at a constant η = 1.04 cp. [b] Obtained from the GLE simulations with $G_\infty = 1.6 \times 10^{+10}$ dynes/cm^2. [c] Obtained from the OLE simulations.

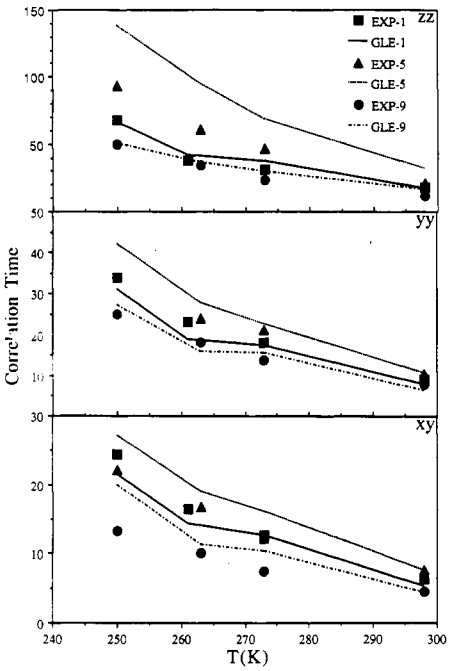

Figure 14. Comparison of the NMR experimental results with the GLE simulations at various temperatures for 1-decanol dissolved in deuterated diglyme.

sult, τ_{zz} = 113 ± 14 ps, at 233 K may be attributable to the influence of *slow* relaxation modes on the friction force and/or of solvent packing on potentials of mean force. At lower temperature more solute and solvent molecules tend to populate in the trans state. The formation of a locally ordered phase would make the cage surrounding the solute molecule sufficiently rigid to significantly "screen" the influence of rapidly fluctuating motions. Thus, slow motional modes, negligible at higher temperatures, may have a greater contribution to the frequency-dependent friction forces at low temperatures. One possible slow mode is rotational reorientation of the solvent molecules. With a normalized amplitude of 0.1, for C_r, a value of τ_{zz} = 121 ps at the central bead is obtained in our simulation.

The asymmetry of the Cartesian correlation times in 1-decanol as one moves away from the chain center arises from the differences in the torsional potentials of the C–C–C–OH and C–C–C–C linkages at each end and from a hydrogen bond anchoring effect at the hydroxyl carbon.

In contrast to the results in solvents with internal rotation the OLE simulations for 1-decanol in methylene chloride exhibit good agreement with the experimental values.[165] Methylene chloride is a solvent without internal segmental rotational modes. Thus, motion associated with the structural relaxation mode is either absent or shifted to a faster time domain. In both cases, decay of the correlation between the segmental motion in 1-decanol and the solvent motion may become so fast in comparison with the characteristic times of the motions in the solute that the OLE method becomes fully capable of providing an accurate description of 1-decanol in methylene chloride.

E. Temperature Dependence at a Fixed Viscosity

In contrast to motion in a vacuum, the temperature dependence of molecular motion in solution is partly attributed to the viscosity of the solvent. If the internal motion (i.e., isomerization transitions) dominates the overall rotation of the relaxation processes, the temperature dependence of the relevant correlation times should be Arrhenius like with an activation energy roughly equal to one barrier height between trans and gauche states. For the R–B torsional potential, the trans-gauche barrier is 2.95 kcal/mol, much larger than the thermal energy kT in the temperature range of the experimental data. By varying the temperature, while holding the zero-frequency viscosity fixed, one can determine the apparent activation energy arising from the contributions other than the solvent viscosity. These estimated activation energies for *n*-nonane from GLE and OLE simulations are listed in Table VII. Except for the slow-motion modes (i.e., the end-to-end direction and the *zz* mode at the central bead) the GLE simulations predict significantly higher apparent activation energies for the motion of all other Cartesian modes than the OLE simulations. This is apparently due to the underestimation in the OLE model of the contribution from the internal torsional motion to the relaxation of local Cartesian motion. In the GLE simulations, the reorientation of the end-to-end direction, which has the longest correlation time, requires the least amount of apparent activation energy, whereas the *xy* mode at position C-2, which has the shortest correlation time, requires the largest amount of apparent activation energy.

The effective activation energies for the Cartesian modes at penultimate beads are always larger than the corresponding modes at the central bead. This result suggests that isomerization transitions are more involved in relaxing the Cartesian modes at the outer beads than near the central bead. This result is in accord with the physical intuition that the torsional motion about end bonds can be realized by the swing of small $-CH_3$ groups and, thus, requires exclusion of only a small amount of solvent volume, whereas motion about the bonds near the center of the chain requires swings of the attached tails through large volumes thereby imposing considerable frictional drag. The cooperative motion of the nearby bonds such as the

formation of "kinks" and "jogs" as in the crankshaft rotational model[169] will facilitate torsional motion near the chain center. As this type of motion requires an activation energy of roughly one barrier height,[170] which exceeds the simulation results, it can only be assumed that the cooperative modes do not dominate the overall rotation in the structural relaxation in *n*-nonane.

Implementation of other solute-solvent interaction mechanisms may further improve the accuracy of GLE simulations. The effect of hydrodynamic interaction ignored in this study may either increase or decrease the calculated correlation times.[186,187] Its implementation in stochastic dynamics simulations requires the extension of the current hydrodynamic theories of friction forces to include both frequency-dependent viscoelastic responses of the fluid and position-dependent cross-correlation of random forces.

VIII. Conclusions

Historically, the Bloch equations were invaluable in their contribution to our understanding of the manner in which relaxation and rf irradiation combine to describe the time evolution of isolated nuclear spins that have been perturbed from their equilibrium state. As the field grew in sophistication, however, studies revealed relaxation behavior that could not be explained by this relatively straightforward approach. In typical organic systems, for example, one invariably encounters the general dominance of the ^{13}C and ^{1}H dipole–dipole interaction. This mechanism, which involves pairwise interactions among spins, requires a density matrix treatment and the associated formalism contained in this review. The experimental conditions under which the full impact of coupled spin relaxation may be observed involve perturbing and measuring the return to equilibrium of separate lines of a spin multiplet. To obtain information on the various relaxation channels available, even for relatively simple coupled spin systems, placed new demands on early workers in this field, but the benefits of such additional effort eventually proved to be of great value in the type and quality of information that may be obtained on molecular dynamics in liquids. It has been our purpose in this review to illustrate the nature of molecular motional information that is available from multiplet spin relaxation studies. The opportunity to provide intimate details of anisotropic molecular reorientation of not only rigid molecules but also of internal segmental motion in flexible chains would now seem to more than justify the additional effort of securing coupled relaxation data.

The opportunity to provide a complete dynamical profile, at least in principle, for all magnetic nuclei in a flexible molecule creates new opportunities for those interested in the effect of microscopic molecular motions and their impact on chemical and physical properties. With the emergence of two, three, and higher dimensional spectroscopy has come the realization that the same multiple relaxation pathways, important in coupled relaxation, now influence the multiple coherences common to these multidimensional experiments. The field of coupled relaxation in one dimension passed through a period of time when the unusual features encountered in these early experiments were considered more anomalies than the rule. Considerable early debate centered on the relative importance of the deviations in spin behavior due to cross-correlated interactions and the anomalous character of the data; ensuing years would seem to have proven that major multiplet spin magnetizations can indeed be induced in even simple spin systems and hopefully we have been successful in identifying some of the interesting physical and chemical features that these techniques provide on all degrees of molecular motion, both internal and overall. Recent coupled relaxation effects observed in two and higher dimensional NMR spectra would now seem to suggest that anomalous spin behavior in these interesting experiments may be more the rule than the exception. Furthermore, the spin preparations used in multidimensional NMR spectroscopy involve spectral perturbations that are similar to the experiments used to introduce magnetization into interesting relaxation channels. Thus, coupled relaxation parameters are likely to become readily available from the impressive multidimensional NMR studies now in progress on macromolecules with weights of many thousands of Daltons. The two-dimensional format provides expanded capability to obtain simultaneously information on numerous magnetic spin sites within a molecule and, therefore, have the potential to provide extensive dynamical maps of relatively large molecular systems of both industrial and biomedical importance. Our hope is that such a rich and diverse source of anisotropic motional information for numerous nuclei in a single molecule will result in the view that this type of data is a virtue to be sought after and not merely an inconvenience or a problem impeding investigators trying to extract structural information from multiplet intensities.

Acknowledgments. We wish to acknowledge the Public Health Service and the National Institutes of Health for their continued support under GM 08521-31 for over two decades of coupled relaxation efforts at the University of Utah. It is with a sense of deep appreciation that we dedicate this review to our esteemed colleague and good friend, Lawrence Glen Werbelow. Larry's indefatigable commitment to coupled relaxation for over two decades contributed greatly to the development of this field and accelerated the arrival of the present day when the use of coupled relaxation principles is rapidly becoming the norm and not the exception. As a true visionary, Larry has possessed the necessary evangelical zeal to spread the principles of spin relaxation over two continents. His contributions can only loom greater as time progresses.

References

(1) Purcell, E. M.; Torrey, H. C.; Pound, R. V. *Phys. Rev.* **1946**, *69*, 37–8.
(2) Bloch, F.; Hansen, W. W.; Packard, M. *Phys. Rev.* **1946**, *70*, 474–85.
(3) Bloch, F. *Phys. Rev.* **1946**, *70*, 460–474.
(4) Wangsness, R. K.; Bloch, F. *Phys. Rev.* **1951**, *89*, 728–739.
(5) Redfield, A. G. *IBM J. Res. Develop.* **1957**, *1*, 19–31.
(6) Abragam, A. *The Principles of Nuclear Magnetism*; Oxford University Press: Oxford, 1961.
(7) Redfield, A. G. In *Advances in Magnetic Resonance*; J. S. Waugh, Ed.; Academic Press: New York, 1965; Vol. 1; pp 1–32.
(8) Werbelow, L. G.; Grant, D. M. In *Advances in Magnetic Resonance*; Waugh, J. S., Ed.; Academic Press: New York, 1977; Vol. 9; pp 189–299.
(9) Vold, R. L.; Vold, R. R. In *Progress in Nuclear Magnetic Resonance Spectroscopy*; Emsley, J. W., Feeney, J., Sutcliffe, L. H., Ed.; Pergamon Press: Oxford, 1978; Vol. 12; pp 79–134.

(10) Canet, D. *Prog. in NMR Spectroscopy* **1989**, *21*, 237.
(11) Rose, M. E. *Elementary Theory of Angular Momentum*; Wiley: New York, 1957.
(12) Ernst, R. R.; Bodenhausen, G.; Workaum, A. *Principles of Nuclear Magnetic Resonance in One and Two Dimensions*; Oxford University Press: Oxford, 1987.
(13) Oschkinat, H.; Pastore, A.; Bodenhausen, G. *J. Am. Chem. Soc.* **1987**, *109*, 4110–11.
(14) Mueller, N.; Bodenhausen, G.; Ernst, R. R. *J. Magn. Reson.* **1987**, *75*, 297–34.
(15) Griesinger, C.; Ernst, R. R. *Chem. Phys. Lett.* **1988**, *152*, 239–47.
(16) Wimperis, S.; Bodenhausen, G. *Mol. Phys.* **1989**, *66*, 897–919.
(17) Oschkinat, H.; Limat, D.; Emsley, L.; Bodenhausen, G. *J. Magn. Reson.* **1989**, *81*, 13–42.
(18) Dalvit, C.; Bodenhausen, G. *Chem. Phys. Lett.* **1989**, *161*, 554–60.
(19) Dalvit, C.; Bodenhausen, G. *Adv. Magn. Reson.* **1990**, *14*, 1–33.
(20) Di Bari, L.; Kowalewski, J.; Bodenhausen, G. *J. Chem. Phys.* **1990**, *93*, 7698–705.
(21) Farrar, T. C.; Decatur, J. D. *J. Phys. Chem.* **1990**, *94*, 7395–401.
(22) Slichter, C. P. *Principles of Magnetic Resonance*, 2nd ed.; Springer-Verlag: Berlin, 1978.
(23) Wang, C. H.; Grant, D. M. *J. Chem. Phys.* **1976**, *64*, 1522–30.
(24) Mehring, M. *High Resolution NMR Spectroscopy in Solids*; Springer-Verlag: Heidelberg, 1976; Vol. 11, p 243.
(25) Alger, T. D.; Grant, D. M.; Liepert, T.; Mayne, C. L.; Pugmire, R. J. *J. Magn. Reson.* **1979**, *34*, 599–616.
(26) Bain, A. D.; Martin, J. S. *J. Magn. Reson.* **1978**, *31*, 301–9.
(27) Bain, A. D.; MacDonald, J. C.; Mazurek, M. *J. Magn. Reson.* **1981**, *44*, 531–41.
(28) Newmark, R. D. Ph.D. Thesis, University of Utah, 1985.
(29) Courtieu, J. M.; Mayne, C. L.; Grant, D. M. *J. Chem. Phys.* **1977**, *66*, 2669–77.
(30) Werbelow, L. G.; Grant, D. M.; Black, E. P.; Courtieu, J. M. *J. Chem. Phys.* **1978**, *69*, 2407–19.
(31) Werbelow, L. G.; Grant, D. M. *Chem. Phys. Lett.* **1978**, *54*, 571–4.
(32) Poupko, R.; Vold, R. L.; Vold, R. R. *J. Phys. Chem.* **1980**, *84*, 3444–8.
(33) Bernassau, J. M.; Black, E. P.; Grant, D. M. *J. Chem. Phys.* **1982**, *76*, 253–6.
(34) Courtieu, J.; Lai, N. T.; Nguyen, T. L.; Bernassau, J. M.; Grant, D. M. *J. Chem. Phys.* **1982**, *76*, 257–64.
(35) Black, E. P.; Bernassau, J. M.; Mayne, C. L.; Grant, D. M. *J. Chem. Phys.* **1982**, *76*, 265–72.
(36) Dickerson, W. H.; Vold, R. R.; Vold, R. L. *J. Phys. Chem.* **1983**, *87*, 166–72.
(37) Canet, D.; Brondeau, J. *Chem. Phys. lett.* **1983**, *100*, 70–5.
(38) Vold, R. L.; Vold, R. R. *Isr. J. Chem.* **1983**, *23*, 315–22.
(39) Vold, R. R. *NMR in Liquid Crystals*; Emsley, J. W., Veracini, C. A., Eds.; Reidel: Dordrecht, 1985; p 253.
(40) Vold, R. R.; Vold, R. L. *J. Chem. Phys.* **1988**, *88*, 1443–57.
(41) Vold, R. L.; Vold, R. R.; Warner, M. *J. Chem. Soc., Faraday Trans.* **1988**, *84*, 997–1013.
(42) Vold, R. R.; Vold, R. L. *J. Chem. Phys.* **1988**, *88*, 4655–9.
(43) Farrar, T. C.; Quintero, A. R. A. *J. Phys. Chem.* **1987**, *91*, 3224–8.
(44) Farrar, T. C.; Locker, I. C. *J. Chem. Phys.* **1987**, *87*, 3281–7.
(45) Farrar, T. C.; Quintero, A. R. A.; Locker, I. C. *Z. Phys. Chem. (Munich)* **1987**, *151*, 25–33.
(46) Decatur, J. D.; Farrar, T. C. *J. Phys. Chem.* **1989**, *93*, 8294–9.
(47) Nery, H.; Canet, D. *J. Magn. Reson.* **1981**, *42*, 370–80.
(48) Nery, H.; Canet, D.; Toma, F.; Fermandjian, S. *J. Am. Chem. Soc.* **1983**, *105*, 1482–6.
(49) Werbelow, L.; Canet, D.; Nery, H. *J. Magn. Reson.* **1984**, *60*, 405–14.
(50) Jaccard, G.; Wimperis, S.; Bodenhausen, G. *Chem. Phys. Lett.* **1987**, *138*, 601–6.
(51) Werbelow, L. G. *J. Magn. Reson.* **1987**, *71*, 151–3.
(52) Hartzell, C. J.; Stein, P. C.; Lynch, T. J.; Werbelow, L. G.; Earl, W. L. *J. Am. Chem. Soc.* **1989**, *111*, 5114–19.
(53) Elbayed, K.; Canet, D. *Mol. Phys.* **1989**, *68*, 1033–46.
(54) Werbelow, L. *J. Phys. Chem.* **1990**, *94*, 6663–6.
(55) Chenon, M. T.; Coupry, C.; Werbelow, L. G. *J. Phys. Chem.*, submitted for publication.
(56) Mackor, E. L.; MacLean, C. *Prog. NMR Spectrosc.* **1967**, *3*, 129.
(57) Pyper, N. C. *Mol. Phys.* **1971**, *21*, 1–33.
(58) Blicharski, J. S.; Nosel, W.; Schneider, H. *Ann. Phys. (Leipzig)* **1971**, *27*, 17.
(59) Blicharski, J. S.; Nosel, W. *Acta Phys. Polon.* **1972**, *A42*, 223.
(60) Werbelow, L. G.; Grant, D. M. *J. Magn. Reson.* **1975**, *20*, 554–64.
(61) Lyerla, J. R. J.; Grant, D. M. *MTP Int. Rev. Sci.: Phys. Chem., Ser. One* **1972**, *4*, 155–200.
(62) Zeidler, M. D. *Ber. Bunsenges. Phys. Chem.* **1968**, *72*, 481.
(63) Pyper, N. C. *Mol. Phys.* **1971**, *22*, 433–58.
(64) Bain, A. D.; Lynden, B. R. M. *Mol. Phys.* **1975**, *30*, 325–56.
(65) Mayne, C. L.; Alderman, D. W.; Grant, D. M. *J. Chem. Phys.* **1975**, *63*, 2514–23.
(66) Mayne, C. L.; Grant, D. M.; Alderman, D. W. *J. Chem. Phys.* **1976**, *65*, 1684–95.
(67) Farrar, T. C.; Becker, E. D. *Pulse and Fourier Transform NMR, Introduction to Theory and Methods*; Academic Press: New York, 1971.
(68) Bloembergen, N.; Purcell, E. M.; Pound, R. V. *Phys. Rev.* **1948**, *73*, 679–712.
(69) Fano, U. *Rev. Mod. Phys.* **1957**, *29*, 74–93.
(70) Lyerla, J. R. J.; Grant, D. M.; Bertrand, R. D. *J. Phys. Chem.* **1971**, *75*, 3967–71.
(71) Alger, T. D.; Hamill, W. D. J.; Pugmire, R. J.; Grant, D. M.; Silcox, G. D.; Solum, M. *J. Phys. Chem.* **1980**, *84*, 632–6.
(72) Alger, T. D.; Solum, M.; Grant, D. M.; Silcox, G. D.; Pugmire, R. J. *Anal. Chem.* **1981**, *53*, 2299–304.
(73) Buckingham, A. D.; Malm, S. M. *Mol. Phys.* **1971**, *22*, 1127.
(74) Facelli, J. C.; Orendt, A. M.; Grant, D. M.; Michl, J. *Chem. Phys. Lett.* **1984**, *112*, 147–9.
(75) Beeler, A. J.; Orendt, A. M.; Grant, D. M.; Cutts, P. W.; Michl, J.; Zilm, K. W.; Downing, J. W.; Facelli, J. C.; Schindler, M. S.; Kutzelnigg, W. *J. Am. Chem. Soc.* **1984**, *106*, 7672–6.
(76) Courtieu, J.; Mayne, C. L.; Grant, D. M.; Bernassau, J. M. *J. Magn. Reson.* **1982**, *48*, 346–53.
(77) Maryott, A. A.; Farrar, T. C.; Malmberg, M. S. *J. Chem. Phys.* **1971**, *54*, 64–71.
(78) Farrar, T. C.; Druck, S. J.; Shoup, R. R.; Becker, E. D. *J. Am. Chem. Soc.* **1972**, *94*, 699–703.
(79) Shoup, R. R.; Farrar, T. C. *J. Magn. Reson.* **1972**, *7*, 48–54.
(80) Farrar, T. C.; Maryott, A. A.; Malmberg, M. S. *Annu. Rev. Phys. Chem.* **1972**, *23*, 193–216.
(81) Becker, E. D.; Shoup, R. R.; Farrar, T. C. *Pure Appl. Chem.* **1972**, *32*, 51–66.
(82) Werbelow, L. *J. Chem. Phys.* **1982**, *77*, 5849.
(83) Chenon, M. T.; Bernassau, J. M.; Coupry, C. *Mol. Phys.* **1985**, *54*, 277–86.
(84) Foucat, L.; Chenon, M. T.; Werbelow, L. *J. Phys. Chem.* **1990**, *94*, 5791–5.
(85) Lyerla, J. R. J.; Grant, D. M.; Wang, C. H. *J. Chem. Phys.* **1971**, *55*, 4676–7.
(86) Wang, C. H.; Grant, D. M.; Lyerla, J. R. J. *J. Chem. Phys.* **1971**, *55*, 4674–5.
(87) Lyerla, J. R. J.; Grant, D. M. *J. Phys. Chem.* **1972**, *76*, 3213–16.
(88) Werbelow, L. G.; Marshall, A. G. *Mol. Phys.* **1974**, *28*, 113–29.
(89) Alger, T. D.; Freeman, R.; Grant, D. M. *J. Chem. Phys.* **1972**, *57*, 2168–71.
(90) Khazanovich, T. N.; Zitserman, V. Y. *Mol. Phys.* **1971**, *21*, 65.
(91) Simon, H. E.; Vold, R. L. *J. Magn. Reson.* **1976**, *24*, 399–409.
(92) Werbelow, L.; Pouzard, G.; Thevand, A. *J. Chim. Phys. Phys. Chim. Biol.* **1979**, *76*, 941–6.
(93) Werbelow, L. G.; Marshall, A. G. *J. Magn. Reson.* **1973**, *11*, 299–313.
(94) Werbelow, L. G.; Grant, D. M. *J. Magn. Reson.* **1978**, *29*, 603–5.
(95) Werbelow, L.; Thevand, A.; Pouzard, G. *J. Chem. Soc., Faraday Trans.* **1979**, *75*, 971–4.
(96) Canet, D.; Vold, R. L.; Vold, R. R. *J. Chem. Phys.* **1976**, *64*, 900–1.
(97) Vold, R. L.; Vold, R. R.; Canet, D. *J. Chem. Phys.* **1977**, *66*, 1202–16.
(98) Kratochwill, A.; Vold, R. L.; Vold, R. R. *J. Chem. Phys.* **1979**, *71*, 1319–24.
(99) Nery, H.; Canet, D. *Mol. Phys.* **1978**, *35*, 213–22.
(100) Werbelow, L. G.; Grant, D. M. *J. Chem. Phys.* **1975**, *63*, 544–56.
(101) Werbelow, L. G.; Grant, D. M. *J. Chem. Phys.* **1975**, *63*, 4742–9.
(102) Werbelow, L. G. *J. Magn. Reson.* **1979**, *34*, 123–7.
(103) Canet, D.; Nery, H.; Brondeau, J. *J. Chem. Phys.* **1979**, *70*, 2098–107.
(104) Thevand, A.; Pouzard, G.; Werbelow, L. *J. Phys. Chem.* **1981**, *85*, 29–35.
(105) Werbelow, L. G.; Marshall, A. G. *Chem. Phys. Lett.* **1973**, *22*, 568–71.
(106) Fagerness, P. E.; Grant, D. M.; Kuhlmann, K. F.; Mayne, C. L.; Parry, R. B. *J. Chem. Phys.* **1975**, *63*, 2524–32.
(107) Kratochwill, A.; Vold, R. L. *J. Magn. Reson.* **1980**, *40*, 197–207.
(108) Nery, H.; Canet, D.; Rivail, J. L. *Chem. Phys.* **1981**, *62*, 123–9.
(109) Solomon, I. *Phys. Rev.* **1955**, *99*, 559.
(110) Shimizu, H.; Fujiwara, S. *J. Chem. Phys.* **1961**, *34*, 1501.
(111) Mackor, E. L.; MacLean, C. *J. Chem. Phys.* **1965**, *42*, 4254–61.
(112) Mackor, E. L.; MacLean, C. *J. Chem. Phys.* **1966**, *44*, 64.
(113) Kuhlmann, K. F.; Grant, D. M.; Harris, R. K. *J. Chem. Phys.* **1970**, *52*, 3439–48.
(114) Konigsberger, E.; Sterk, H. *J. Chem. Phys.* **1985**, *83*, 2723–26.

(115) Noggle, J. H.; Schirmer, R. E. *The Nuclear Overhauser Effect; Chemical Applications*; Academic Press: New York, 1971.
(116) Daragan, V. A.; Khasanovich, T. N.; Stepanyants, A. U. *Chem. Phys. Lett.* **1974**, *26*, 89.
(117) Debye, P. *Polar Molecules*; Dover: New York, 1929.
(118) Perrin, F. *J. Phys. Radium* **1934**, *5*, 497.
(119) Perrin, F. *J. Phys. Radium* **1936**, *7*, 1.
(120) Woessner, D. E. *J. Chem. Phys.* **1962**, *37*, 647.
(121) Shimizu, H. *J. Chem. Phys.* **1962**, *37*, 765.
(122) Shimizu, H. J. *Chem. Phys.* **1964**, *40*, 754.
(123) Woessner, D. E.; Snowden, B. S.; Strom, E. T. *Mol. Phys.* **1968**, *14*, 265.
(124) Huntress, W. T. *J. Chem. Phys.* **1968**, *48*, 3524.
(125) Huntress, W. T. *Adv. Magn. Reson.* **1970**, *4*, 1.
(126) Hubbard, P. S. *J. Chem. Phys.* **1970**, *52*, 563.
(127) Lyerla, J. R. J.; Grant, D. M.; Harris, R. K. *J. Phys. Chem.* **1971**, *75*, 585–8.
(128) Campbell, I. D.; Freeman, R. *J. Magn. Reson.* **1973**, *11*, 143–62.
(129) Campbell, I. D.; Freeman, R.; Turner, D. L. *J. Magn. Reson.* **1975**, *20*, 172–6.
(130) Canet, D.; Brondeau, J.; Nery, H.; Marchall, J. P. *Chem. Phys. Lett.* **1980**, *72*, 184–8.
(131) Hubbard, P. S. *Phys. Rev.* **1958**, *109*, 1153.
(132) Hubbard, P. S. *J. Chem. Phys.* **1969**, *51*, 1647.
(133) Grant, D. M.; Werbelow, L. G. *J. Magn. Reson.* **1976**, *21*, 369–71.
(134) Favro, L. D. *Phys. Rev.* **1960**, *119*, 53.
(135) Wang, S. C. *Phys. Rev.* **1929**, *34*, 243–252.
(136) Fuson, M. M.; Brown, M. S.; Grant, D. M.; Evans, G. T. *J. Am. Chem. Soc.* **1985**, *107*, 6695–8.
(137) Jakobsen, H. J.; Linde, S. A.; Sorensen, S. *J. Magn. Reson.* **1974**, *15*, 385.
(138) Bovee, W. M. M. J. *Mol. Phys.* **1975**, *29*, 1673–84.
(139) Muller, L.; Kumar, A.; Ernst, R. R. *J. Chem. Phys.* **1975**, *63*, 5490–1.
(140) Liu, F.; Mayne, C. L.; Grant, D. M. *J. Magn. Reson.* **1989**, *84*, 344–50.
(141) Liu, F.; Horton, W. J.; Mayne, C. L.; Xiang, T. X.; Grant, D. M. Submitted for publication.
(142) Mayne, C. L. Ph.D. Thesis, University of Utah, 1976.
(143) Fuson, M. M.; Prestegard, J. H. *J. Chem. Phys.* **1982**, *76*, 1539–49.
(144) Chenon, M. T.; Bernassau, J. M.; Mayne, C. L.; Grant, D. M. *J. Phys. Chem.* **1982**, *86*, 2733–43.
(145) Levy, G. C. *Acc. Chem. Res.* **1973**, *6*, 161–9.
(146) Grant, D. M.; Chenon, M. T.; Mayne, C. L.; Werbelow, L. G. *Proc. 20th Colloq. Spectrosc. Intn., Prague, Czech.* **1977**, *2*, 207–221.
(147) Stark, R. E.; Vold, R. L.; Vold, R. R. *J. Magn. Reson.* **1979**, *33*, 421–36.
(148) Brown, M. S.; Mayne, C. L.; Grant, D. M.; Chou, T. C.; Allred, E. L. *J. Phys. Chem.* **1984**, *88*, 2708–13.
(149) Brown, M. S.; Grant, D. M.; Horton, W. J.; Mayne, C. L.; Evans, G. T. *J. Am. Chem. Soc.* **1985**, *107*, 6698–707.
(150) Fuson, M. M.; Prestegard, J. H. *Biochemistry* **1983**, *22*, 1311–16.
(151) Fuson, M. M.; Prestegard, J. H. *J. Am. Chem. Soc.* **1983**, *105*, 168–76.
(152) Fuson, M. M.; Prestegard, J. H. *J. Magn. Reson.* **1980**, *41*, 179–84.
(153) Fuson, M. M.; Grant, D. M. *Macromolecules* **1988**, *21*, 944–9.
(154) Fuson, M. M.; Anderson, D. J.; Liu, F.; Grant, D. M. *Macromolecules* **1991**, *24*, 2594–97.
(155) Prestegard, J. H.; Grant, D. M. *J. Am. Chem. Soc.* **1978**, *100*, 4664–8.
(156) Courtieu, J.; Jullien, J.; Nguyen, T. L.; Guillois, A.; Gonord, P.; Kan, S. K.; Mayne, C. L. *J. Chem. Phys.* **1980**, *72*, 953–9.
(157) Black, E. P. Ph.D. Thesis, University of Utah, 1980.
(158) Kuhlmann, K. F.; Grant, D. M. *J. Chem. Phys.* **1971**, *55*, 2998–3007.
(159) Collins, S. W.; Alger, T. D.; Grant, D. M.; Kuhlmann, K. F.; Smith, J. C. *J. Phys. Chem.* **1975**, *79*, 2031–7.
(160) Ladner, K. H.; Dalling, D. K.; Grant, D. M. *J. Phys. Chem.* **1976**, *80*, 1783–6.
(161) Myers, R. J.; Gwinn, W. D. *J. Chem. Phys.* **1952**, *20*, 1420.
(162) Jung, W. G.; Zeidler, M. D.; Chieux, P. *Mol. Phys.* **1989**, *68*, 473–85.
(163) Gilchrist, J. l. G. *Chem. Phys.* **1982**, *70*, 353–66.
(164) Knauss, D. C.; Evans, G. T.; Grant, D. M. *Chem. Phys. Lett.* **1980**, *71*, 158–63.
(165) Liu, F.; Xiang, T.-X.; Grant, D. M. Submitted for publication.
(166) Schatzki, T. F. *Polym. Prepr.* **1965**, *6*, 646.
(167) Jelinski, L. W.; Dumais, J. J.; Engel, A. K. *Macromolecules* **1983**, *16*, 492–6.
(168) Helfand, E. *J. Chem. Phys.* **1971**, *54*, 4651–61.
(169) Skolnick, J.; Helfand, E. *J. Chem. Phys.* **1980**, *72*, 5489–5500.
(170) Helfand, E. *Science* **1984**, *226*, 647–50.
(171) Xiang, T.-X.; Liu, F.; Grant, D. M. *J. Chem. Phys.* **1991**, *94*, 4463–71.
(172) Xiang, T.-X.; Liu, F.; Grant, D. M. Manuscript in preparation.
(173) Zwanzig, R.; Bixon, M. *Phys. Rev. A* **1970**, *2*, 2005–12.
(174) Metiu, H.; Oxtoby, D. W.; Freed, K. F. *Phys. Rev. A* **1977**, *15*, 361–71.
(175) MacPhail, R. A.; Kivelson, D. *J. Chem. Phys.* **1984**, *80*, 2102–14.
(176) Sceats, M. G.; Dawes, J. M. *J. Chem. Phys.* **1985**, *83*, 1298–304.
(177) Ryckaert, J. P.; Bellemans, A. *Chem. Phys. Lett.* **1975**, *30*, 123–5.
(178) Zhu, S. B.; Lee, J.; Robinson, G. W.; Lin, S. H. *J. Chem. Phys.* **1989**, *90*, 6335–9.
(179) Zhu, S. B.; Lee, J.; Robinson, G. W.; Lin, S. H. *Chem. Phys. Lett.* **1988**, *148*, 164–8.
(180) Zhu, S. B.; Lee, J.; Robinson, G. W. *J. Chem. Phys.* **1988**, *88*, 7088–96.
(181) Scott, R. A.; Scheraga, H. A. *J. Chem. Phys.* **1966**, *44*, 3054–69.
(182) Jorgensen, W. L. *J. Phys. Chem.* **1983**, *87*, 5304–14.
(183) Jorgensen, W. L. *J. Phys. Chem.* **1986**, *90*, 1276–84.
(184) Pastor, R. W.; Karplus, M. *J. Phys. Chem.* **1988**, *92*, 2636–41.
(185) Xiang, T.-X.; Liu, F.; Grant, D. M. *J. Chem. Phys.* **1991**, in press.
(186) Pear, M. R.; McCammon, J. A. *J. Chem. Phys.* **1981**, *74*, 6922–5.
(187) Ladanyi, B. M.; Hynes, J. T. *J. Chem. Phys.* **1982**, *77*, 4739–46.